DEBRECENI EGYETEM

TERMÉSZETTUDOMÁNYI KAR

Four-jet production in electron-positron annihilation

Ph.D. thesis

by

Zoltán Nagy

University of Debrecen
Faculty of Sciences
Debrecen, 2000

Four-jet production in electron-positron annihilation

Értekezés a doktori (Ph.D.) fokozat megszerzése érdekében
a fizika tudományában.

Írta: Nagy Zoltán okleveles fizikus
Készült a Debreceni Egyetem Természettutományi Karán fizika doktori programja
(részecskefizika alprogramja) keretében.

Témavezető: Dr. .....

Elfogadásra javaslom: 2000 ....

Az értekezést bírálóként elfogadásra javaslom:

Dr. ....

Dr. ....

Dr. ....

Jelölt az értekezést 2000 ....-n sikeresen megvédte:

A bírálóbizotság elnöke: Dr. ....

A bírálóbizotság tagjai:

Dr. ....

Dr. ....

Dr. ....

Dr. ....

Debrecen-2000

Ez a dolgozat a Magyar Tudományos Akadémia Atommag Kutató Intézetében készült 2000-ben. A dolgozat alapjául szolgáló eredmények illetve tudományos közlemények a Kossuth Lajos Tudományegyetem Elméleti Fizikai Tanszékén születtek 1997 és 1998 között.

Ezen értekezést a Debreceni Egyetem fizika doktori program részecskefizika alprogramja keretében készítettem 1998 és 2000 között és ezúton benyújtom a Debreceni Egyetem doktori Ph.D. fokozatának elnyerése céljából.

Debrecen, 2000. április 20.

Nagy Zoltán

Tanúsítom, hogy Nagy Zoltán doktorjelölt 1998 és 2000 között a fent megnevezett doktori alprogram keretében irányításommal végezte munkáját. Az értekezésben foglaltak a jelölt önálló munkáján alapulnak, az eredményekhez önálló alkotó tevékenységével meghatározóan hozzájárult. Az értekezést elfogadásra javaslom.

Debrecen, 2000. április 20.

Dr. Trócsányi Zoltán
témavezető

Contents

Chapter 1

Introduction

It is generally believed that the strong interaction which acts between the constituents of hadrons, is described by the theory of Quantum Chromodynamics (QCD). The two type of the constituents, called partons, are presented by the quarks and gluons which correspond to matter and force carriers respectively. There are indications that the QCD explains the experimental observation that the quarks and the gluons only appear as confined states and do not occur as free particles. The fact that the hadrons are observed instead of partons (quarks and gluons), is theoretical explained by the principle of color confinement: only colorless objects occur in nature. Prediction of QCD for any strong interacted process can be obtained in principle which turns out to be very hard. However under specific conditions it is possible to compute some quantities by means of perturbative method. This approach is justified by asymptotic freedom of QCD. With this property of QCD and the renormalization group techniques one can define the running coupling constant $\alpha_s(Q)$ which become zero in the limit $Q \to \infty$. This behaviour in the high scale region allows us to make perturbative expansion in $\alpha_s(Q)$. The lowest order of this perturbative expansion corresponds to the naïve parton model approach or to so-called leading order approximation (LO). However, the LO calculation can predict only the order of magnitude of a given cross section and the rough features of a certain observable. The accuracy of the perturbative expansion is controlled by the size of the higher-order calculations. Any QCD prediction thus requires (at least) a next-to-leading order (NLO) calculation and the NLO definitions of the related components (e.g $\alpha_s(Q)$).

These higher-order computations have been carried out over a period of about twenty years, often long after the accuracy of experimental data has made them necessary, because of the difficulties in the setting up a general and straightforward calculational procedure.

One of these difficulties is the treatment of the matrix elements. Because of the complexity of the non-abelian vertices the expression of the matrix elements becomes huge by increasing the external legs of matrix element. This problem arise at leading order too. Otherwise, the loop matrix elements contain integrals over the

loop momenta. In principle and some important cases [42] the problem of the one-integrals is solved, but the two loop integrals are known only in some special cases. At this moment, the calculation of the higher loop amplitudes is hopeless.

The other difficulty is in necessity of factorizing the long- and short-distance components of the scattering processes and is reflected in the perturbative calculation by the presence of divergences. The cancellation of these divergences is main task of the next-to-leading (or higher order) calculation. There are many general method have been developed for calculating NLO cross sections. When I started my works in the topic of perturbative QCD I also had took a share in the developing an NLO calculation method [8].

In this dissertation I discuss the theoretical description of the four-jet production in electron-positron annihilation at NLO level. The motivations of this project are the followings.

The electron-positron annihilation is the cleanest way to test QCD in high energy elementary particle reactions and measure the strong coupling constant α_s. The other ingredient of the QCD, that is in principle free, is the underlying gauge group. Although by now nobody questions that QCD is based upon SU(3) gauge theory, the "full" measurement of QCD, that is the simultaneous measurement of the strong coupling and the eigenvalues of the quadratic Casimirs of the underlying gauge theory, the C_F and C_A color charges, is not a purely academic exercise. The possible existence of light gluinos [62] influences both the value of α_s and the measured value of the color charges. Thus the only consistent framework to check whether the data favor or exclude the additional degrees of freedom is a simultaneous fit of these parameters to data. The sensitivity of a given observable on the color charges however, is influenced by the fact that in perturbation theory the three gluon coupling appears at tree level first for four-jet final states. Therefore, four-jet observables seem to be the best candidates to measure the color factors.

On the other hand the knowledge of the weight of the QCD four-jet events is important in the point of view some other non-QCD processes. For example the the the $e^+e^- \to W^+W^-$ events lead to four-jet final state. The QCD four-jet events mean the main background for Higgs and other new particle searches.

The outline of this thesis is as follows. In Chapter 2 a brief introduction is given elements of QCD (Lagrangian, regularization, running coupling,...). In Chapter 3 the description of the hadronic final states are discussed. The number of physical quantities are defined which help us to characterize the events and we give the general scheme of the theoretical description. In the Chapter 4 one of the general method [53] is presented for calculating NLO jet cross sections in e^+e^- annihilation. In the Chapter 5 the physical results for some relevant four-jet quantities are presented. In Appendix A and Appendix B the four- and five-parton matrix elements are given.

Chapter 2

Basics of QCD

In this chapter the basics of perturbative QCD are briefly discussed. First we define the Lagrangian and then present the QCD Feynman rules. We give a short overview about the regularization, renormalization and the renormalization group equations. The solution of the renormalization group equations presents the asymptotic behaviour of the coupling constant and the masses.

2.1 The QCD Lagrangian

QCD is a renormalizable quantum field theory of the strong interaction. Its fundamentals fields are the Dirac spinor fields describing particles of spin $1/2$, called quarks with fractional electromagnetic charge and the gauge fields corresponding to electromagnetic chargeless and massless particles of spin 1, called gluons. The underlying gauge group is the $SU(3)$. The Lagrangian is defined by sum of the two terms

$$L_{eff}^{QCD} = L_{inv} + L_{gauge} \ , \tag{2.1}$$

where the first term is the classical gauge invariant term was defined at first by Yang and Mills in [10].

$$L_{inv} = \sum_f \bar{\psi}_f (\mathrm{i}\hat{D} - m_f)\psi_f - \frac{1}{4} G_a^{\mu\nu} G_{\mu\nu}^a \ , \tag{2.2}$$

where m_f denotes the mass of the quark with flavour f and $G_a^{\mu\nu}$ is the strength tensor of the gauge field. We introduced the covariant derivative in the fundamental representation of gauge group.

$$\hat{D} = \gamma_\mu D^\mu \ , \qquad D^\mu = \partial^\mu + \mathrm{i}g_s t^a A_a^\mu \tag{2.3}$$

$$G_{\mu\nu}^a = \partial_\mu A_\nu^a - \partial_\nu A_\mu^a - \mathrm{i}g_s F_{bc}^a A_\mu^b A_\nu^c \ , \tag{2.4}$$

where g_s denote the strong coupling constant. Here t^a and F^a_{bc} are the fundamental and adjoint representation of the generators of the gauge group. The fields ψ_f are the quark fields and A^μ_a are the gluon fields.

Because of the gauge invariance, the A^μ_a gauge fields are determined up to a gauge transformation. During the quantization this freedom give to rise any problem. We have to fix the gauge. The physical quantities are independent of this gauge choice. In the case of covariant Lorentz gauge the gauge fixing term L_{gauge} in the expression of Lagrangian can be written as follows

$$L_{gauge} = -\frac{1}{2\xi}(\partial_\mu A^\mu_a)^2 + \partial_\mu \eta^*_a(\partial^\mu \eta^a - \mathrm{i}g_s F^a_{bc}\eta^b A^{\mu c}) \ , \tag{2.5}$$

or in the case of axial gauge

$$L_{gauge} = -\frac{1}{2\xi}(n_\mu A^\mu_a)^2 \ , \tag{2.6}$$

where ξ is an arbitrary parameter and the n^μ is a space or light like ($n^2 \leq 0$) four-vector. In Eq. (2.5) the last term is the contribution of non-physical Faddeev-Popov ghost fields. These fields are fermionic with scalar kinematic term in the Lagrangian.

The fundamental t^a and adjoint F^a_{bc} representation of generators of the gauge group satisfied the relation of the Lie-algebras

$$[t^a, t^b]_{\alpha\beta} = \mathrm{i}f^{abc}t^c_{\alpha\beta} \ , \qquad [F^a, F^b]_{df} = \mathrm{i}f^{abc}F^c_{df} \ , \tag{2.7}$$

where $f^{abc} = f_{abc}$ is the structure constants are related to the adjoint representation via $F^a_{bc} = -\mathrm{i}f_{abc}$. The quadratic Casimir invariants C_F and C_A are defined by

$$\sum_{a=1}^{N_A}(t^a t^{\dagger a})_{\alpha\beta} = C_F\delta_{\alpha\beta} \, , \quad \sum_{a=1}^{N_A}(F^a F^{\dagger a})_{cd} = C_A\delta_{cd} \, , \quad \mathrm{Tr}(t^a t^{\dagger b}) = T_R\delta^{ab} \, , \tag{2.8}$$

where N_A is the number of the t^a generators. The last equation in (2.8) is the normalization equation. The usual normalization is the $T_R = 1/2$ choose. In the case of $SU(N_c)$ the quadratic Casimirs are $C_F = (N_c^2 - 1)/(2N_c)$, $C_A = N_c$.

2.2 Feynman rules

During the perturbative calculation we use the Feynman rules which are derived from the Lagrangian. Using these rules we can calculate the amplitudes of any process. In Table (2.1) the Feynman rules are given in standard notation in the cases of Lorentz and axial gauge. The rules of the Faddeev-Popov ghost fields is given in Table (2.2). In this table we also listed the color truncated Feynman rules. More details can be found about these rules in the paper of Mangano-Parke [41]

Table 2.1: Feynman rules for QCD

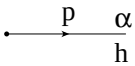	Quark leg with momentum p, color α and helicity h. Standard notation: $\bar{u}_\alpha(p)$ Color truncated: $\langle p \pm \vert \ , \quad h = \pm \ , \quad m = 0$
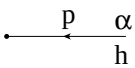	Antiquark leg with momentum p, color α and helicity h. Standard notation: $v_\alpha(p)$ Color truncated: $\vert p \pm \rangle \ , \quad h = \mp \ , \quad m = 0$
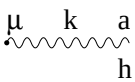	Gluon leg with momentum k, color a and helicity h. Standard notation: $\varepsilon^a_\mu(k, h = \pm)$ Color truncated: $\varepsilon^\pm_\mu(k,p) = \pm \dfrac{\langle k \pm \vert \gamma_\mu \vert p \pm \rangle}{\sqrt{2}\langle p \mp \vert k \mp \rangle} \ , \quad h = \pm \ ,$ where p is an arbitrary reference momentum.
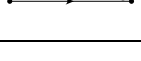	Standard notation: $\mathrm{i}\delta_{\alpha\beta}(\hat{p} + m)/(p^2 - m^2 + \mathrm{i}0)$ Color truncated: $\mathrm{i}\hat{p}/p^2 \ , m = 0$
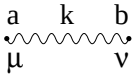	Standard notation: $-\mathrm{i}\delta_{ab}P_{\mu\nu}/(k^2 + \mathrm{i}0)$ - Lorentz gauge: $P_{\mu\nu} = g_{\mu\nu} - (1-\xi)k_\mu k_\nu/(k^2 + \mathrm{i}0)$ - Axial gauge: $P_{\mu\nu} = g_{\mu\nu} + k_\mu k_\nu (n^2 + \xi k^2)(k \cdot n)^{-2}$ $\quad - (n_\mu k_\nu + n_\nu k_\mu)(k \cdot n)^{-1}$ Color truncated: $-\mathrm{i}g_{\mu\nu}/k^2$
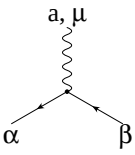	Standard notation: $\mathrm{i}g_s\gamma_\mu t^a_{\alpha\beta}$ Color truncated: $\mathrm{i}(g_s/\sqrt{2})\gamma_\mu$
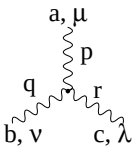	Standard notation: $\mathrm{i}g_s F^a_{bc} V_{\mu\nu\lambda}(p,q,r)$ Color truncated: $\mathrm{i}(g_s/\sqrt{2})V_{\mu\nu\lambda}(p,q,r)$ $V_{\mu\nu\lambda}(p,q,r) = g_{\mu\lambda}(p-r)_\nu + g_{\nu\lambda}(r-q)_\mu + g_{\mu\nu}(q-p)_\lambda$ (all momenta outgoing)
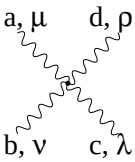	Standard notation: $\mathrm{i}g_s^2\big(F^x_{ab}F^x_{cd}(g_{\mu\lambda}g_{\nu\rho} - g_{\mu\rho}g_{\nu\lambda})$ $\quad + F^x_{ad}F^x_{bc}(g_{\mu\nu}g_{\lambda\rho} - g_{\mu\lambda}g_{\nu\rho}) + F^x_{ac}F^x_{bd}(g_{\mu\nu}g_{\lambda\rho} - g_{\mu\rho}g_{\nu\lambda})\big)$ Color truncated: $\mathrm{i}g_s^2\left(g_{\mu\lambda}g_{\nu\rho} - \frac{1}{2}(g_{\mu\rho}g_{\nu\lambda} + g_{\mu\nu}g_{\lambda\rho})\right)$

Table 2.2: Feynman rules for ghost fields

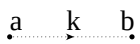	Standard notation: -Lorentz gauge: $\mathrm{i}\delta_{ab}/(k^2+\mathrm{i}0)$ -Axial gauge: no ghost fields
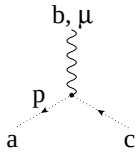	Standard notation: -Lorentz gauge: $\mathrm{i}g_s p_\mu F^b_{ac}$ -Axial gauge: no ghost fields

2.3 Regularization

In a given order of the perturbative calculation a physical amplitude can be written as a sum of the all topologically independent Feynman diagrams. The higher order diagrams contain closed loops. These loop diagrams mean the quantum corrections. These integrals (loop, phase space) contain various singularities. If we want to calculate for example a cross section in naive way we won't be able to interpret that result. We have to regularize the theory and in this regularized theory the calculated quantities are finite and removed the regularization remains finite. A n-point Green function can be written in the following form

$$G^{(n)}(p_1,...,p_n) = \int \left[\prod_i \frac{d^4 l_i}{(2\pi)^4}\right] \left[\prod_j \frac{1}{k_j^2 - m_j^2 + \mathrm{i}0}\right] N(\{p,l\}) \ , \qquad (2.9)$$

where $p_1,..,p_n$ denote the external momenta and l_i's are the loop momenta. The numerator in Eq.(2.9) $N(\{p,l\})$ is a function of the external and internal momenta. The momenta k_j's are linear expression of the external and internal momenta. In this expression the integrand contains infrared (IR) and ultraviolet divergences (UV) in the worst case. The UV divergences arise from the big loop energy region. This shows IR behavior when one of the particle lines is on-shell ($k_j^2 = m_j^2$).

There are many regularization scheme in the literature but we are interesting in that scheme which is able to regularize both in the UV and IR regions. Otherwise, it has to preserve the physical requirements (Lorentz and gauge invariance, unitary, etc). In this sense the dimensional regularization is the most suitable for gauge theory. In this regularization scheme the dimension of the spacetime is shifted by 2ϵ where ϵ a real or complex number. The effects of the dimensional regularization are the followings

1. Change dimension of the the space time.

$$d = 4 \quad \longrightarrow \quad d = 4 - 2\epsilon \qquad (2.10)$$

2. The action must remain dimensionless. From this condition we find for the strong coupling constant

$$\mathrm{g}_s \longrightarrow \mathrm{g}_s\mu^\epsilon \ , \tag{2.11}$$

where μ is an arbitrary scale parameter.

3. The vector indices run between 1 and d.

$$4 = \sum_{\nu=1}^{4} 1 \longrightarrow d = \sum_{\nu=1}^{d} 1 \ , \qquad \frac{d^4k}{(2\pi)^4} \longrightarrow \frac{d^dk}{(2\pi)^d} \tag{2.12}$$

4. The dimension of the Dirac-matrices is d.

$$\{\gamma^\mu, \gamma^\nu\} = 2g^{\mu\nu} \ , \qquad g^\mu_\mu = d \ , \qquad \mu, \nu = 1, ..., d \tag{2.13}$$

Let see a simple example for a divergent integral in the regularized theory

$$\begin{aligned} I_s(4-2\epsilon) &= \int \frac{d^{4-2\epsilon}}{(2\pi)^{4-2\epsilon}} \frac{1}{(k^2 - m^2 + \mathrm{i}0)^s} \\ &= (-1)^s \mathrm{i}(4\pi)^{\epsilon-2}(m^2 - \mathrm{i}0)^{2-s-\epsilon} \frac{\Gamma(s-2+\epsilon)}{\Gamma(s)} \end{aligned} \tag{2.14}$$

where $\Gamma(s)$ is the Euler-gamma function. In $d = 4$ dimension this integral has one UV pole if $s = 2$.

2.4 Renormalization

The renormalization is a procedure which makes our physical predictions free from UV divergences. This renormalization procedure is well defined in all order of the perturbative calculation and can be evaluated. We renormalize the fields and the parameters by the Z_i renormalization constants. These constants are defined well only in the regularized theory since these constants contain poles in the term of variable ϵ (as $1/\epsilon^p$and $p > 0$ integer).

Let define the renormalized and bare quantities (fields and parameters) by the followings

$$(A^\mu_a)_B = Z_A^{1/2} A^\mu_a \tag{2.15}$$
$$(\psi_f)_B = Z_\psi^{1/2} \psi_f \tag{2.16}$$
$$(\eta_a)_B = Z_\eta^{1/2} \eta_a \tag{2.17}$$
$$\xi_B^{-1} = Z_\xi Z_A^{-1} \xi^{-1} \tag{2.18}$$
$$(\mathrm{g}_s)_B = Z_g \mathrm{g}_s \mu^\epsilon \tag{2.19}$$
$$(m_f)_B = Z_m Z_\psi^{-1} m_f \tag{2.20}$$

where the index B denotes the bare quantities which are infinite in the non-regularized theory. The Z_i renormalization can be expanded in the number of loop giving

$$Z_i = \sum_{n=0}^{\infty} \left(\frac{\alpha_s}{2\pi}\right)^n \sum_{j=1}^{n} \frac{Z_i^{(n,j)}(m/\mu)}{\epsilon^j} \ , \tag{2.21}$$

where $\alpha_s = \mathrm{g}_s^2/(4\pi)$. The renormalized Lagrangian is defined by

$$L_{eff}(\varphi_B, \xi_B, (\mathrm{g}_s)_B, (m_f)_B) = L_{eff}(\varphi, \xi, \mathrm{g}_s, m_f) + L_{count}(\varphi, \xi, \mathrm{g}_s, m_f, Z_i) \ , \tag{2.22}$$

where φ denotes the all fields. The effective L_{eff} is defined by Eq.(2.2, 2.3, 2.5, 2.6). At the same time Eq.(2.22) defines the L_{count} counter term.

The Z_i renormalization constants are defined unambiguously up to the poles. There are many renormalization schemes. The simplest renormalization scheme is the minimal subtraction scheme (MS). In this case we subtract only the poles. The renormalization constants of this scheme are the followings

$$\begin{aligned}
Z_A &= 1 + \frac{\alpha_s}{2\pi}\left(C_A\left(\frac{13}{6} - \frac{\xi}{2}\right) - \frac{4}{3}T_R n_f\right)\frac{1}{2\epsilon} && (2.23)\\
Z_\psi &= 1 - \frac{\alpha_s}{2\pi}\xi C_F \frac{1}{2\epsilon} && (2.24)\\
Z_m &= 1 - \frac{\alpha_s}{2\pi}(3+\xi) C_F \frac{1}{2\epsilon} && (2.25)\\
Z_\xi &= 1 && (2.26)\\
Z_g &= 1 - \frac{\alpha_s}{2\pi}\left(\frac{11}{3}C_A - \frac{4}{3}T_R n_f\right)\frac{1}{4\epsilon} && (2.27)\\
Z_\eta &= 1 - \frac{\alpha_s}{2\pi}(\xi - 3) C_A \frac{1}{8\epsilon} && (2.28)
\end{aligned}$$

where n_f is the number of the flavours. An other simple and popular renormalization scheme is the modified minimal subtraction scheme ($\overline{MS}$) is defined by the redefinition of the $1/\epsilon$ pole

$$\frac{1}{\epsilon} \ \longrightarrow \ \frac{1}{\epsilon} - \gamma_E + \ln(4\pi) \ , \tag{2.29}$$

where γ_E is the Euler number.

Renormalization group equation

The theoretical predictions for the physical quantities must be independent of the renormalization scheme. This equivalent with that the Green functions and the physical quantities are independent of the μ parameter. Otherwise a F physical or non-

physical (e.g. Green functions) quantity satisfies the renormalization group equation

$$\Big[\mu\frac{\partial}{\partial\mu}+\beta(\alpha_s,\xi,x_i)\frac{\partial}{\partial\alpha_s}+\delta(\alpha_s,\xi,x_i)\frac{\partial}{\partial\xi} -\gamma_m(\alpha_s,\xi,x_i)\sum_f x_f\frac{\partial}{\partial x_f}-\gamma(\alpha_s,\xi,x_i)\Big]F(\alpha_s,\xi,x_i;\mu,...)=0 \ , \quad (2.30)$$

where the introduced universal functions, which depend on the $\alpha_s, \xi, x_i = m_i/\mu$ parameters, are defined by

$$\mu\frac{d\alpha_s}{d\mu} = \beta(\alpha_s,\xi,x_A) \ , \quad (2.31)$$

$$\mu\frac{dm_f}{d\mu} = -m_f\gamma_m(\alpha_s,\xi,x_i) \ , \qquad f=1,...,n_f \ , \quad (2.32)$$

$$\mu\frac{d\xi}{d\mu} = \delta(\alpha_s,\xi,x_A) \ , \quad (2.33)$$

and the γ anomalous dimension

$$\gamma(\alpha_s,\xi,x_i) = n_A\gamma_A(\alpha_s,\xi,x_i)+n_\psi\gamma_\psi(\alpha_s,\xi,x_i)+n_\eta\gamma_\eta(\alpha_s,\xi,x_i) \ , \quad (2.34)$$

$$\mu\frac{dZ_A}{d\mu} = Z_A\gamma_A(\alpha_s,\xi,x_i) \ , \quad (2.35)$$

$$\mu\frac{dZ_\psi}{d\mu} = Z_\psi\gamma_\psi(\alpha_s,\xi,x_i) \ , \quad (2.36)$$

$$\mu\frac{dZ_\eta}{d\mu} = Z_\eta\gamma_\eta(\alpha_s,\xi,x_i) \ , \quad (2.37)$$

where n_A, n_ψ, n_η are the number of truncated gluon, quark, ghost external legs of the F. If F is a scattering amplitude (S-matrix) then $n_A = n_\psi = n_\eta = 0$ and F doesn't depend on the ξ gauge parameter because of a physical quantities are independent of the gauge choice ($\partial F/\partial\xi = 0$). We always calculate in a given order of the perturbative calculation, so the scale independence is also required in that same order ($dF/d\mu = \mathcal{O}(\alpha_s(\mu)^n)$ and n is positive). Because of this cut in the series of α_s, the results will depend on the renormalization scale parameter.

Running parameters

The solution of Eq.(2.31) gives the scale dependences of the coupling and masses. Functions β and γ_m are determined by the renormalization constants. At two-loop level the renormalization equations for the coupling and for the masses are the followings

$$\mu\frac{d\overline{\alpha}_s}{d\mu} = -\overline{\alpha}_s^2\beta_0-\overline{\alpha}_s^3\beta_1+... \quad (2.38)$$

$$\mu\frac{dm_f}{d\mu} = -m_f(\overline{\alpha}_s\gamma_0+\overline{\alpha}_s^2\gamma_1+...) \ , \qquad f=1,...,n_f \ , \quad (2.39)$$

where $\overline{\alpha}_s = \alpha_s/(2\pi)$ and the β_i, γ_i coefficients are

$$\beta_0 = \frac{11}{3}C_A - \frac{4}{3}T_R n_f \ , \qquad \beta_1 = \frac{17}{3}C_A^2 - 2C_F T_R n_f - \frac{10}{3}C_A T_R n_f \ , \tag{2.40}$$

$$\gamma_0 = 3C_F \ , \qquad \gamma_1 = \frac{3}{4}C_F^2 + \frac{97}{12}C_A C_F - \frac{5}{3}C_F T_R n_f \ . \tag{2.41}$$

The solution of equation of coupling constant is given by

$$\overline{\alpha}_s(\mu) = \frac{\overline{\alpha}_s(\nu)}{w(\mu)}\left(1 - \frac{\beta_1}{\beta_0}\overline{\alpha}_s(\nu)\frac{\ln(w(\mu))}{w(\mu)}\right) \ , \tag{2.42}$$

$$w(\mu) = 1 - \beta_0 \overline{\alpha}_s(\nu)\ln\left(\frac{\nu}{\mu}\right) \ , \tag{2.43}$$

where ν is an arbitrary reference scale. By the experiments, the strong coupling at the Z^0 peak is $\alpha_s(\nu = 91.187\ \mathrm{GeV}) = 0.118 \pm 0.006$. From Eq.(2.42) we can obtain the asymptotic behavior of the coupling. In the limit $\mu \longrightarrow \infty$, $\overline{\alpha}_s \longrightarrow 0$. So, asymptotically the effective coupling vanishes (the theory presents asymptotic freedom). And the solution for the masses is given by

$$\begin{aligned} m_f(\mu) &= m_f(\nu)\exp\left(-\int_\nu^\mu \frac{d\lambda}{\lambda}\gamma_m(\overline{\alpha}_s(\lambda))\right) \\ &= m_f(\nu)\exp\left(\int_{\overline{\alpha}_s(\nu)}^{\overline{\alpha}_s(\mu)} \frac{du}{u}\frac{\gamma_0 + u\gamma_1 + ...}{\beta_0 + u\beta_1 + ...}\right) \ , \end{aligned} \tag{2.44}$$

where the dots denotes the higher order contributions. Performed the integral in Eq.(2.44) we can obtain the asymptotically behavior of the masses

$$m_f(\mu) \longrightarrow m_f(\nu)\left(\frac{\overline{\alpha}_s(\mu)}{\overline{\alpha}_s(\nu)}\right)^{\frac{\gamma_0}{\beta_0}} \ , \qquad \mu \longrightarrow \infty \ , \qquad f = 1, ..., n_f \ . \tag{2.45}$$

At high scale the masses vanish. In Table (2.3) the mass of the various quark flavours has been listed at $\mu = 1$ GeV scale. With the exception of the *top*-quark, the quark

Table 2.3: Quark masses at $\mu = 1$ GeV scale.

$m_d = 2, ..., 8$ MeV ,	$m_u = 5, ..., 15$ MeV ,
$m_s = 100, ..., 300$ MeV ,	$m_c = 1, ..., 1.6$ GeV ,
$m_b = 4.1, ..., 4.5$ GeV ,	$m_t = 179 \pm 8$ GeV .

masses are very small. At high scale the masses vanish and the effect of the quark masses means negligible contributions. During the calculations we work with five quark flavours ($n_f = 5$) and them masses are neglected.

Asymptotic freedom is useful for quantities that are dominated by the short distance behavior of the theory. Such quantities, which are termed infrared safe, can

not depend sensitively on the masses of quarks, nor can they suffer from infrared divergences (particle emission with small energy, collinear emission, ...). Infrared safety is one of the fundamental concepts of perturbative QCD and it makes essential use of the renormalization group. We consider an infrared safe physical quantity $F(Q^2/\mu^2, \alpha_s(\mu), m^2(\mu)/\mu^2)$, where Q is an large invariant, much greater than Λ_{QCD}. We assume that F has been scaled by an overall factor of Q to make it dimensionless. Because F is physical, it cannot depend on μ,

$$F\left(\frac{Q^2}{\mu^2}, \alpha_s(\mu), \frac{m^2(\mu)}{\mu^2}\right) = F\left(1, \alpha_s(Q), \frac{m^2(Q)}{Q^2}\right) \quad . \tag{2.46}$$

Now we can expand in the coupling at the scale of large momenta of the problem and use asymptotic freedom. This procedure can be used if F happens to be infrared safe when it is behavior in the large μ limit is the following

$$F\left(\frac{Q^2}{\mu^2}, \alpha_s(\mu), \frac{m^2(\mu)}{\mu^2}\right) \xrightarrow{\mu \to 0} F\left(\frac{Q^2}{\mu^2}, \alpha_s(\mu), 1\right) + \mathcal{O}\left((\frac{m^2(\mu)}{\mu^2})^a\right) \quad , \tag{2.47}$$

where $a > 0$. The effect of the quark masses vanishes as a power of $m_f(\mu)/\mu$. So, the quantity F can be written as a power series of α_s as

$$F(Q) = C_0 + \frac{\alpha_s(Q)}{2\pi} C_1 + \left(\frac{\alpha_s(Q)}{2\pi}\right)^2 C_2 + \cdots \quad , \tag{2.48}$$

where the C_i kinematical coefficients don't depend on Q and masses.

Chapter 3

Hadron production in e^+e^- annihilation

In high energy particle collisions the most important processes are the clearly hadronic processes. For example at the LEP1 collider the number of the hadronic event are about the 70% of the total number of events. Because of the largeness of the α_s QCD coupling constant, the relevant interaction is the strong interaction (QCD) in these processes. The QCD particles (quarks and gluons) only appear as confined state (hadrons) and don't occur a free particles. Otherwise the large number of the hadronic event makes the test of QCD possible. We must describe the physics of the hadrons using the physics of the partons (quarks and gluons). We will see in high energy processes the prediction of QCD well describes the hadronic events.

In this chapter we discuss the cross section of hadronic events and theoretical description of the jet production.

3.1 Total hadronic cross section

Because of the final state is total we can apply the principle of parton-hadron duality which declares the equivalence of the partonic and hadronic Hilbert-space. This identity can be proofed in those cases when we aren't interesting in the structure of the final state namely, we want to calculate the total hadronic cross section.

$$\sum_{\text{hadrons}} |h\rangle\langle h| = \sum_{q,g} |\text{gluons, quarks}\rangle\langle\text{gluons, quarks}| \tag{3.1}$$

This identity allows us to calculate the total hadronic cross section at parton level. Defining the ratio of the hadronic and leptonic cross sections

$$R(Q) = \frac{\sigma(e^+e^- \to \text{hadrons})}{\sigma(e^+e^- \to \mu^+\mu^-)} \ , \tag{3.2}$$

the result can be expanded in the power of α_s [14]

$$\begin{aligned} R(Q) &= \sum_{i=1}^{n_f} q_i^2 \big(1 + \overline{\alpha}_s(\mu) r_1 + \overline{\alpha}_s^2(\mu)[r_2 + r_1 \beta_0 \ln x_\mu] \\ &+ \overline{\alpha}_s^3(\mu)[r_3 + (2 r_2 \beta_0 + r_1 \beta_1) \ln x_\mu + r_1 \beta_0^2 \ln^2 x_\mu]\big) \ , \end{aligned} \tag{3.3}$$

where $\overline{\alpha}_s = \alpha_s/(2\pi)$ is the coupling constant, $x_\mu = \mu/Q$ is the renormalization scale, Q is the total center-of-mass energy and q_i is the electric charge of the quark flavour i in units of electromagnetic coupling constant. If the number of the active fermion flavours is $n_f = 5$ then r_1, r_2, r_3 scale independent coefficients are the followings

$$r_1 = 2 \ , \qquad r_2 = 5.636 \ , \qquad r_3 = -102.44 \ , \tag{3.4}$$

where the underlying gauge group is fixed to $SU(3)$. Fig. (3.1) shows the renormalization scale dependence of the result in the various order of the perturbative calculation. The label LO denotes the leading order contribution, NLO is the next-to-leading order result and NNLO is the next-to-next-to-leading order result.

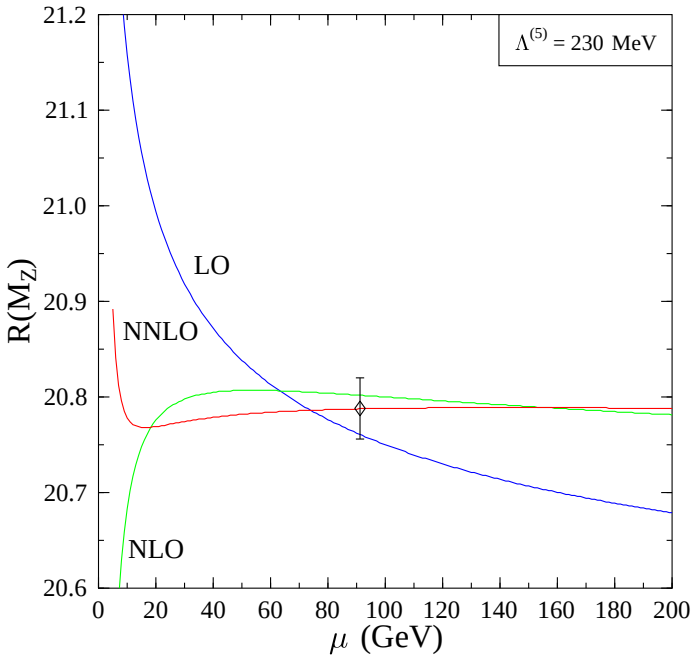

Figure 3.1: Scale dependence of $R(M_{Z^0})$ at LO, NLO and NNLO level. The experimental result at the Z^0 peak is $R(M_{Z^0}) = 20.788 \pm 0.032$.

3.2 Structure of the hadronic events

In the high energy collision there are many events which involves two or more hadronic jets. The **hadronic jet** can be defined as *shower* of collinear hadrons. Such jet events are shown in Fig. (3.2). In other word, the hadronic events have structure and the theory has to be able to describe this structure. In high energy processes

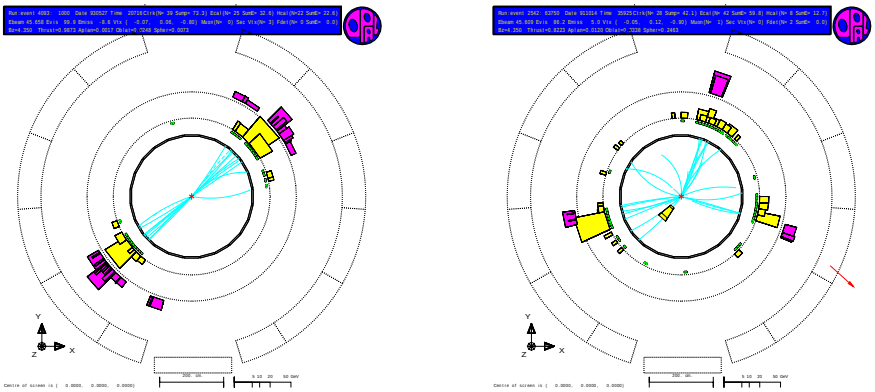

Figure 3.2: Two and three jets events in e^+e^- annihilation.

the hadronic events and jets can be described various way. We can measure the geometric properties of the events (collinearity, coplanarity). Generally we can ask the weight of those events which geometric properties are characterized by $O_1, O_2, ...$ are $C_1, C_2, ...$, where $C_1, C_2, ...$ are fixed. The $O_1, O_2, ...$ parameter are called *event shapes*. The event shape variables don't arrange the hadrons into jets but sometimes these are defined to enhance jet like configurations. We can define such algorithms which arrange the hadrons into jets. In this case we can measure the weight of the n-jet events. These algorithms are called *jet finding algorithms*. In the following, let see some example for the event shapes and for the jet finding algorithms.

Let us consider an m-hadron final state produced by electron-positron annihilation

$$e^+(p_+) + e^-(p_-) \longrightarrow h_1(p_1) + \cdots + h_m(p_m) \ , \qquad p_+ + p_- = Q \ , \tag{3.5}$$

where p_+, p_- are the momenta of the incoming leptons and $p_1, ..., p_m$ are the momenta of the outgoing hadrons. This momenta are represented in the center-of-mass frame of the incoming leptons.

Event shapes

We define here some well known event shapes variable which characterize the geometric properties of the events.

i) **Thrust** [16] This variable characterizes the collinearity of the events.

$$T(p_1,...,p_m) = \max_{\vec{n}_T} \frac{\sum_{i=1}^{m} |\vec{p}_i \cdot \vec{n}_T|}{\sum_{i=1}^{m} |\vec{p}_i|} \quad , \tag{3.6}$$

where the vector $\vec{n}_T$ (thrust axis) is chosen to maximize this sum. If there are only two hadrons in the final state then $T = 1$. For arbitrary number of particles

$$\frac{1}{2} \leq T \leq 1 \quad . \tag{3.7}$$

Other two thrust like variable can be defined. The **thrust major** is defined by the $\vec{n}_{T_{\rm maj}}$ thrust major axis which is perpendicular to $\vec{n}_T$ and maximizes the (3.6) expression. The **thrust minor** is defined similarly by the thrust minor axis. The $\vec{n}_{T_{\rm min}}$ thrust minor axis is perpendicular to both $\vec{n}_{T_{\rm maj}}$ and $\vec{n}_T$ and this also maximizes the (3.6) expression. If we have only three hadrons in the final state then $T_{\rm min} = 0$. So the thrust minor characterizes the coplanarity of the event.

ii) **C and D parameter** [17] These parameters are defined by the eigenvalues of the momentum tensor

$$\theta^{\alpha\beta} = \sum_{i=1}^{m} \frac{\vec{p}_i^{\,\alpha} \vec{p}_i^{\,\beta}}{|\vec{p}_i|^2} \Big/ \sum_{i=1}^{m} |\vec{p}_i|^2 \quad . \tag{3.8}$$

Let denote λ_1, λ_2, λ_3 the three eigenvalues of the $\theta^{\alpha\beta}$ momentum tensor and the definition of the C and D parameters are the followings

$$C(p_1,...,p_m) = 3(\lambda_1\lambda_2 + \lambda_1\lambda_3 + \lambda_2\lambda_3) \quad , \tag{3.9}$$

$$D(p_1,...,p_m) = 27\lambda_1\lambda_2\lambda_3 \quad . \tag{3.10}$$

For two-hadron final states both C and D vanish, while for three-hadron final states only C is non vanishing and its allowed range is between zero and $3/4$ ($0 \leq C \leq 0.75$). For larger number of particles

$$0 \leq C, D \leq 1 \quad . \tag{3.11}$$

The C-parameter enhances the 3-jet like events on the range $0 \leq C \leq 0.75$ and enhances the 4-jet events on the range $0.75 \leq C \leq 1$. The D-parameter characterizes the coplanarity of the events.

Finally, we define the distribution of event shape variables and the average value of shape variables

$$\Sigma(O) = \frac{1}{N} \sum_{\substack{i=1 \\ \text{events}}}^{N} \int_{O}^{O+\Delta O} dO\, O\, \delta\left(O - O(p_1,...,p_{m_i})\right) \quad , \tag{3.12}$$

$$\langle O \rangle_\delta = \frac{1}{N} \sum_{\substack{i=1 \\ \text{events}}}^{N} O(p_1,...,p_{m_i}) \Theta\left(O(p_1,...,p_{m_i}) > \delta\right) \quad , \tag{3.13}$$

where $p_1, ..., p_{m_i}$ are the momenta of the hadrons of the i-th event, and N is the number of events.

Jet finding algorithms

There are several jet clustering algorithms defined. We discuss here **E, E0, P**, **JADE** [22], **Durham** [25], **Geneva** [26] and **Cambridge** [27] jet clustering algorithms. The most general definition of the clustering algorithm involves three components: an ordering variable v_{ij}, test variable y_{ij}, and a combination procedure. In the cases of E, E0, JADE and Durham algorithms the ordering and the test variable are same ($v_{ij} \equiv y_{ij}$). In these cases no ordering procedure. These algorithms are called *JADE-type* algorithms which are defined according to the following iterative procedure.

1. Define the resolution parameter y_{cut}.
2. For every pair of hadrons h_k, h_l compute the resolution variable y_{kl}. In the table (3.1) are defined the various definition of the resolution variables.
3. If y_{ij} is the smallest value of y_{kl} computed in 2. and $y_{ij} < y_{cut}$, combine (p_i, p_j) into a single jet (pseudoparticle) $p_{(ij)}$ according to a recombination prescription.
4. Repeat this procedure from step 2. until all pairs of objects (particles and/or pseudoparticles) have $y_{ij} > y_{cut}$. Whatever objects remain at this stage are called jets.

The Cambridge algorithm is defined as follows. As before, one starts with a table of the energies E_i of primary objects and their relative angles as given by the ordering variable $v_{ij} = 2(1 - \cos\theta_{ij})$.

1. Define the resolution parameter y_{cut}.
2. If only one object remains in the table, then store this as a jet and stop.
3. Otherwise, select the pair of objects (ij) having the minimal value of the ordering variable v_{ij}. Order the pair such that $E_i \leq E_j$.
4. Inspect the value of the test variable,

$$y_{ij} = \frac{E_i^2}{Q^2} v_{ij} \quad . \tag{3.14}$$

   If $y_{ij} < y_{cut}$, then update the table by deleting i and j, introducing a new particle (ij) with 4-momentum $p_{ij} = p_i + p_j$, and recompute the relevant values of the ordering variable. If $y_{ij} > y_{cut}$, then store i as a jet and delete it form the table.
5. Go to step 2.

Table 3.1: The definition of the resolution variables and the recombination schemes of various jet clustering algorithms; $\vec{p}_i$ denotes a three-vector and the Lorentz-vector can be written as $p_i \equiv (E_i, \vec{p}_i)$. The $v_{ij} = 2(1 - \cos\theta_{ij})$ is the relative angle of vectors (i, j).

Algorithm	Resolution	Combination
E	$y_{ij} = \frac{(p_i + p_j)^2}{Q^2}$	$p^\mu_{(ij)} = p^\mu_i + p^\mu_j$
E0	$y_{ij} = \frac{(p_i + p_j)^2}{Q^2}$	$E_{(ij)} = E_i + E_j$ $\vec{p}_{(ij)} = E_{(ij)} \frac{\vec{p}_i + \vec{p}_i}{\lvert\vec{p}_i + \vec{p}_j\rvert}$
P	$y_{ij} = \frac{(p_i + p_j)^2}{Q^2}$	$\vec{p}_{(ij)} = \vec{p}_i + \vec{p}_j$ $E_{(ij)} = \lvert\vec{p}_i + \vec{p}_j\rvert$
JADE	$y_{ij} = \frac{E_i E_j}{Q^2} v_{ij}$	$p^\mu_{(ij)} = p^\mu_i + p^\mu_j$
Durham	$y_{ij} = \frac{\min\{E_i^2, E_j^2\}}{Q^2} v_{ij}$	$p^\mu_{(ij)} = p^\mu_i + p^\mu_j$
Geneva	$y_{ij} = \frac{4}{9} \frac{E_i E_j}{(E_i + Ej)^2} v_{ij}$	$p^\mu_{(ij)} = p^\mu_i + p^\mu_j$

The jet clustering algorithms arrange the hadrons into jets. This arrangement is depend on the resolution parameter y_{cut}. In the other words, we can define the n-jet function by

$$r^{(n)}(p_1, ..., p_m; y_{cut}) = \begin{cases} 1 & \text{if the algorithm found } n\text{-jets} \\ 0 & \text{if the algorithm didn't find } n\text{-jets} \end{cases} \tag{3.15}$$

where $p_1, ..., p_m$ are the momenta of the hadrons and y_{cut} is the resolution parameter.The weight of the n-jet (jet-rates) events is defined by

$$R_n(y_{cut}) = \frac{1}{N} \sum_{\substack{i=1 \\ \text{events}}}^{N} r^{(n)}(p_1, ..., p_{m_i}; y_{cut}) \ , \tag{3.16}$$

where $p_1, ..., p_{m_i}$ are the momenta of the hadrons of the ith event. From the definition of the jet rates we found the following identity

$$\sum_{n=2}^{\infty} R_n(y_{cut}) \ = \ 1 \ . \tag{3.17}$$

Notice that, we can always write any physical quantities (the distributions, jet rates and the average value of the event shapes,...) in the following general form

$$P(O_1, O_2, ...) = \frac{1}{N} \sum_{\substack{i=1 \\ \text{events}}}^{N} F_J^{(m_i)}(p_1, ..., p_{m_i}; O_1, O_2, ...) \ , \tag{3.18}$$

where the function $F_J^{(m_i)}$ is called *jet measure function*. In the point of the theoretical calculation this function has to fulfill some important requirements. These requirements will be discussed explicitly in Chapter 4. On the other hand we can generalize the jet measure function. Introduced the jet function which is function of the events and the $O_1, O_2, ..$ parameters. With this notation the Eq. (3.18) can be written as

$$P(O_1, O_2, ...) = \frac{1}{N} \sum_{\substack{i=1 \\ \text{events}}}^{N} F_J(\Gamma_i; O_1, O_2, ...) \ , \tag{3.19}$$

where Γ_i denotes the ith hadronic events. In the simplest case an event is fully characterized by the number of hadrons and their momenta. Thus the action of the function $F_J(...)$ on an event Γ

$$F_J(\Gamma; O_1, O_2, ...) = F_J^{(m_\Gamma)}(p_1, ..., p_{m_\Gamma}; O_1, O_2, ...) \ , \tag{3.20}$$

where $p_1, ..., p_{m_\Gamma}$ are the momenta of the hadrons in event Γ.

3.3 Jet and weighted cross sections

By the experimental tests, the weight of the $2, 3, 4$-jet events are approximately proportional to the power of α_s strong coupling by the follows

$$2\text{jets} : 3\text{jets} : 4\text{jets} : ... = \mathcal{O}(\alpha_s^0) : \mathcal{O}(\alpha_s^1) : \mathcal{O}(\alpha_s^2) : ... \ . \tag{3.21}$$

This indicates that the perturbative QCD may be applied to discussion of hadronic jet process. We can try a similar description which was used in the total hadronic cross section case where the hadronic states was replaced with partonic states in the final state. In that case it was allowed by the parton-hadron duality. In the jet cross section case this is not or only approximately true. The jet function are defined in Eq. (3.18) means a cut in the space of the hadronic states. There is no guarantee as regards we can find the equivalent of this cut in the partonic Hilbert-space. But this fact is not hopeless. The difference between hadron and parton level jet functions vanishes as an inverse power of total center of mass energy ($\mathcal{O}(1/Q)$). So, for the partonic jet function has been found

$$\bar{F}_J^{(n)}(p_1, ..., p_n; O_1, O_2, ...) = F_J^{(n)}(p_1, ..., p_n; O_1, O_2, ...) + \mathcal{O}\left(\frac{1}{Q}\right) \ , \tag{3.22}$$

where $\bar{F}_J^{(n)}$ and $F_J^{(n)}$ denotes the parton and hadron level jet functions and $p_1, ..., p_n$ are the momenta of the partons. Eq. (3.22) is true only in those cases when the jet quantities, which are characterized by the jet functions are independent of the long distance physics. The perturbative QCD can describe only the short distance physics because the long distance physics is represented by infrared and collinear divergences. These divergences arise when some gluons become soft or at least two partons become collinear. So, we can use the approximation of the partonic jet function in Eq. (3.22) in those cases when the hadronic jet function is defined in such a way that their value is independent of the number of soft and collinear hadrons. In this case the theoretical prediction is free from the infrared and collinear divergences. This is formulated in the Kinoshita-Lee-Nauenberg theorem [11].

In the lowest order of perturbative calculation every partons correspond to a jet. This follows the rule in Eq. (3.21). Otherwise we have to take the hadronization correction into consideration. This corrections are calculated by hadronization models. There are many possible models to parameterize the non-perturbative hadronization process of the quarks and gluons. Hence description of hadronic jets following from the original quarks and gluons is model dependent. Typical examples of the hadronization models are the *string model* [29] and the *cluster model* [30]. Fig. (3.3) shows the parton and hadron level 2,3,4 jets rates has been calculated by string hadronization model.

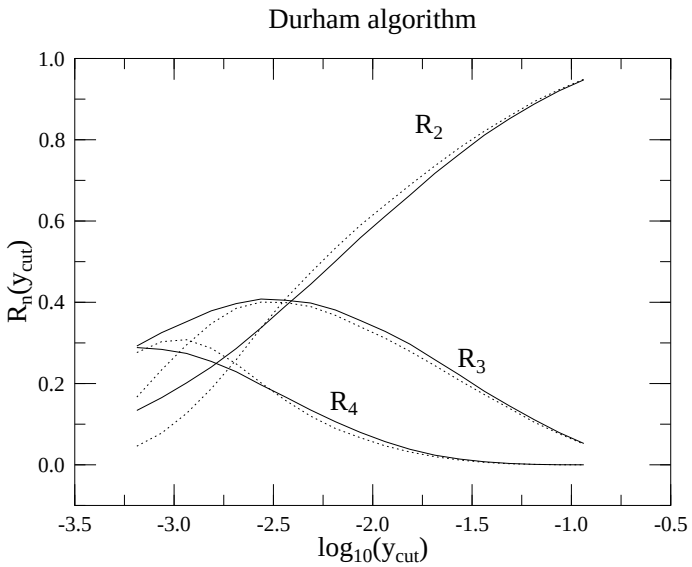

Figure 3.3: The Durham 2,3,4 jet rates.The solid line is the parton level result and the dotted line is the hadron level. This results has been calculated by event generator PYTHIA [32].

Jet cross section

Let define the parton level jet cross section in the regularized theory discussed in Sec. (2.3), where the dimension of the spacetime is $d = 4 - 2\epsilon$. This cross section can be define as a sum of the m-parton contributions. Because of the infrared singularities (previously mentioned soft and collinear divergences) this definition can be only formal. Before any calculation we have to manage the cancellation of the divergences. Thus we have

$$\sigma(O_1, O_2, ...) = \sum_{m=2}^{\infty} \int_m d\sigma_m(O_1, O_2, ...) \ , \tag{3.23}$$

where $\int_m$ denotes the integration over the m-partons phase space and the differential cross sections are defined by

$$\begin{aligned} d\sigma_m(O_1, O_2, ...) \ &= \ \mathcal{N}_{in} \sum_{\{m\}} d\Gamma^{(m)}(p_1, ..., p_m; Q) \, \frac{1}{S_{\{m\}}} \, |M_m(p_1, ..., p_m)|^2 \\ &\quad \cdot \ F_J^{(m)}(p_1, ..., p_m, O_1, O_2, ...) \ , \end{aligned} \tag{3.24}$$

where $\mathcal{N}_{in}$ includes all the factors that are QCD independent. $\sum_{\{m\}}$ denotes the sum over all the configurations with m partons and $S_{\{m\}}$ is the Bose symmetry factor for identical partons in the final state. M_m is the renormalized matrix element are expanded in the number of loop

$$M_m(p_1, ..., p_m) = \sum_{l=0}^{\infty} M_m^{(l)}(p_1, ..., p_m) \ , \tag{3.25}$$

where $l = 0, 1$ gives the tree and one-loop level contributions. The $d = 4 - 2\epsilon$ dimensional phase space which involves the integration over the $p_1, ..., p_m$ of m final state partons will be denoted as follows

$$d\Gamma^{(m)}(p_1, ..., p_m; Q) = \left[\prod_{l=1}^{m} \frac{d^d p_l}{(2\pi)^{d-1}} \, \delta_+(p_l^2) \right] \ (2\pi)^d \delta^{(d)}(p_1 + ... + p_m - Q) \ , \tag{3.26}$$

where Q is the sum of the incoming momenta.

If the jet function is identically one ($F_J^{(m)}(p_1, ..., p_m, O_1, O_2, ..) \equiv 1$) then we get the total cross section from Eq. (3.23). In a general case the cross section can be written as a power series of α_s

$$\sigma(O_1, O_2, ...) = \sigma^{LO}(O_1, O_2, ...) + \sigma^{NLO}(O_1, O_2, ...) + \dots \ , \tag{3.27}$$

where σ^{LO} is Born approximation (*leading order* contribution, LO) of the cross section and σ^{NLO} is the first correction (*next-to-leading order* contribution, NLO) to the Born term.

Let see the explicit expressions of the two contribution in Eq. (3.27) when the jet function is the n-jet rate function. The first non-vanishing term in Eq. (3.23) is

$$\begin{aligned}\sigma^{LO}_{n-jet}(y_{cut}) &= \mathcal{N}_{in}\sum_{\{n\}}\int_n d\Gamma^{(n)}(p_1,...,p_n;Q)\,\frac{1}{S_{\{n\}}}\,|M^{(0)}_n(p_1,...,p_n)|^2 \\ &\cdot\ r^{(n)}(p_1,...,p_n,y_{cut})\ ,\end{aligned} \tag{3.28}$$

where $r^{(n)}$ is the jet function defined in (3.15). The NLO correction term is the sum of two term

$$\sigma^{NLO}_{n-jet}(y_{cut}) = \sigma^{R}_{n-jet}(y_{cut}) + \sigma^{V}_{n-jet}(y_{cut})\ , \tag{3.29}$$

where $\sigma^{R}_{n-jet}(y_{cut})$ $n+1$-parton contribution is given by

$$\begin{aligned}\sigma^{R}_{n-jet}(y_{cut}) &= \mathcal{N}_{in}\sum_{\{n+1\}}\int_{n+1} d\Gamma^{(n+1)}(p_1,...,p_{n+1};Q)\,\frac{1}{S_{\{n+1\}}} \\ &\cdot\quad |M^{(0)}_{n+1}(p_1,...,p_{n+1})|^2\ r^{(n)}(p_1,...,p_{n+1},y_{cut})\ ,\end{aligned} \tag{3.30}$$

and the n-parton contribution

$$\begin{aligned}\sigma^{V}_{n-jet}(y_{cut}) &= \mathcal{N}_{in}\sum_{\{n\}}\int_n d\Gamma^{(n)}(p_1,...,p_n;Q)\,\frac{1}{S_{\{n\}}} \\ &\cdot\quad 2Re\left(M^{(0)}_n(p_1,...,p_n)M^{(1)}_n(p_1,...,p_n)^\dagger\right) \\ &\cdot\quad r^{(n)}(p_1,...,p_n,y_{cut})\ .\end{aligned} \tag{3.31}$$

Both the σ^R and the σ^V are divergent if $d=4$, although their sum is finite. The divergences come from soft (when a gluon energy becomes zero) and collinear (two momenta become collinear) regions. In the next chapter we will present a method which helps us to regularize the two pieces of the NLO correction. This method is called *dipole subtraction method* developed by Catani-Seymour [53].

Chapter 4

Calculation of NLO jet cross sections

There are two type of algorithm used for NLO calculation: one based on the phase space slicing method and the other based on the subtraction method. The main difference between these algorithms is that only a minimal part of the full calculation is treated analytically, namely only those contributions giving rise to the singularities. In a simple example we can demonstrate the differences between these two algorithms.

Let $f(x)$ a complicated function which is finite in $x = 0$. We would like to calculate the following integral

$$I = \lim_{\epsilon \to 0} \left(\int_0^1 \frac{dx}{x} x^\epsilon f(x) - \frac{1}{\epsilon} f(0) \right) \quad , \tag{4.1}$$

where the function $f(x)$ is too complicated to perform the integral analytically. The I integral is finite in the limit $\epsilon \to 0$ but the two pieces of the right-hand side of Eq. (4.1) are separately divergent.

One of the usual method is the slicing method when the phase space is divided into two part $0 < x < \delta$ and $\delta < x < 1$, where the parameter δ is chosen in such a way that allowing us to use the simple approximation $f(x) \simeq f(0)$ on the $[0, \delta]$ range. This gives

$$\begin{aligned} I &\simeq \lim_{\epsilon \to 0} \left(f(0) \int_0^\delta \frac{dx}{x} x^\epsilon + \int_\delta^1 \frac{dx}{x} x^\epsilon f(x) - \frac{1}{\epsilon} f(0) \right) \\ &= f(0) \ln \delta + \int_\delta^1 \frac{dx}{x} f(x) \quad . \end{aligned} \tag{4.2}$$

Now the integral in the second term can be performed by Monte Carlo integration. As long as δ is small, the result will be independent of δ. This method was applied for e^+e^-annihilation [50] by Giele and Glover and for hadron-hadron collision by Giele, Glover and Kosower. [51].

The other method is the subtraction method which use the following identity

$$I = \lim_{\epsilon \to 0} \int_0^1 \frac{dx}{x} x^\epsilon [f(x) - g(x)] + \lim_{\epsilon \to 0} \left(\int_0^1 \frac{dx}{x} x^\epsilon g(x) - \frac{1}{\epsilon} f(0) \right) \ , \tag{4.3}$$

where the function g(x) is a proper approximation of $f(x)$ and have same behaviour in the limit $x \to 0$ as $f(x)$. Furthermore, the function $g(x)x^{\epsilon-1}$ has to be analytically integrable. Thus, we have

$$I = \int_0^1 \frac{dx}{x} [f(x) - g(x)] + C \ , \tag{4.4}$$

where C is the results of the second term on the right-hand side of Eq. (4.3). The first term can be performed by Monte Carlo integration. In the case when $g(x) = f(0)$ the constant C is zero. This method was applied first for $e^+e^-$by Ellis, Ross and Terrano [48] and in some other general NLO cross section calculation method [8, 52, 53].

In this chapter we discuss the general idea of the subtraction method of NLO jet cross section calculations and we give the description of the dipole subtraction method that was developed by Catani and Seymour [53]. In Sec. (4.5) we discuss the relevant details of numerical implementation of phase space integrals.

4.1 The subtraction procedure

At the end of previous chapter we have seen that a NLO jet cross section is sum of two terms as follows

$$\sigma = \sigma^{LO} + \sigma^{NLO} \ . \tag{4.5}$$

Here the LO cross section σ^{LO} is obtained by integrating the fully exclusive cross section $d\sigma^B$ over the phase space for the corresponding jet quantity. Suppose also that this LO calculation involves m partons in the final state. Thus, we can write

$$\sigma^{LO} = \int_m d\sigma^B \ , \tag{4.6}$$

where all quantities are evaluated in the regularized theory (in $d = 4 - 2\epsilon$ space-time dimensions).

Let see now the NLO correction term. We have to consider the exclusive cross section $d\sigma^R$ with $m+1$ partons in the final state and the one-loop correction $d\sigma^V$ with m partons in the final state

$$\sigma^{NLO} \equiv \int d\sigma^{NLO} = \int_{m+1} d\sigma^R + \int_m d\sigma^V \ . \tag{4.7}$$

The two integrals in Eq. (4.7) are separately divergent in the $d = 4$ dimensional space-time although their sum is finite. Therefore, before any numerical calculation

can be attempted, the separate pieces have to be regularized. In the regularized theory the divergences are replaced by double poles $1/\epsilon^2$ and single poles $1/\epsilon$.

The general idea of the subtraction method for writing a general-purpose Monte Carlo program is to use the following identity

$$d\sigma^{NLO} = \left[d\sigma^R - d\sigma^A\right] + d\sigma^A + d\sigma^V \quad , \tag{4.8}$$

where $d\sigma^A$ is a proper approximation of $d\sigma^R$ such as to have same pointwise singular behaviour as $d\sigma^R$. Thus, $d\sigma^A$ acts as a local counterterm for $d\sigma^R$ and, introducing the phase space integration,

$$\sigma^{NLO} = \int_{m+1} \left[d\sigma^R - d\sigma^A\right] + \int_{m+1} d\sigma^A + \int_m d\sigma^V \quad . \tag{4.9}$$

In Eq. (4.9) we can safely perform the limit $\epsilon \to 0$ under the integral sign in the first term on the right-hand side of this equation. So, this first term can be integrated numerically in $d = 4$ dimension.

All the singularities are associated to the last two terms on the right-hand side of Eq. (4.9). If one is able to perform analytically the integration of $d\sigma^A$ over the one-parton subspace leading to the ϵ poles, one can combine these poles with those in $d\sigma^V$, thus cancelling all the divergences[1], performing the limit $\epsilon \to 0$ and carrying out numerically the remaining integration over the m-parton phase space. The final structure of the calculation is written as follows

$$\sigma^{NLO} = \int_{m+1} \left[d\sigma^R_{\epsilon=0} - d\sigma^A_{\epsilon=0}\right] + \int_m \left[d\sigma^V + \int_1 d\sigma^A\right]_{\epsilon=0} \quad . \tag{4.10}$$

This identity can be implemented in a partonic Monte Carlo program, which generates weighted partonic events with $m+1$ and m final state partons.

Note that the subtracted term $d\sigma^R - d\sigma^A$ in Eq. (4.10) is integrable in four dimension by definition. The cancellation of the divergences is guaranteed by the jet function defined in Eq. (3.18). This functions have to be defined in such a way that their actual value is independent of the number of soft an collinear hadrons (partons) produced in the final state. In particular, this value has to be same in a given m parton configuration and all $m+1$-parton configuration that are kinematically degenerate with it (one of a parton become soft or two partons become collinear). We have

$$F_J^{(m+1)} \longrightarrow F_J^{(m)} \quad , \tag{4.11}$$

in that cases where $m+1$-parton and m-parton configurations are kinematically degenerate. The jet function with this property are called *infrared safe* jet functions. In Sec. (3.2) we have defined some infrared safe jet functions (e.g thrust, jet clusters,...).

The key of the subtraction procedure is the actual form of the counter term $d\sigma^A$. We have to find an expression for $d\sigma^A$ which fulfils the following properties:

[1] The cancellation of the infrared divergences is generally proofed by the Kinoshita-Lee-Nauenberg theorem [11].

1. for any given process has to be obtained in that way which is independent of the particular jet function
2. it has to exactly match the singular behaviour of $d\sigma^R$
3. its form has to be particularly convenient for Monte Carlo integration techniques
4. it has to be exactly integrable analytically in $d = 4 - 2\epsilon$ dimension over a single-parton subspaces leading to soft and collinear divergences.

In the next sections we will give a possible definition of the counterterm $d\sigma^A$.

4.2 Dipole factorization formulae

Notation

The matrix element which involves m QCD partons in the final state has the following structure

$$M_m^{c_1,...,c_m;s_1,...,s_m}(p_1,...,p_m) \ , \tag{4.12}$$

where $\{c_1,...,c_m\}$, $\{s_1,...,s_m\}$ and $\{p_1,..,p_m\}$ denotes respectively the color indices ($a = 1,...,\ N_c^2 - 1$ for gluon leg , $\alpha = 1,..,N_c$ for quark or antiquark), spin indices ($\mu = 1,...,d$ for gluons, $s = 1,2$ for massless fermions) and the momenta. In the $d = 4 - 2\epsilon$ space number of the helicity states are d for gluons and 2 for massless fermions.

It's useful to introduce a basis $\{|c_1,...,c_m > \otimes |s_1,...,s_m >\}$ in the color+helicity space in such a way that

$$M_m^{c_1,..,c_m;s_1,..,s_m}(p_1,..,p_m) \equiv \Big(< c_1,..,c_m| \otimes < s_1,..,s_m| \Big) |1,..,m >_m \ . \tag{4.13}$$

Thus $|1,...,m >_m^{(0)}$ is an vector in the color + helicity space. According to this notation the matrix element squared M_m (sum over helicities and colors in the final state) can be written as

$$|M_m|^2 = {}_m\!< 1,...,m|1,...,m >_m \ . \tag{4.14}$$

The loop expansion of the matrix element is given by

$$|1,...,m >_m = \sum_{l=0}^{\infty} \left(\frac{\alpha_s}{2\pi}\right)^l |1,...,m >_m^{(l)} \ , \tag{4.15}$$

where α_s is the strong coupling. The $l = 0$ case correspond to the tree level and the case $l = 1$ to the 1-loop level. The loop expansion of the matrix element squared is

the following

$$|M_m|^2 = \sum_{p=0}^{\infty} \left(\frac{\alpha_s}{2\pi}\right)^p |M_m^{(p)}|^2 \equiv {}^{(0)}_{m}\!<1,...,m|1,...,m>^{(0)}_{m} + \frac{\alpha_s}{2\pi}\, 2\,\mathrm{Re}\, {}^{(0)}_{m}\!<1,...,m|1,...,m>^{(1)}_{m} + \cdots \quad .(4.16)$$

We also define the color-correlated tree level amplitudes as

$$|M_m^{(0)\ i,k}|^2 \equiv {}^{(0)}_{m}\!<1,...,m|\, \boldsymbol{T}_i \cdot \boldsymbol{T}_k \,|1,...,m>^{(0)}_{m}$$
$$= \left[M_m^{(0)\ a_1..b_i..b_k..a_m}(p_1,..,p_m)\right]^* T^c_{b_i a_i} T^c_{b_k a_k} M_m^{(0)\ a_1..a_i..a_k..a_m}(p_1,..,p_m)\,, (4.17)$$

where $T^a_{cb} \equiv i f_{cab}$ if the particle i is a gluon and $T^a_{\alpha\beta} \equiv t^a_{\alpha\beta}$ if the particle i is a quark and $T^a_{\alpha\beta} \equiv \bar{t}^a_{\alpha\beta} = -t^a_{\beta\alpha}$ if it is an antiquark. The color-charge algebra is

$$\boldsymbol{T}_i \cdot \boldsymbol{T}_j = \boldsymbol{T}_j \cdot \boldsymbol{T}_i \quad \text{if} \ \ i \neq j; \qquad \boldsymbol{T}_i^2 = C_i, \tag{4.18}$$

where C_i are the quadratic Casimirs of the gauge group ($C_i = C_A$ if i is a gluon and $C_i = C_F$ if i is a quark or an antiquark).

Note that by definition, each vector $|1,...,m>_m$ is an color singlet. Therefore color conservation is simply

$$\sum_{i=1}^{m} \boldsymbol{T}_i |1,...,m>_m = 0. \tag{4.19}$$

Dipole formulae

In Eq. (4.7) the real emission part $d\sigma^R$ is proportional to the $m+1$-parton tree level matrix element $|M^{(0)}_{m+1}|^2$. The dependence of the matrix element of the p_j final state parton is singular in two different phase space region: in the *soft* region, defined by limit $p_j \to 0$; in the *collinear* region, defined by $(p_j \parallel p_i)$ (where p_i is momentum of another QCD parton). This singular behaviour of the tree level matrix element is universal, that is, it is not dependent on very detailed structure of $|M^{(0)}_{m+1}|^2$ itself. The origin of this universality is the factorization property of the tree level matrix element. Thus, the singular behaviour of $M^{(0)}_{m+1}$ is essentially factorizable with respect to $M^{(0)}_m$ and the singular factor.

The dipole factorization formulae in the limit $p_i \cdot p_j \to 0$ is given by

$$|M^{(0)}_{m+1}(p_1,...,p_{m+1})|^2 = \sum_{k\neq i,j} \mathcal{D}_{ij,k}(p_1,...,p_{m+1}) + \ldots \tag{4.20}$$

where the dots denote the finite (or square root singular) contributions and the dipole contribution $\mathcal{D}_{ij,k}$ is defined by

$$\mathcal{D}_{ij,k}(p_1,...,p_{m+1}) = \frac{-1}{2p_i \cdot p_j}$$
$$\cdot\, {}^{(0)}_{m}\!<1,..,\widetilde{ij},..,\widetilde{k},..,m+1|\, \frac{\boldsymbol{T}_k \cdot \boldsymbol{T}_{ij}}{\boldsymbol{T}_{ij}^2}\, \boldsymbol{V}_{ij,k}\, |1,..,\widetilde{ij},..,\widetilde{k},..,m+1>^{(0)}_{m} \quad .(4.21)$$

The m-parton matrix element on the right-hand side of Eq. (4.21) is obtained from the original $m+1$-parton matrix element by replacing the partons i and j with a single parton $\widetilde{ij}$ (*the emitter*) and the parton k with parton $\widetilde{k}$ (*the spectator*). The momenta of the emitter and the spectator are defined in different ways in different dipole formulae

$$\widetilde{p}^{\mu}_{ij} = p^{\mu}_i + p^{\mu}_j - \frac{y_{ij,k}}{1-y_{ij,k}}\, p^{\mu}_k \ , \quad \widetilde{p}^{\mu}_k = \frac{1}{1-y_{ij,k}}\, p^{\mu}_k \ , \tag{4.22}$$

where the variable $y_{ij,k}$ is given by

$$y_{ij,k} = \frac{p_i p_j}{p_i p_j + p_j p_k + p_k p_i} \ , \qquad \tilde{z}_i = 1 - \tilde{z}_j = \frac{p_i \widetilde{p}_k}{\widetilde{p}_{ij}\widetilde{p}_k} \ . \tag{4.23}$$

The momenta of the emitter and spectator are on-shell ($\widetilde{p}^2_{ij} = \widetilde{p}^2_k = 0$)) and preserve the momentum conservation

$$p^{\mu}_i + p^{\mu}_j + p^{\mu}_k = \widetilde{p}^{\mu}_{ij} + \widetilde{p}^{\mu}_k \ . \tag{4.24}$$

The $\boldsymbol{V}_{ij,k}$ are matrices in the helicity space of emitter. For fermion and gluon splitting we have (where s and s' are the spin indices of the fermion $\widetilde{ij}$ in $< .., \widetilde{ij}, ..|$ and $|.., \widetilde{ij}, .. >$ respectively)

$$\begin{aligned} < s|\boldsymbol{V}_{q_i g_j,k}(\tilde{z}_i; y_{ij,k})|s' > &\equiv V_{q_i g_j,k}\, \delta_{ss'} \\ &= 8\pi\mu^{2\epsilon}\alpha_s\, C_F \ \left[\frac{2}{1-\tilde{z}_i(1-y_{ij,k})} - \ (1+\tilde{z}_i) - \epsilon(1-\tilde{z}_i)\right] \ \delta_{ss'} \ . \end{aligned} \tag{4.25}$$

For the quark, antiquark and for gluon, gluon splitting (μ, ν are the spin indices of the gluon $\widetilde{ij}$) we have

$$\begin{aligned} < \mu|\boldsymbol{V}_{q_i\bar{q}_j,k}(\tilde{z}_i)|\nu > &\equiv V^{\mu\nu}_{q_i\bar{q}_j,k} \\ &= 8\pi\mu^{2\epsilon}\alpha_s\, T_R \ \left[-g^{\mu\nu} - \frac{2}{p_i p_j}\left(\tilde{z}_i p^{\mu}_i - \tilde{z}_j p^{\mu}_j\right)\left(\tilde{z}_i p^{\nu}_i - \tilde{z}_j p^{\nu}_j\right)\right] , \end{aligned} \tag{4.26}$$

$$\begin{aligned} < \mu|\boldsymbol{V}_{g_i g_j,k}(\tilde{z}_i; y_{ij,k})|\nu > &\equiv V^{\mu\nu}_{g_i g_j,k} \\ &= 16\pi\mu^{2\epsilon}\alpha_s\, C_A \ \left[- g^{\mu\nu}\left(\frac{1}{1-\tilde{z}_i(1-y_{ij,k})} + \frac{1}{1-\tilde{z}_j(1-y_{ij,k})} - 2\right)\right. \\ &\quad \left. +(1-\epsilon)\frac{1}{p_i p_j}\left(\tilde{z}_i p^{\mu}_i - \tilde{z}_j p^{\mu}_j\right)\left(\tilde{z}_i p^{\nu}_i - \tilde{z}_j p^{\nu}_j\right)\right] . \end{aligned} \tag{4.27}$$

4.3 NLO jet cross section

In this section we define the leading order cross section and give formal conditions for the jet function. We also define the $d\sigma^A$ subtraction term. We will see the realization of the cancellation of infrared divergences.

Leading order and the jet function

In the term of the QCD matrix elements, the Born level cross section in d dimension is the following

$$d\sigma^B = \mathcal{N}_{in} \sum_{\{m\}} d\Gamma^{(m)}(p_1,...,p_m;Q)\, \frac{1}{S_{\{m\}}} |M_m^{(0)}(p_1,...,p_m)|^2 F_J^{(m)}(p_1,...,p_m), \quad (4.28)$$

where $\mathcal{N}_{in}$ includes all the non QCD factors, $\sum_{\{m\}}$ denotes the sum over all the configurations with m final state partons, $d\Gamma^{(m)}$ is the partonic phase space defined in Eq. (3.26) and $S_{\{m\}}$ is the Bose symmetry factor for identical partons in the final state.

The phase space function $F_J^{(m)}(p_1,...,p_m)$ is the jet function, defines the jet observables. In generally F_J may contain θ-functions, δ-functions, numerical and kinematic factors or any combination of these. The essential properties of F_J is that the jet function, we are interested in has to be infrared and collinear safe. From a formal viewpoint this implies that F_J fulfils the following properties

$$F_J^{(n+1)}(p_1,..,p_j,..,p_{n+1}) \to F_J^{(n)}(p_1,...,p_{n+1}) \quad \text{if } p_j \to 0\ , \quad (4.29)$$

$$F_J^{(n+1)}(p_1,..,p_i,..,p_j,..,p_{n+1}) \to F_J^{(n)}(p_1,..,p_i+p_j,..,p_{n+1}) \quad \text{if } p_i \parallel p_j\ , \quad (4.30)$$

and for all $n \geq m$

$$F_J^{(m)}(p_1,...,p_m) \to 0 \quad \text{if } p_i \cdot p_j \to 0\ . \quad (4.31)$$

Eqs. (4.29, 4.30) guarantee that the jet observables are infrared safe for any number n of final state partons. Eq. (4.31) ensures that the leading order cross section is well defined.

The cross section $d\sigma^R$ has same expression as $d\sigma^B$, apart form the replacement $m \to m+1$.

The subtraction term

The $d\sigma^A$ local subtraction term is provided by the dipole factorization formulae introduced in Sec. (4.2). Thus we can defined

$$\begin{aligned} d\sigma^A &= \mathcal{N}_{in} \sum_{\{m+1\}} d\Gamma^{(m+1)}(p_1,...,p_{m+1};Q)\, \frac{1}{S_{\{m+1\}}} \\ &\cdot \sum_{\substack{i,j \\ \text{pairs}}} \sum_{k\neq i,j} \mathcal{D}_{ij,k}(p_1,...,p_{m+1})\, F_J^{(m)}(p_1,..\widetilde{p}_{ij},\widetilde{p}_k,..,p_{m+1})\ . \quad (4.32) \end{aligned}$$

Here $\mathcal{D}_{ij,k}(p_1,...,p_{m+1})$ are the dipole contributions in Eq. (4.21) and $F_J^{(m)}(...)$ is the jet function for the corresponding m-parton state $\{p_1,..\widetilde{p}_{ij},\widetilde{p}_k,..,p_{m+1}\}$.

The definition in Eq. (4.32) makes the difference $(d\sigma^R - d\sigma^A)$ integrable in $d = 4$ dimension. Its explicit expression is

$$\begin{aligned} d\sigma^R - d\sigma^A &= \mathcal{N}_{in} \sum_{\{m+1\}} d\Gamma^{(m+1)}(p_1, ..., p_{m+1}; Q)\, \frac{1}{S_{\{m+1\}}} \\ &\cdot \Big\{ |M^{(0)}_{m+1}(p_1, ..., p_{m+1})|^2\, F_J^{(m+1)}(p_1, ..., p_{m+1}) \\ &- \sum_{\substack{i,j \\ \text{pairs}}} \sum_{k \neq i,j} \mathcal{D}_{ij,k}(p_1, ..., p_{m+1})\, F_J^{(m)}(p_1, ..\widetilde{p}_{ij}, \widetilde{p}_k, .., p_{m+1}) \Big\} \,. \end{aligned} \tag{4.33}$$

Integral of the subtraction term

The subtraction term $d\sigma^A$ have to be been able to integrate analytically over the one-parton subspace in d dimension leading to soft an collinear divergences. The definition of the dipole momenta in Eq. (4.22) allow us to exactly factorize the $m+1$-parton phase space into a m-parton phase space times a single-parton contribution as follows

$$d\Gamma^{(m+1)}(p_1, ..., p_{m+1}; Q) = d\Gamma^{(m)}(p_1, .., \widetilde{p}_{ij}, \widetilde{p}_k, .., p_{m+1}; Q)\, [dp_i(\widetilde{p}_{ij}, \widetilde{p}_k)] \quad , \tag{4.34}$$

where the one-parton subspace in the term of variables $y_{ij,k}$, $\tilde{z}_i$ defined in Eq. (4.23) is given by

$$[dp_i(\widetilde{p}_{ij}, \widetilde{p}_k)] = \frac{d^d p_i}{(2\pi)^{d-1}}\, \delta_+(p_i^2)\, \Theta(1 - \tilde{z}_i)\, \Theta(1 - y_{ij,k})\, \frac{(1 - y_{ij,k})^{d-3}}{1 - \tilde{z}_i} \,. \tag{4.35}$$

Using the phase space factorization property in Eq. (4.34) and the explicit expression of the dipole contribution $\mathcal{D}_{ij,k}$ in Eq. (4.21) and performed the integral over the one-parton subspace the result can be written in the following form

$$\begin{aligned} \int_{m+1} d\sigma^A &= \int_m \left[\int_1 d\sigma^A \right] = \int_m \mathcal{N}_{in} \sum_{\{m\}} d\Gamma^{(m)}(p_1, ..., p_m; Q)\, \frac{1}{S_{\{m\}}} \frac{\alpha_s}{2\pi} \\ &\cdot \; {}^{(0)}_{m}\!< 1, ..., m|\, \boldsymbol{I}(\epsilon)\, |1, ..., m >^{(0)}_{m}\; F_J^{(m)}(p_1, ..., p_m) \quad , \end{aligned} \tag{4.36}$$

where the $\boldsymbol{I}(\epsilon)$ insertation operator is defined by

$$\boldsymbol{I}(p_1, .., p_m; \epsilon) = -\frac{1}{\Gamma(1 - \epsilon)} \sum_i \frac{1}{\boldsymbol{T}_i^2} \mathcal{V}_i(\epsilon) \sum_{k \neq i} \boldsymbol{T}_i \cdot \boldsymbol{T}_k \left(\frac{4\pi\mu^2}{2 p_i \cdot p_k} \right)^{\epsilon} \,. \tag{4.37}$$

The singular factor $\mathcal{V}_i(\epsilon)$ is defined by

$$\mathcal{V}_i(\epsilon) = \boldsymbol{T}_i^2 \left(\frac{1}{\epsilon^2} - \frac{\pi^2}{3} \right) + \gamma_i\, \frac{1}{\epsilon} + \gamma_i + K_i + \mathcal{O}(\epsilon) \quad , \tag{4.38}$$

where we have introduced the following constants

$$\gamma_{i=q,\bar{q}} = \frac{3}{2} C_F \,, \quad \gamma_{i=g} = \frac{11}{6} C_A - \frac{2}{3} T_R n_f \,, \tag{4.39}$$

$$K_{i=q,\bar{q}} = \left(\frac{7}{2} - \frac{\pi^2}{6}\right) C_F \ , \quad K_{i=g} = \left(\frac{67}{18} - \frac{\pi^2}{6}\right) C_A - \frac{10}{9} T_R n_f \ , \qquad (4.40)$$

where n_f is the number of the quark flavours.

Virtual contribution

The $d\sigma^V$ virtual contribution is defined by the one-loop renormalized matrix element as follows

$$\begin{aligned} d\sigma^V &= \mathcal{N}_{in} \sum_{\{m\}} d\Gamma^{(m)}(p_1, ..., p_m; Q) \, \frac{1}{S_{\{m\}}} \frac{\alpha_s}{2\pi} \\ &\cdot \quad 2\mathrm{R}e \left({}^{(0)}_{m}\!< 1, ..., m | 1, ..., m >^{(1)}_{m} \right) \, F_J^{(m)}(p_1, .., p_m) \ , \end{aligned} \qquad (4.41)$$

where $|1, ..., m >^{(1)}_m$ is the one-loop contribution to the matrix element.

The renormalized one-loop matrix element ($\overline{\mathrm{MS}}$ matrix element) is untinged the ultraviolet divergences but contains infrared (IR) singularities. The structure of this IR divergences is well known [43]. The IR divergences arise from two kinematically degenerate region: a) when the loop momentum become soft or/and the loop momentum become collinear with an external momentum. Using dimensional regularization, when the space-time dimension is $d = 4 - 2\epsilon$, performed the loop integration these two singular behaviors result in poles $1/\epsilon^2$ (soft and collinear) and $1/\epsilon$ (soft or collinear). The singular part of the one-loop matrix element can be expressed by the tree level matrix element and a singular singular factor

$$|1, ..., m >^{(1)}_m = \boldsymbol{I}^{(1)}(p_1, .., p_m; \epsilon) |1, ..., m >^{(0)}_m + |1, ..., m >^{(1), \, fin}_m \ , \qquad (4.42)$$

where $|1, ..., m >^{(1), \, fin}_m$ denotes the finite part of the one-loop matrix element in the limit $\epsilon \to 0$ and $\boldsymbol{I}^{(1)}(\epsilon)$ is the one loop insertation operator which is defined by

$$\boldsymbol{I}^{(1)}(p_1, .., p_m; \epsilon) = \frac{1}{2} \frac{1}{\Gamma(1-\epsilon)} \sum_i \frac{1}{\boldsymbol{T}_i^2} \mathcal{V}_i^{sing}(\epsilon) \sum_{k \neq i} \boldsymbol{T}_i \cdot \boldsymbol{T}_k \left(\frac{4\pi\mu^2}{-2 p_i \cdot p_k} \right)^{\epsilon} \ , \qquad (4.43)$$

where the singular function $\mathcal{V}_i^{sing}(\epsilon)$ depend only on the parton flavour and is given by

$$\mathcal{V}_i^{sing}(\epsilon) = \boldsymbol{T}_i^2 \frac{1}{\epsilon^2} + \gamma_i \frac{1}{\epsilon} \ . \qquad (4.44)$$

Finally, some note about the regularization schemes. We use dimensional regularization. The key of this regularization method is the analytic continuation of loop momenta to $d = 4 - 2\epsilon$ space-time dimensions. Having done this, one is left with some freedom regarding the dimensionality of momenta of the external particles as well as the number of polarizations of both external and internal particles. This leads

to different regularization schemes (RS). The customary is the conventional dimensional regularization scheme (CDR). This is the most natural choosing because no distinction is made between particles in the loop and external particles. All particles momenta are d-dimensional and one considers $d-2$ helicity states for gluons and 2 helicity states for massless quarks.

In the loop calculations the mostly used regularization scheme is the dimensional reduction scheme (DR). In this case for all particles (gluon and massless quark) the number of helicity states are 2 and the dimension of the external particles momenta are $d=4$ as against loop momenta which dimension is $d=4-2\epsilon$.

Of course the loop amplitudes and the α_s coupling depend on the different regularization schemes. In the one-loop case the RS-dependence is simply

$$|1,...,m>_m^{(1),\mathrm{RS}} = \frac{1}{2}\sum_i \tilde{\gamma}_i^{\mathrm{RS}} |1,...,m>_m^{(0),\mathrm{RS}} + |1,...,m>_m^{(1)} \quad , \tag{4.45}$$

where the finite coefficients $\tilde{\gamma}_i^{\mathrm{RS}}$ depend only on the flavour of external partons. By definition the CDR scheme is the reference scheme ($\tilde{\gamma}_i^{\mathrm{CDR}}=0$). In the case of DR the transitional factors $\tilde{\gamma}_i^{\mathrm{DR}}$ are the followings

$$\tilde{\gamma}_g^{\mathrm{DR}} = \frac{1}{6}C_A \quad , \qquad \tilde{\gamma}_q^{\mathrm{DR}} = \tilde{\gamma}_{\bar{q}}^{\mathrm{DR}} = \frac{1}{2}C_F \quad . \tag{4.46}$$

The regularization scheme dependence of the strong coupling α_s is the following in case of DR

$$\alpha_s^{\mathrm{DR}} = \alpha_s\left(1+\frac{C_A}{6}\frac{\alpha_s}{2\pi}\right) \quad , \tag{4.47}$$

where α_s is the customary $\overline{\mathrm{MS}}$ strong coupling.

4.4 Final result

The result of the calculation of NLO cross section in e^+e^-annihilation are summarized below.

The cross in Eq. (4.5) contains a LO and a NLO component. The LO cross section that involves m final state partons is given by

$$\sigma^{LO} \quad = \quad \int_m d\sigma^B = \int d\Gamma^{(m)}\ |\hat{M}_m^{(0)}(p_1,...,p_m)|^2\ F_J^{(m)}(p_1,...,p_m) \quad , \tag{4.48}$$

where $\hat{M}_m^{(0)}$ is the generalised tree level matrix element squared which is defined by

$$|\hat{M}_m^{(0)}(p_1,...,p_m)|^2 = \mathcal{N}_{in}\sum_{\{m\}}\frac{1}{S_{\{m\}}}|M_m^{(0)}(p_1,...,p_m)|^2 \quad . \tag{4.49}$$

According to Eq. (4.10), the NLO correction can be written as a sum of a $m+1$ and a m-parton integral

$$\sigma^{NLO} = \sigma^{NLO}_{\{m+1\}} + \sigma^{NLO}_{\{m\}} \quad . \tag{4.50}$$

The $m+1$-parton contribution is the following

$$\begin{aligned}
\sigma^{NLO}_{\{m+1\}} &= \int_{m+1} \left[d\sigma^R_{\epsilon=0} - d\sigma^A_{\epsilon=0} \right] \\
&= \int d\Gamma^{(m+1)} \Big\{ \, |\hat{M}^{(0)}_{m+1}(p_1,...,p_{m+1})|^2 \; F^{(m+1)}_J(p_1,...,p_{m+1}) \\
&- \sum_{\substack{i,j \\ \text{pairs}}} \sum_{k \neq i,j} \hat{\mathcal{D}}_{ij,k}(p_1,...,p_{m+1}) \; F^{(m)}_J(p_1,..\widetilde{p}_{ij},\widetilde{p}_k,..,p_{m+1}) \Big\} \quad , \qquad (4.51)
\end{aligned}$$

where $\hat{\mathcal{D}}_{ij,k}$ is defined by

$$\hat{\mathcal{D}}_{ij,k}(p_1,...,p_{m+1}) = \mathcal{N}_{in} \sum_{\{m+1\}} \frac{1}{S_{\{m+1\}}} \mathcal{D}_{ij,k}(p_1,...,p_{m+1}) \quad . \tag{4.52}$$

The m-parton integral is a Born like contribution. This term is sum of the contributions of the virtual corrections and the integral of subtraction term defined in Eq.(4.32)

$$\begin{aligned}
\sigma^{NLO}_{\{m\}} &= \int_m \left[d\sigma^V + \int_1 d\sigma^A \right]_{\epsilon=0} \\
&= \int d\Gamma^{(m)} \; |\hat{M}^{(1)}_m(p_1,...,p_m)|^2 \; F^{(m)}_J(p_1,...,p_m) \quad , \qquad (4.53)
\end{aligned}$$

where the generalized matrix element squared $|\hat{M}^{(1)}_m|^2$ is given by

$$\begin{aligned}
|\hat{M}^{(1)}_m(p_1,...,p_m)|^2 &= \mathcal{N}_{in} \frac{\alpha_s}{2\pi} \sum_{\{m\}} \frac{1}{S_{\{m\}}} \lim_{\epsilon \to 0} \Big\{ 2\mathrm{R}e \left({}^{(0)}_{m}\!< 1,...,m|1,...,m >^{(1),\,fin}_{m} \right) \\
&\quad + {}^{(0)}_{m}\!< 1,...,m| \; \boldsymbol{I}(\epsilon) + \boldsymbol{I}^{(1)}(\epsilon) \; |1,...,m >^{(0)}_{m} \Big\} \quad . \qquad (4.54)
\end{aligned}$$

The sum of the two insertation operator $\boldsymbol{I}(\epsilon)$ and $\boldsymbol{I}^{(1)}(\epsilon)$ is finite in the limit $\epsilon \to 0$

$$\lim_{\epsilon \to 0} \Big(\boldsymbol{I}(\epsilon) + 2Re\boldsymbol{I}^{(1)}(\epsilon) \Big) = \sum_{i=1}^{m} \left(\gamma_i + K_i + \frac{1}{6}\pi^2 \boldsymbol{T}_i \right) \quad . \tag{4.55}$$

The both pieces of the NLO correction $\sigma^{NLO}_{\{m\}}$ and $\sigma^{NLO}_{\{m+1\}}$ can be calculated by Monte Carlo integration. I developed a computer program (called `DEBRECEN` [9]) which implements the dipole subtraction method and can calculate n-jet cross section at NLO accuracy.

4.5 Numerical implementation

We have seen in the previous section that the NLO cross section can be calculated by the Monte Carlo integration. The leading order integral in Eq. (4.48) and the m-parton NLO integral in Eq. (4.53) are simple Monte Carlo integration. The integrand of these integrals are finite over all the integration domain. On the other hand the difference of the $m+1$-parton matrix element squared and the dipole contributions defined in Eq. (4.21) contains integrable square root singularities as follows

$$\lim_{p_i \cdot p_j \to 0} [d\sigma^R - d\sigma^A] \propto \frac{1}{\sqrt{p_i \cdot p_j}} \ , \tag{4.56}$$

where this singularities arise from the previously discussed soft and collinear regions. The square root singular function can not be integrated by a simple Monte Carlo (choosing random values uniformly), because the variance of the estimate for the integral is infinite. We have to try to eliminate this type of singularities from the integrand so as to be able to calculate the $m+1$-parton integral of NLO calculation.

Important sampling

The integration over the phase space means a multi-dimensional Monte Carlo integral. In generally, we have to calculate the following type of integrals

$$I[f] = \int_n d\vec{x}\, f(\vec{x}) \ , \tag{4.57}$$

where $f(\vec{x})$ is an integrable function not necessary smooth and $\vec{x} = (x_1, ..., x_n)$, where $x_j \in [0,1]$ for $j = 1, ..., n$. The most simple Monte Carlo one can think of to estimate $I[f]$ to generate random values for $\vec{x}$ uniformly and evaluate the function $f(\vec{x})$. The estimate $E[f]$ for $I[f]$ is then given by

$$E[f] = \frac{1}{N} \sum_{i=1}^{N} f(p_{1_i}, ..., p_{n_i}) \ . \tag{4.58}$$

In the limit $N \to \infty$ this leads to $E[f] = I[f]$. The estimates for the variance and for the error are given by

$$\mathrm{Var}[f] = E[f^2] - E[f]^2 \ , \qquad \mathrm{Err}[f] = \sqrt{\frac{\mathrm{Var}[f]}{N-1}} \ , \tag{4.59}$$

where $\mathrm{Var}[f]$ and $\mathrm{Err}[f]$ denote the variance and the error respectively. If the function f contains integrable singularities (e.g. square root) then the variance goes to infinity in the $N \to \infty$ and the estimation becomes unstable.

In these cases to reduce the value of $\mathrm{Var}[f]$ we apply important sampling. We introduce new integration variables instead of $\vec{x}$

$$I[f] = \int_m d\vec{\rho}\, \frac{f(\vec{x}(\vec{\rho}))}{g(\vec{x}(\vec{\rho}))} \approx E\left[\frac{f \circ \vec{x}}{g \circ \vec{x}}\right] \ , \tag{4.60}$$

in such a way that, the Jacobian factor ($g(\vec{x}(\vec{\rho}))$, where $\rho_j \in [0,1]$ for $j = 1, ..., m$ and $m \geq n$) of the transformation $\vec{x}(\vec{\rho})$ has the same singular behavior as $f(\vec{x})$

$$\frac{f(\vec{x}(\vec{\rho}))}{g(\vec{x}(\vec{\rho}))} \longrightarrow \text{constant} \ , \tag{4.61}$$

in the singular limits.

In the those cases when we can not find that integral transformation which can handle simultaneously the all singular limits of function $f(\vec{x})$ but we can define in every singular limits a transformations which handle only that singularity, then the Jacobian $g(\vec{x})$ can be written as follows

$$g(\vec{x}) = \sum_{i=1}^{n_s} \alpha_i g_i(\vec{x}) \ , \tag{4.62}$$

where n_s denotes the number of the singular limits of $f(\vec{x})$, the functions $g_i(\vec{x})$ are the Jacobian of the transformations and the constants α_i are arbitrary positive weights with the following normalization condition

$$\sum_{i=1}^{n_s} \alpha_i = 1 \ , \tag{4.63}$$

and these weight should be chosen in such a way that, they minimize the variance. With this Jacobian the, integral is a weighted sum

$$I[f] = \sum_{i=1}^{n_s} \alpha_i \int_{m_i} d\vec{\rho}_i \left[\frac{f(\vec{x})}{g_1(\vec{x}) + \cdots + g_{n_s}(\vec{x})} \right]_{\vec{x}=\vec{x}_i(\vec{\rho}_i)} \ , \tag{4.64}$$

where $\vec{x}_i(\vec{\rho}_i)$ are the corresponding transformations and the estimate for the integral is the following

$$I[f] = \sum_{i=1}^{n_s} \alpha_i E \left[\frac{f \circ \vec{x}_i}{g \circ \vec{x}_i} \right] \ , \tag{4.65}$$

where the function $g(\vec{x})$ is defined in Eq.(4.62). This integration method is called *multi channel integration method* [55].

We apply this sampling method for the phase space integral which involves integrable singularities.

Phase space integral

In the NLO jet calculation we have a $m+1$-parton phase space integral involving integrable square root singular matrix element squared like in Eq. (4.56). So, we want to calculate the following type of integrals

$$I[f] = \int d\Gamma^{(m+1)}(p_1, ..., p_{m+1}; Q)\, f(p_1, ..., p_{m+1}) \ , \tag{4.66}$$

where $d\Gamma^{(m+1)}$ denotes the phase space integral measure. Now, we introduce the following multi channel Jacobian to eliminate the all singularities of the integrand:

$$G(p_1,...,p_{m+1}) = \sum_{\substack{i,j,k=1 \\ i\neq j\neq k}}^{m+1} \alpha_{ij,k} \frac{(2\pi)^2}{(s_{ik}+s_{jk})\sqrt{(1-\tilde{z}_i)y_{ij,k}}} \ , \tag{4.67}$$

where the $y_{ij,k}$ and $\tilde{z}_i$ kinematic variables are defined in Eq. (4.23), $\alpha_{ij,k}$ are the channel weight parameters and $s_{mn} = 2p_m \cdot p_n$ is the usual Lorentz dot product. With this definition of the Jacobian and using the factorization property of the phase space given in Eq. (4.34), the integral can be written as

$$\begin{aligned} I[f] &= \int d\Gamma^{(m+1)}(p_1,...,p_{m+1};Q)\, G(p_1,...,p_{m+1}) \frac{f(p_1,...,p_{m+1})}{G(p_1,...,p_{m+1})} \\ &= \sum_{\substack{i,j,k=1 \\ i\neq j\neq k}}^{m+1} \alpha_{ij,k} \int d\Gamma^{(m)}(p_1,..,\widetilde{p}_{ij},..,\widetilde{p}_k,..p_{m+1};Q) \\ &\cdot \int_0^{2\pi} \frac{d\phi_i}{2\pi} \frac{1}{2}\int_0^1 \frac{dy_{ij,k}}{\sqrt{y_{ij,k}}} \frac{1}{2}\int_0^1 \frac{d\tilde{z}_i}{\sqrt{1-\tilde{z}_i}} \frac{f(p_1,...,p_{m+1})}{G(p_1,...,p_{m+1})} \ . \end{aligned} \tag{4.68}$$

Now, we introduce new integration variables instead of $\{\tilde{z}_i, y_{ij,k}, \phi_i\}$, as follows

$$\tilde{z}_i = 1-\rho_{z_i}^2 \ , \qquad y_{ij,k} = \rho_{y_{ij,k}}^2 \ , \qquad \phi_i = 2\pi\rho_{\phi_i} \ . \tag{4.69}$$

These integral transformations lead us to a simpler expression

$$\begin{aligned} I[f] &= \int d\Gamma^{(m+1)}(p_1,...,p_{m+1};Q)\, G(p_1,...,p_{m+1}) \frac{f(p_1,...,p_{m+1})}{G(p_1,...,p_{m+1})} \\ &= \sum_{\substack{i,j,k=1 \\ i\neq j\neq k}}^{m+1} \alpha_{ij,k} \int d\Gamma^{(m)}(p_1,..,\widetilde{p}_{ij},..,\widetilde{p}_k,..p_{m+1};Q) \\ &\cdot \int_0^1 d\rho_{\phi_i}\, d\rho_{y_{ij,k}}\, d\rho_{z_i} \frac{f(p_1,...,p_{m+1})}{G(p_1,...,p_{m+1})} \ . \end{aligned} \tag{4.70}$$

Using the previously equation easy to see that the $m+1$-parton integral of the Jacobian factor is equal to the m-parton total phase space weight

$$I[G] = \int d\Gamma^{(m)}(p_1,...,p_m;Q) \ . \tag{4.71}$$

Using the multi channel important sampling method we can create an algorithm which can generate well sampled events. Let see the main steps of this algorithm

1. Generate a phase space with m outgoing parton $\{q_1,...,q_m\}_m$ by any phase space algorithm. For example, by algorithm called `RAMBO` [54] which is simple and well known. This generates flat phase space with constant phase space weight for every events. The weight of ith m-parton event is denoted by $W_i^{(m)}$.

2. Choose a three indices (i,j,k) in such a way that $i,k=1,...,m$, $j=1,...,m+1$ and $i \neq k$. This choices determine the channel weights. If the indices are chosen uniformly then the channel weights in the expression of the $G(p_1,...)$ in the Eq. (4.67) are constant $\alpha_{ij,k}=1/(m(m^2-1))$.

3. Generate the random values $\rho_z, \rho_y, \rho_\phi$ uniformly and calculate the kinematic variables z, y, ϕ by Eq. (4.69).

4. Calculate the momentum set $\{p_1,...,p_{m+1}\}_{m+1}$ using the definition of the dipole momenta in Eq. (4.22). In the center of mass frame of q_i and q_k we have

$$\begin{aligned} p_l &= q_l \qquad \text{if} \qquad l=1,..,m \quad \text{and} \quad l \neq i,k \ , \\ p_k &= (1-y)q_k \ , \quad p_{m+1}=p \ , \quad p_i = q_i + y\, q_k - p \ , \end{aligned} \tag{4.72}$$

   where the temporary momentum p can be expressed by variables z, y, ϕ

$$p = \frac{\sqrt{s_{ik}}}{2}(z+(1-z)\,y,\ (1-z)\,y-z,\ p_\perp \cos\phi_i,\ p_\perp \sin\phi_i) \ , \tag{4.73}$$

   where $p_\perp^2 = 4\,z\,(1-z)\,y$ is the transverse momentum squared and $s_{ik}=2q_i\cdot q_k$.

5. Permute the momenta p_j and p_{m+1} ($p_j \leftrightarrow p_{m+1}$).

6. Calculate the weight of the $m+1$-parton configuration which is obtained by

$$W^{(m+1)} = \frac{W^{(m)}}{G(p_1,...,p_{m+1})} \ . \tag{4.74}$$

With this phase space algorithm a $m+$-parton integral can be written as an m-parton integral by the follows

$$I[f] = \int d\Gamma^{(m)}(q_1,...,q_m;\,Q) \sum_{j=1}^{m+1} \sum_{\substack{i,k=1 \\ i\neq k}}^{m} \beta_{i,j,k} \int_0^1 d\rho_\phi\, d\rho_y\, d\rho_z \frac{f(p_1,...,p_{m+1})}{G(p_1,...,p_{m+1})}, \tag{4.75}$$

where $\beta_{i,j,k} = \alpha_{im+1,k_{|j\leftrightarrow m+1}}$. In first term of the left hand side of Eq. (4.75) the momentum set $\{p_1,...,p_{m+1}\}_{m+1}$ are generated by the previously described algorithm. Note, this momentum set depend on the i,j,k sum parameters.

Chapter 5

Four-Jet production in e^+e^- annihilation

Electron-positron annihilation into hadrons is the cleanest process to test Quantum Chromodynamics (QCD) [12] in high energy elementary particle reactions. In this process the initial state is completely known and there is a lot of quantities, for instance the total cross section and jet related correlations, that depend on the long distance properties of the theory very little. These quantities can be calculated in perturbative QCD as a function of a single parameter, the strong coupling. For this reason the various QCD tests at electron-positron colliders [56, 57, 58, 59, 60, 61] can be regarded as experiments for determining α_s.

The other ingredient of QCD, that is in principle free, is the underlying gauge group. Although by now nobody questions that QCD is based upon SU(3) gauge theory, the "full" measurement of QCD, that is the simultaneous measurement of the strong coupling and the eigenvalues of the quadratic Casimirs of the underlying gauge theory, the C_F and C_A color charges, is not a purely academic exercise. The possible existence of light gluinos [62] influences both the value of α_s and the measured value of the color charges (or, assuming $SU(3)_c$, the value of the light fermionic degrees of freedom n_f). Thus the only consistent framework to check whether the data favor or exclude the additional degrees of freedom is a simultaneous fit of these parameters to data.

In principle any observable depends on these basic parameters. The sensitivity of a given observable on the color charges however, is influenced by the fact that in perturbation theory the three gluon coupling appears at tree level first for four-jet final states. In the total cross section and for three-jet like quantities the adjoint color charge appears only in the radiative corrections. Therefore, four-jet observables seem to be the best candidates to measure the color factors. Indeed, during the first phase of operation of the Large Electron Positron Collider (LEP) four-jet events were primarily used for measuring C_F and C_A [63]. These measurements however,

were not complete in the sense mentioned above. The lack of knowledge about the perturbative prediction for four-jet observables at O(α_s^3) prevented the experimental collaborations from fixing the absolute normalization of the perturbative prediction, therefore, α_s could not be measured using the same observables.

The important developments that made possible the for-jet NLO calculation were the calculation techniques for NLO jet cross sections [8, 52, 53] and the one-loop amplitudes for the relevant subprocesses, i.e., for $e^+e^- \to 4$ partons become available. In Refs. [45, 46] Campbell, Glover and Miller introduced FORTRAN programs that calculate the NLO squared matrix elements of the $e^+e^- \to \gamma^* \to \bar{q}q\bar{Q}Q$ and $\bar{q}qgg$ processes. In Refs. [44, 47] Bern, Dixon, Kosower and Wienzierl gave analytic formulas for the helicity amplitudes of the same processes with the $e^+e^- \to Z^0 \to 4$ partons channel included as well. For the sake of completeness, in our work we use the amplitudes of Refs. [47] for the loop corrections (see Appendix B). Although the tree-level helicity amplitudes for the $e^+e^- \to 5$ partons subprocesses had been known [40], we calculated them anew and present the results in terms of Weyl spinors conforming with the notation used for describing the one-loop helicity amplitudes [47]. We also present the previously unpublished color linked helicity dependent Born matrix elements for the $e^+e^- \to 4$ partons processes (see Appendix A).

Based on the previously discussed subtraction method, the author developed a Monte Carlo program (called `DEBRECEN`) which can calculate four-jet cross section at NLO level. Furthermore, three other program have been developed irrespectively of our work (`MENLO PARC` [70], `EERAD2` [72] and `MERCUTIO` [73]).

In this chapter we discuss the phenomenology of the four-jet production. The four-jet observables can be classified into three major groups: i) four-jet rates; ii) four-jet event shape variables; iii) four-jet angular correlations. We calculated the jet rates E0, Durham and Geneva algorithm for three different value of y_{cut} parameter[1, 6] and compared our results with the results of three other program. The Durham jet rates were compared with ALEPH data [6, 7]. Using the Durham and Cambridge algorithms we calculated the four-jet shape variables y_4^D and y_4^C [6]. We also calculated the following four-jet event shape variables: D-parameter and acoplanarity [18] in Ref. [1], Π_1 and Π_4 Fox-Wolfram moments [19] in Ref. [4] and C-parameter ($C > 0.75$) in Ref. [6]. We also determined the four-jet angular correlations and compared with ALEPH data [5]. Some of the mentioned algorithms and variables are defined in Sec. (3.2).

5.1 Jet rates

The most important multi-jet observables that are used for determining the underlying parton structure of hadronic events are the multi-jet rates. In e^+e^- annihilation the widely known Durham [25] algorithm have become indispensable for this purpose. Recently a new jet clustering, the Cambridge algorithm was proposed as an improved version of the Durham scheme [27]. This scheme is designed to minimize

the formation of "junk jets" — jets formed from hadrons of low transverse momenta, unconnected to the underlying parton structure. As a result, the hadronization corrections to the mean jet multiplicities were found smaller when the Cambridge algorithm is employed than for the Durham clustering [27]. However, it was shown in Ref. [28] that the small hadronization corrections found for the Cambridge algorithm in the study of the mean jet rate are due to cancellations among corrections for the individual jet production rates. Apart from the very small values of the resolution parameter, $y_{cut} < 10^{-3.2}$, for the individual rates the Durham clustering shows comparably small (for $y_{cut} > 10^{-2}$), or even much smaller hadronization corrections. In this section we present the NLO production rates for four jets using both algorithms and compare the size of the radiative corrections.

Note, we compared the various Monte Carlo programs (`MENLO PARC`, `DEBRECEN`, `EERAD2` and `MERCUTIO`) for the Durham jet clustering algorithm. The result are shown in the Table (5.1).

Table 5.1: The four-jet fraction as calculated by `MENLO PARC`, `DEBRECEN` , `EERAD2` and `MERCUTIO`, for Durham jet algorithms and varying y_{cut}.

Algorithm	y_{cut}	`MENLO PARC`	`DEBRECEN`
Durham	0.005	$(1.04 \pm 0.02) \cdot 10^{-1}$	$(1.05 \pm 0.01) \cdot 10^{-1}$
	0.01	$(4.70 \pm 0.06) \cdot 10^{-2}$	$(4.66 \pm 0.02) \cdot 10^{-2}$
	0.03	$(6.82 \pm 0.08) \cdot 10^{-3}$	$(6.87 \pm 0.04) \cdot 10^{-3}$
	y_{cut}	`EERAD2`	`MERCUTIO`
	0.005	$(1.05 \pm 0.01) \cdot 10^{-1}$	$(1.06 \pm 0.01) \cdot 10^{-1}$
	0.01	$(4.65 \pm 0.02) \cdot 10^{-2}$	$(4.72 \pm 0.01) \cdot 10^{-2}$
	0.03	$(6.86 \pm 0.03) \cdot 10^{-3}$	$(6.96 \pm 0.03) \cdot 10^{-3}$

The four-jet rates are defined as the ratio of the four-jet cross section to the total hadronic cross section:

$$R_4 = \frac{\sigma_{4-\mathrm{jet}}}{\sigma_{\mathrm{tot}}}(y_{cut}) = \eta^2 B_4(y_{cut}) + \eta^3 \left(C_4(y_{cut}) - \frac{3}{2} B_4(y_{cut}) \right) \quad , \tag{5.1}$$

where we used $\sigma_{\mathrm{tot}} = \sigma_0(1 + 1.5\eta)$ and $\eta = \alpha_s C_F/(2\pi)$. The renormalization scale dependence of the cross section is obtained by the substation $\eta \to \eta(\mu)(1 + \beta_0/C_F\, \eta(\mu)\, \ln x_\mu)$, where $x_\mu = \mu/\sqrt{s}$. Setting the color charges to the SU(3) values, we plot the scale independent $B_4(y_{cut})$ and $C_4(y_{cut})$ functions in Figs. (5.1 and 5.2) and tabulate the values for $C_4(y_{cut})$ in Table (5.2).

Comparing the values for the two Born functions, we see that at leading order the Cambridge algorithm gives slightly higher rates and the difference increases with decreasing y_{cut}. On the other hand, the correction functions become smaller for Cambridge clustering with decreasing y_{cut}. The result of these opposite trends is

Table 5.2: Correction functions to the four-jet rates for Durham and Cambridge algorithms.

$\log_{10}(y_{cut})$	$C^{\mathrm{D}}_{y_{cut}}$	$C^{\mathrm{C}}_{y_{cut}}$
-0.9	$(4.209 \pm 0.655) \cdot 10^{-2}$	$(4.375 \pm 0.655) \cdot 10^{-2}$
-1.0	$(9.449 \pm 0.220) \cdot 10^{-1}$	$(9.499 \pm 0.230) \cdot 10^{-1}$
-1.1	$(5.411 \pm 0.055) \cdot 10^{0}$	$(5.300 \pm 0.057) \cdot 10^{0}$
-1.2	$(1.769 \pm 0.011) \cdot 10^{1}$	$(1.700 \pm 0.012) \cdot 10^{1}$
-1.3	$(4.321 \pm 0.032) \cdot 10^{1}$	$(4.044 \pm 0.033) \cdot 10^{1}$
-1.4	$(8.893 \pm 0.034) \cdot 10^{1}$	$(8.142 \pm 0.038) \cdot 10^{1}$
-1.5	$(1.619 \pm 0.005) \cdot 10^{2}$	$(1.459 \pm 0.006) \cdot 10^{2}$
-1.6	$(2.705 \pm 0.009) \cdot 10^{2}$	$(2.400 \pm 0.010) \cdot 10^{2}$
-1.7	$(4.201 \pm 0.012) \cdot 10^{2}$	$(3.683 \pm 0.014) \cdot 10^{2}$
-1.8	$(6.221 \pm 0.020) \cdot 10^{2}$	$(5.403 \pm 0.021) \cdot 10^{2}$
-1.9	$(8.730 \pm 0.029) \cdot 10^{2}$	$(7.490 \pm 0.032) \cdot 10^{2}$
-2.0	$(1.191 \pm 0.004) \cdot 10^{3}$	$(1.009 \pm 0.005) \cdot 10^{3}$
-2.1	$(1.563 \pm 0.006) \cdot 10^{3}$	$(1.308 \pm 0.007) \cdot 10^{3}$
-2.2	$(2.000 \pm 0.010) \cdot 10^{3}$	$(1.653 \pm 0.010) \cdot 10^{3}$
-2.3	$(2.478 \pm 0.011) \cdot 10^{3}$	$(2.023 \pm 0.012) \cdot 10^{3}$
-2.4	$(3.007 \pm 0.024) \cdot 10^{3}$	$(2.402 \pm 0.025) \cdot 10^{3}$
-2.5	$(3.542 \pm 0.023) \cdot 10^{3}$	$(2.749 \pm 0.027) \cdot 10^{3}$
-2.6	$(4.029 \pm 0.033) \cdot 10^{3}$	$(3.020 \pm 0.036) \cdot 10^{3}$
-2.7	$(4.469 \pm 0.052) \cdot 10^{3}$	$(3.198 \pm 0.063) \cdot 10^{3}$
-2.8	$(4.797 \pm 0.067) \cdot 10^{3}$	$(3.220 \pm 0.077) \cdot 10^{3}$
-2.9	$(4.869 \pm 0.099) \cdot 10^{3}$	$(2.999 \pm 0.108) \cdot 10^{3}$
-3.0	$(4.878 \pm 0.120) \cdot 10^{3}$	$(2.608 \pm 0.132) \cdot 10^{3}$
-3.1	$(4.482 \pm 0.166) \cdot 10^{3}$	$(1.678 \pm 0.178) \cdot 10^{3}$
-3.2	$(3.430 \pm 0.256) \cdot 10^{3}$	$(-3.254 \pm 27.6) \cdot 10^{1}$
-3.3	$(1.783 \pm 0.300) \cdot 10^{3}$	$(-2.093 \pm 0.32) \cdot 10^{3}$

that the K factors, defined are smaller for the Cambridge algorithm for small values of y_{cut}, which is demonstrated in Fig. (5.3).

The smaller K factors also mean smaller renormalization scheme dependence, which can be seen from comparing Figs. (5.4 and 5.5). The usual interpretation of the smaller scale dependence is that the effect of the uncalculated higher orders are expected to be smaller in the case of Cambridge clustering. It is interesting to note that in the middle y_{cut} region ($10^{-3.2} < y_{cut} < 10^{-2}$), where the hadronization corrections for the Cambridge clustering were found significantly *larger* than for the Durham algorithm, the theoretical uncertainty due to the renormalization scale ambiguity is *smaller* for the Cambridge than that for the Durham clustering. Of course, one has to keep in mind that the μ-dependence bands are not upper bounds on errors that arise from truncation of the perturbation series, just suggestions. In particular, if

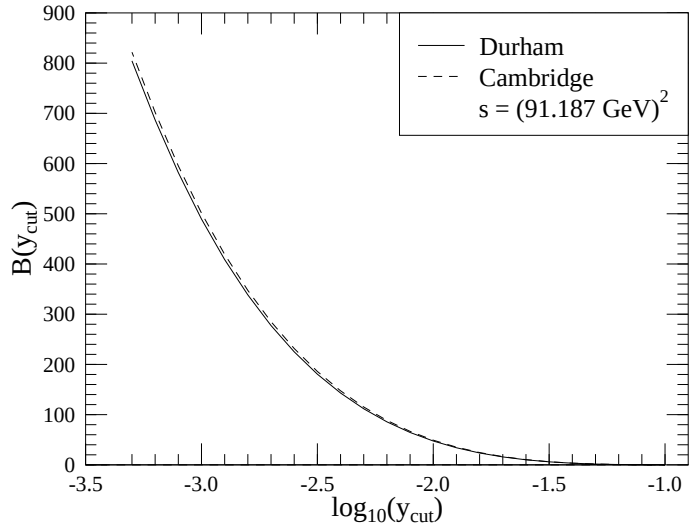

Figure 5.1: The Born function B_4 for the four-jet rate as a function of the resolution variable y_{cut} with Durham (solid) and Cambridge (dashed) algorithms.

there is an artificial narrowing of the μ-dependence bands, e.g. at a crossover point, they almost certainly do not represent the size of the truncation error at that point.

$$K(y_{cut}) = 1 + \eta(\sqrt{s})\frac{C_4(y_{cut})}{B_4(y_{cut})} \quad , \tag{5.2}$$

Four-jet fractions decrease very rapidly with increasing resolution parameter y_{cut}. As a result, most of the available four-jet data are below $y_{cut} = 0.01$. It is well-known that for small values of y_{cut} the fixed order perturbative prediction is not reliable, because the expansion parameter $\alpha_s \ln^2 y_{cut}$ logarithmically enhances the higher order corrections. One has to perform the all order resummation of the leading and next-to-leading logarithmic (NLL) contributions. This resummation is possible for the Durham algorithm using the coherent branching formalism [36] and the procedure is the same for the Cambridge algorithm [27]. The four-jet rate in the next-to-leading logarithmic approximation is given by [36]

$$\begin{aligned} R_4^{\rm NLL} &= 2[\Delta_q(Q)]^2\Bigg[\left(\int_{Q_0}^{Q} dq\, \Gamma_q(Q,q)\,\Delta_g(q,Q_0)\right)^2 \\ &+ \int_{Q_0}^{Q} dq\, \Gamma_q(Q,q)\,\Delta_g(q,Q_0) \\ &\quad \cdot \int_{Q_0}^{q} dq' \left(\Gamma_g(q,q')\,\Delta_g(q',Q_0) + \Gamma_f(q')\Delta_f(q',Q_0)\right)\Bigg] \quad . \end{aligned} \tag{5.3}$$

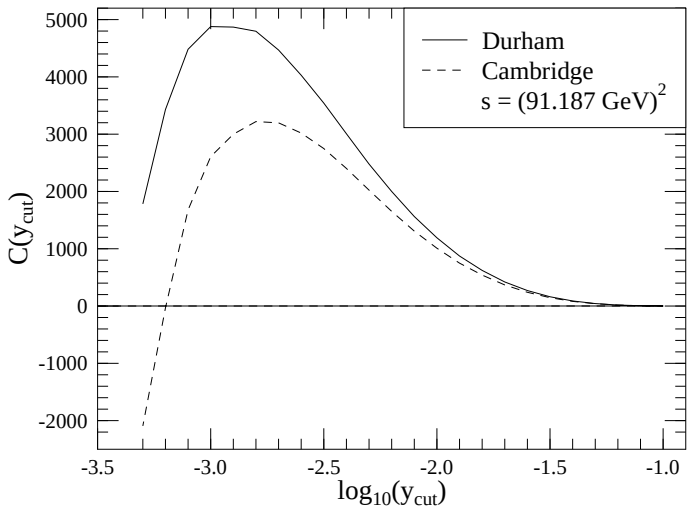

Figure 5.2: The correction function C_4 for the four-jet rate as a function of the resolution variable y_{cut} with Durham (solid) and Cambridge (dashed) algorithms.

In Eq. (5.3) the functions $\Delta_a(Q, Q_0)$ are the Sudakov form factors which express the probability of parton branching evolution from scale $Q_0 = Q\sqrt{y_{cut}}$ to scale Q without resolvable branching. The Sudakov factors are defined in terms of the $P_{ab}(\alpha_s(q), z)$ vertex probabilities as follows

$$\Delta_a(Q, Q_0) = \exp\left(-\sum_b \int_{Q_0}^{Q} \frac{dq}{q} \int dz \, \frac{\alpha_s(q)}{2\pi} \, P_{ab}(\alpha_s(q), z)\right) \quad . \tag{5.4}$$

It was shown in Ref. [37] that one can obtain an improved theoretical prediction for the differential two-jet rate if the vertex probabilities are taken at next-to-leading order [34], which we also consider in our analysis:

$$P_{qq}(\alpha_s, z) = C_F \left(\frac{1+z^2}{1-z} + \frac{\alpha_s}{2\pi} K \frac{2}{1-z}\right) \quad , \tag{5.5}$$

$$P_{gg}(\alpha_s, z) = 2C_A \left(\frac{z}{1-z} + \frac{1-z}{z} + z(1-z) + \frac{\alpha_s}{2\pi} K \frac{2}{z(1-z)}\right) \quad , \tag{5.6}$$

$$P_{gq}(\alpha_s, z) = T_R n_f \left(z^2 + (1-z)^2\right) \quad . \tag{5.7}$$

The K coefficient is renormalization scheme dependent. In the $\overline{\rm MS}$ scheme it is given by [33]

$$K = C_A \left(\frac{67}{18} - \frac{\pi^2}{6}\right) - \frac{10}{9} T_R n_f \quad . \tag{5.8}$$

Performing the z integral in Eq. (5.4) (upper and lower bound of z integral are determined by the collinear behaviour of the Durham algorithm), one obtains the

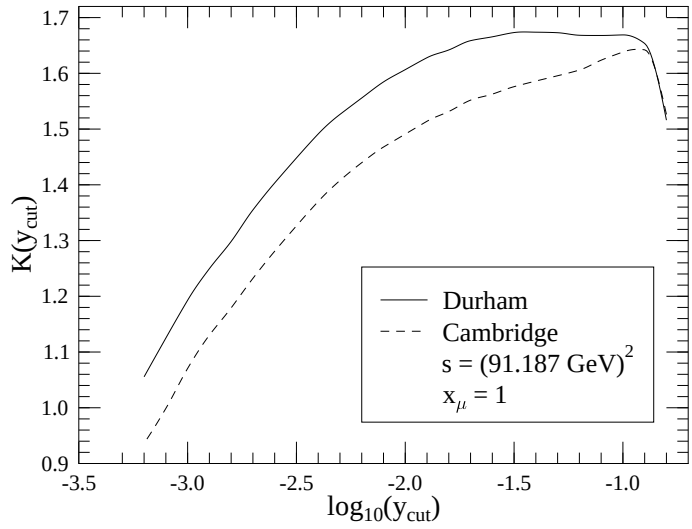

Figure 5.3: K factors as a function of the resolution variable y_{cut} for Durham (solid) and Cambridge (dashed) algorithms.

Sudakov factors as integrals of the emission probabilities $\Gamma_a(Q,q)$ in the following form:

$$\Delta_q(Q,Q_0) = \exp\left(-\int_{Q_0}^{Q} dq\,\Gamma_q(Q,q)\right) \ , \tag{5.9}$$

$$\Delta_g(Q,Q_0) = \exp\left(-\int_{Q_0}^{Q} dq\,\left[\Gamma_g(Q,q)+\Gamma_f(q)\right]\right) \ , \tag{5.10}$$

$$\Delta_f(Q,Q_0) = \frac{\left[\Delta_q(Q,Q_0)\right]^2}{\Delta_g(Q,Q_0)} \ , \tag{5.11}$$

and the NLL emission probabilities are

$$\Gamma_q(Q,q) = \frac{2C_F}{\pi}\frac{\alpha_s(q)}{q}\left[\left(1+\frac{\alpha_s(q)}{2\pi}\,K\right)\ln\frac{Q}{q}-\frac{3}{4}\right] \ , \tag{5.12}$$

$$\Gamma_g(Q,q) = \frac{2C_A}{\pi}\frac{\alpha_s(q)}{q}\left[\left(1+\frac{\alpha_s(q)}{2\pi}\,K\right)\ln\frac{Q}{q}-\frac{11}{12}\right] \ , \tag{5.13}$$

$$\Gamma_f(Q,q) = \frac{n_f}{3\pi}\frac{\alpha_s(q)}{q} \ . \tag{5.14}$$

We relate the $\alpha_s(q)$ strong coupling appearing in the emission probabilities to the strong coupling at the relevant renormalization scale, $\alpha_s(\mu)$, according to the one-

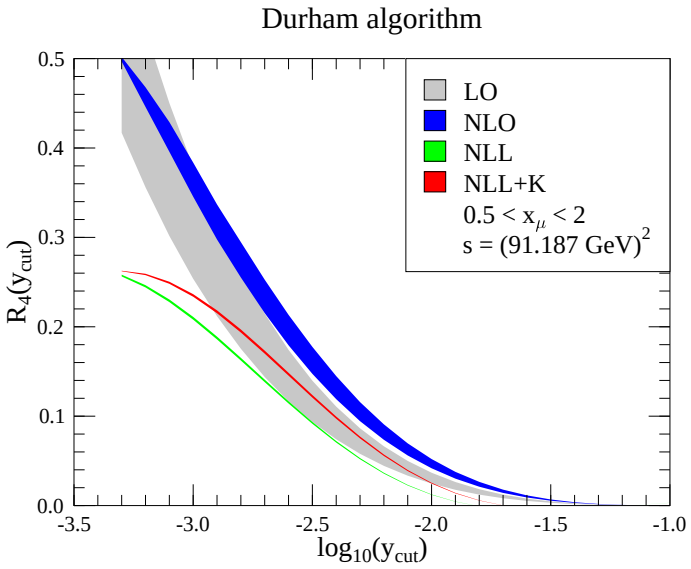

Figure 5.4: The QCD prediction for the four-jet rate with Durham clustering at Born level (light gray band) and at NLO (dark band). The two narrow bands show the four-jet rate in the NLL approximation ($K = 0$, lower band) and in improved NLL approximation (upper band) as explained in the text. The bands indicate the theoretical uncertainty due to the variation of the renormalization scale x_μ between 0.5 and 2.

loop formula

$$\alpha_s(q) = \frac{\alpha_s(\mu)}{1 - \beta_0 \frac{\alpha_s}{2\pi} \ln\left(\frac{\mu}{q}\right)} \quad , \tag{5.15}$$

where we use Eq. (2.42) for expressing $\alpha_s(\mu)$ in terms of $\alpha_s(M_Z) = 0.118$. We could also use a two-loop formula for $\alpha_s(q)$, but the result would differ only in subleading logarithms.

The result of this resummation together with its renormalization scale dependence is also shown in Figs. (5.4 and 5.5) (narrow bands). The lower band corresponds to the usual NLL approximation ($K = 0$), and the upper band is the result of the improved resummation. We can see clearly from the figures that the fixed-order and the NLL approximations differ significantly. One expects that for large values of y_{cut} the former, and for small values of y_{cut} the latter is the reliable description, therefore, the two results have to matched.

The Durham and Cambridge four-jet rates can be resummed at leading and next-to-leading logarithmic order, but they do not satisfy a simple exponentiation [35]. For observables that do not exponentiate the viable matching schemes are the R matching

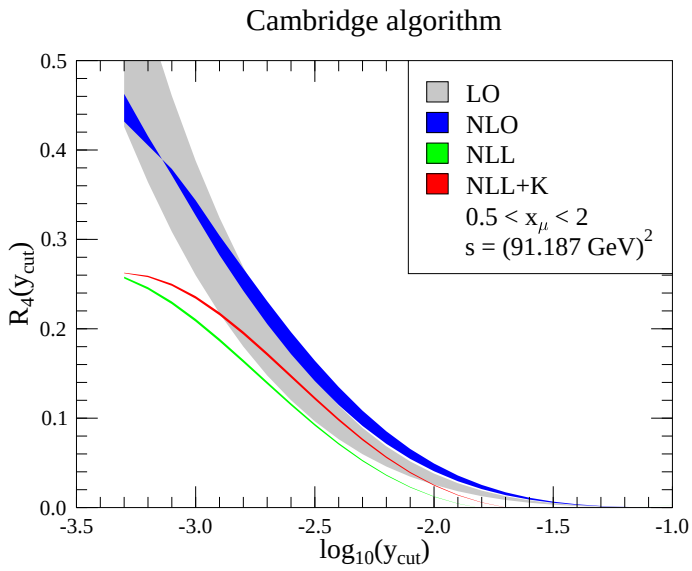

Figure 5.5: The QCD prediction for the four-jet rate with Cambridge clustering at Born level (light gray band) and at NLO (dark band). The two narrow bands show the four-jet rate in the NLL approximation ($K = 0$, lower band) and in improved NLL approximation (upper band) as explained in the text. The bands indicate the theoretical uncertainty due to the variation of the renormalization scale x_μ between 0.5 and 2.

or the modified R matching [36, 58]. We use R matching according to the following formula:

$$R_4^{\mathrm{R-match}} = R_4^{\mathrm{NLL}} + \eta^2 \left(B_4 - B_4^{\mathrm{NLL}}\right) + \eta^3 \left(C_4 - C_4^{\mathrm{NLL}} - \frac{3}{2}\left(B_4 - B_4^{\mathrm{NLL}}\right)\right), \quad (5.16)$$

where B_4^{NLL} and C_4^{NLL} are the coefficients in the expansion of R_4^{NLL} as in Eq. (5.1).

In Fig. (5.6) we show the theoretical prediction at the various levels of approximation: in fixed order perturbation theory at Born level (LO), at NLO (NLO), resummed and R-matched prediction (NLO+NLL) and improved resummed and R-matched prediction (NLO+NLL+K). Also shown is the four-jet rate measured by the ALEPH collaboration at the Z^0 peak [64] corrected to parton level using the PYTHIA Monte Carlo [32]. We used bin-by-bin correction and the consistency of the correction was checked by using the HERWIG Monte Carlo [31]. The two programs gave the same correction factor within statistical error. The errors of the data are the scaled errors of the published hadron level data, and we did not include any systematic error due to the hadron to parton correction. In the inset we indicated the renormalization scale dependence of the 'NLO+NLL+K' prediction.

In Fig. (5.6) deserves several remarks. First of all, we see that the inclusion of the

radiative corrections improves the fixed order description of the data using the natural scale $x_\mu = 1$ for larger values of y_{cut}. Secondly, the importance of resummation in the

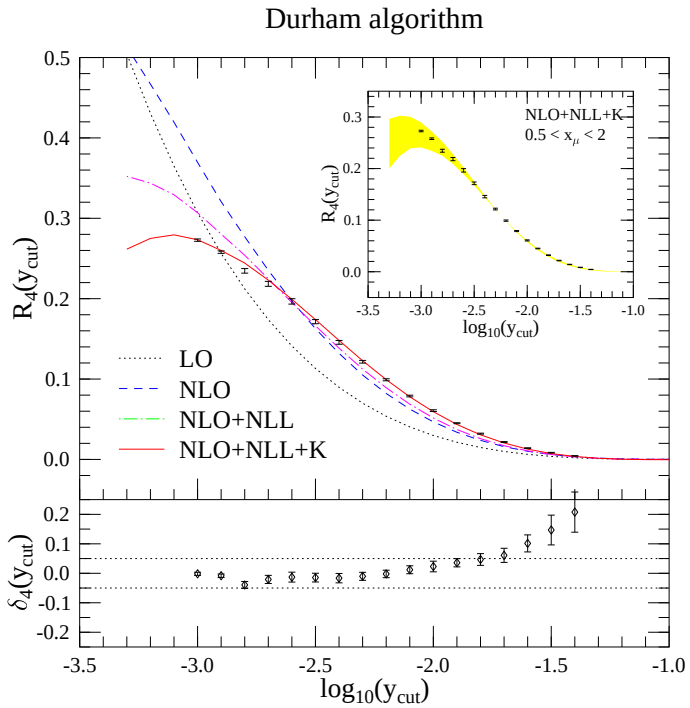

Figure 5.6: The QCD prediction for the four-jet rate with Durham clustering in fixed order perturbation theory at leading (dotted) and NLO (dashed), and fixed order matched with resummed (dashed-dotted) and improved resummed (solid) calculation compared to ALEPH data obtained at the Z^0 peak and corrected to parton level (errorbars). The renormalization scale is set to $x_\mu = 1$. The lower plot shows the relative difference $\delta_4 = (\text{data} - \text{theory})/\text{theory}$, where theory means the NLO prediction matched with improved resummed calculation at $x_\mu = 1$. The inset shows the renormalization scale dependence of the 'theory' prediction with scale variation $0.5 < x_\mu < 2$.

small y_{cut} region is clearly seen, but it is still not sufficient to describe the data at the natural scale, neglected subleading terms are still important.[1] On the other hand, the improved resummation seems to take into account just the right amount of subleading terms and it makes the agreement between data and theory almost perfect over the whole y_{cut} region as can be seen from the lower plot. (Although for $y_{cut} > 10^{-1.7}$ δ_4 falls outside the $\pm 5\,\%$ band, one should keep in mind that in this region the error of

[1] Our 'NLO+NLL' results differ from those in Ref. [70], where $\alpha_s(q)$ in calculating $R_4^{\rm NLL}$ was kept at the fix $\alpha_s(M_Z)$ value [71].

the hadron to parton correction is very large. Also, for the 'NLO+NLL+K' prediction we found remarkably small scale dependence for $y_{cut} > 10^{-3}$. This feature, however, should be taken with care. The improvement, obtained by including the two-loop coefficient K, affects NNLL terms, but there are other contributions of the same order that are not taken into account (e.g., NLO running of α_s and other dynamical effects), which is not the case for the 2-jet rate. The scale dependence of the 'NLO+NLL+K' result would consistently be under control only after the inclusion of the complete set of NNLL terms.

Finally it is worth noting that for $y_{cut} = 10^{-2.6}$ both PYTHIA and HERWIG yield less than 2 % hadronization correction. At the same value of the resolution parameter the theoretical prediction is insensitive to corrections beyond next-to-leading order (the NLO, NLO+NLL, NLO+NLL+K curves cross, the renormalization scale dependence is small), therefore, at this accidental value of y_{cut} the NLO prediction agrees perfectly with the hadron level data.

5.2 Event shape variables

Four-jet event shapes were used extensively by the LEP collaborations for QCD studies [64, 65]. In this subsection we consider four shape variables, the y_4 distributions for the Durham and Cambridge algorithms, the thrust minor ($T_{\rm min}$), the C parameter for C values above 0.75 and the D parameter, which are often used in the experimental analyses.

In the case of event shape distributions we multiply the normalized cross section with the value of the event shape parameter, so we use the parametrisation

$$\Sigma(O_4) \equiv \frac{O_4}{\sigma_0}\frac{d\sigma_4}{dO_4}(O_4) = \eta(\mu)^2 B(O_4) + \eta(\mu)^3 \left[B(O_4)\frac{\beta_0}{C_F}\ln x_\mu^2 + C(O_4) \right] \quad (5.17)$$

and the average value of the shape variable is easily obtained from the differential distribution:

$$\langle O_4 \rangle_\delta = \int_\delta^1 dO_4\, \Sigma(O_4)\,. \quad (5.18)$$

Using this parametrisation we define the K factors of the differential distribution as

$$K(O_4) = 1 + \eta(\sqrt{s})\,\frac{C(O_4)}{B(O_4)}\,. \quad (5.19)$$

In the following we plot the physical cross sections $\Sigma(O_4)$, the $K(O_4)$ factors and tabulate the correction functions $C(O_4)$ for $O_4 = y_4$, $T_{\rm min}$,D and C.

The y_4 value denotes the transition value for y_{cut} at which, when decreasing y_{cut}, the classification of a given event changes from three jets to four jets. The advantage of this variable over the differential four-jet rate is that this variable can be defined on an event by event basis. Depending on the actual resolution variable one obtains the

y_4^D distribution for the Durham clustering and the y_4^C distribution for the Cambridge clustering. We calculated the $B(y_4)$ and $C(y_4)$ functions for both algorithms. The $B(y_4)$ values equal the $y_{cut}B(y_{cut})$ values when $y_4 = y_{cut}$, therefore, we tabulate only the $C(y_4)$ functions for the two algorithms in Table (5.3). We show the NLO

Table 5.3: Correction functions to the differential distributions of the y_4 variables for the Durham and Cambridge algorithm. The parameter values are at the lower edge of the corresponding histogram bin.

y_4	$C(y_4^D)$	$C(y_4^C)$
0.000	$(2.523 \pm 0.425) \cdot 10^3$	$(1.064 \pm 0.350) \cdot 10^3$
0.005	$(2.212 \pm 0.017) \cdot 10^3$	$(1.857 \pm 0.019) \cdot 10^3$
0.010	$(1.376 \pm 0.009) \cdot 10^3$	$(1.166 \pm 0.011) \cdot 10^3$
0.015	$(9.429 \pm 0.071) \cdot 10^2$	$(8.144 \pm 0.080) \cdot 10^2$
0.020	$(6.799 \pm 0.070) \cdot 10^2$	$(5.855 \pm 0.062) \cdot 10^2$
0.025	$(4.930 \pm 0.063) \cdot 10^2$	$(4.346 \pm 0.051) \cdot 10^2$
0.030	$(3.760 \pm 0.042) \cdot 10^2$	$(3.293 \pm 0.043) \cdot 10^2$
0.035	$(2.885 \pm 0.037) \cdot 10^2$	$(2.553 \pm 0.039) \cdot 10^2$
0.040	$(2.164 \pm 0.033) \cdot 10^2$	$(1.947 \pm 0.034) \cdot 10^2$
0.045	$(1.754 \pm 0.026) \cdot 10^2$	$(1.580 \pm 0.027) \cdot 10^2$
0.050	$(1.314 \pm 0.025) \cdot 10^2$	$(1.202 \pm 0.025) \cdot 10^2$
0.055	$(1.024 \pm 0.021) \cdot 10^2$	$(9.508 \pm 0.213) \cdot 10^1$
0.060	$(8.293 \pm 0.292) \cdot 10^1$	$(7.692 \pm 0.296) \cdot 10^1$
0.065	$(6.307 \pm 0.300) \cdot 10^1$	$(5.945 \pm 0.304) \cdot 10^1$
0.070	$(4.636 \pm 0.180) \cdot 10^1$	$(4.445 \pm 0.184) \cdot 10^1$
0.075	$(3.516 \pm 0.117) \cdot 10^1$	$(3.430 \pm 0.114) \cdot 10^1$
0.080	$(2.673 \pm 0.115) \cdot 10^1$	$(2.560 \pm 0.110) \cdot 10^1$
0.085	$(2.271 \pm 0.216) \cdot 10^1$	$(2.214 \pm 0.217) \cdot 10^1$
0.090	$(1.412 \pm 0.204) \cdot 10^1$	$(1.395 \pm 0.206) \cdot 10^1$
0.095	$(1.085 \pm 0.057) \cdot 10^1$	$(1.056 \pm 0.059) \cdot 10^1$
0.100	$(7.412 \pm 0.584) \cdot 10^0$	$(7.377 \pm 0.588) \cdot 10^0$
0.105	$(5.069 \pm 0.537) \cdot 10^0$	$(5.121 \pm 0.529) \cdot 10^0$
0.110	$(2.817 \pm 0.400) \cdot 10^0$	$(2.914 \pm 0.399) \cdot 10^0$
0.115	$(2.652 \pm 0.329) \cdot 10^0$	$(2.428 \pm 0.301) \cdot 10^0$
0.120	$(1.353 \pm 0.221) \cdot 10^0$	$(1.516 \pm 0.183) \cdot 10^0$

perturbative prediction in QCD for $\Sigma(y_4)$ in Fig. (5.7). In the same figure, the inset shows the $K(y_4)$ factors of the distributions. The physical cross sections for the two algorithms are very similar. The $K(y_4)$ factors are quite large, but much smaller than in the case of other four-jet event shape distributions. They depend weakly on the y_4 value for $y_4 > 0.1$ and decrease rapidly with decreasing y_4 below $y_4 = 0.1$. In the case of the Cambridge algorithm the radiative corrections are 15–30 % smaller than those for the Durham algorithm.

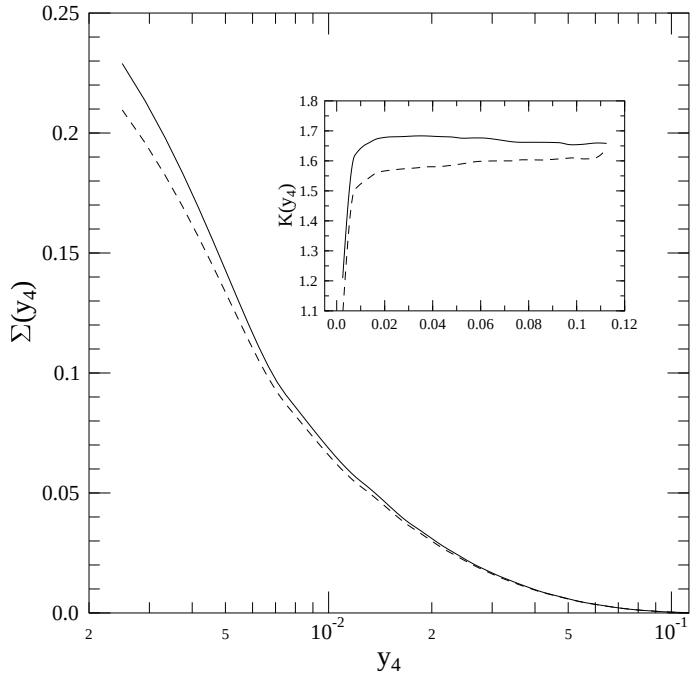

Figure 5.7: The NLO QCD prediction for the y_4^D (solid) and y_4^C (dashed) differential distributions with renormalization scale $x_\mu = 1$. The inset shows the K factors of the distributions.

The event shape variables thrust minor ($T_{\rm min}$), C and D parameters are defined in Sec. (3.2). The kinematical limit of the C parameter for three-parton processes is C = 0.75. Therefore, in the region C $\in [0.75, 1]$ the four-parton processes contribute to the leading order prediction, and our program is capable to calculate the radiative correction to the distribution. The results of such a calculation for the Born functions $B(T_{\rm min})$, $B(C)$ and $B(D)$ agree with the known results (see e.g., [49]). The $C(T_{\rm min})$ and $C(C)$ correction functions are given in Table (5.4).

In the case of event shape differential distributions the NLO corrections should logarithmically diverge at the edge of the phase space. This divergence occurs at zero for the y_4, $T_{\rm min}$ and D parameter distributions and is regularized by the multiplication with the value of the variable (see Eq. (5.17)). This is not the case for the C parameter, because it diverges at C = 0.75. Nevertheless, we obtained a finite and positive contribution in the first bin owing to bin smearing as we have checked explicitly by refining the bin width.

Figs. (5.8) show the leading and NLO QCD prediction for the $T_{\rm min}$ differential distributions at $x_\mu = 1$. The inset show the K factor which is large indicating 100 % or larger radiative corrections. As a result, the renormalization scale dependence remains large, only the absolute normalization of the distributions increases with a

Table 5.4: Correction functions to the differential distributions of the $T_{\min}$ and C parameter event shape variables. The parameter values are at the lower edge of the corresponding histogram bin.

$T_{\min}$	$C(T_{\min})$	C	$C(C)$	D	$C(D)$
0.00	—	0.75	$(4.775 \pm 1.100) \cdot 10^3$	0.00	$(1.08 \pm 0.06) \cdot 10^4$
0.02	$(3.319 \pm 0.270) \cdot 10^4$	0.76	$(6.082 \pm 0.160) \cdot 10^3$	0.04	$(1.24 \pm 0.02) \cdot 10^4$
0.04	$(2.381 \pm 0.082) \cdot 10^4$	0.77	$(4.610 \pm 0.089) \cdot 10^3$	0.08	$(8.59 \pm 0.12) \cdot 10^3$
0.06	$(1.652 \pm 0.038) \cdot 10^4$	0.78	$(3.663 \pm 0.063) \cdot 10^3$	0.12	$(6.24 \pm 0.12) \cdot 10^3$
0.08	$(1.172 \pm 0.025) \cdot 10^4$	0.79	$(2.904 \pm 0.042) \cdot 10^3$	0.16	$(4.99 \pm 0.11) \cdot 10^3$
0.10	$(8.600 \pm 0.130) \cdot 10^3$	0.80	$(2.406 \pm 0.031) \cdot 10^3$	0.20	$(3.85 \pm 0.06) \cdot 10^3$
0.12	$(6.488 \pm 0.100) \cdot 10^3$	0.81	$(1.948 \pm 0.026) \cdot 10^3$	0.24	$(2.98 \pm 0.05) \cdot 10^3$
0.14	$(4.695 \pm 0.077) \cdot 10^3$	0.82	$(1.625 \pm 0.024) \cdot 10^3$	0.28	$(2.52 \pm 0.05) \cdot 10^3$
0.16	$(3.499 \pm 0.042) \cdot 10^3$	0.83	$(1.365 \pm 0.023) \cdot 10^3$	0.32	$(1.94 \pm 0.05) \cdot 10^3$
0.18	$(2.684 \pm 0.027) \cdot 10^3$	0.84	$(1.135 \pm 0.019) \cdot 10^3$	0.36	$(1.59 \pm 0.04) \cdot 10^3$
0.20	$(2.010 \pm 0.021) \cdot 10^3$	0.85	$(9.194 \pm 0.130) \cdot 10^2$	0.40	$(1.37 \pm 0.03) \cdot 10^3$
0.22	$(1.498 \pm 0.017) \cdot 10^3$	0.86	$(7.906 \pm 0.110) \cdot 10^2$	0.44	$(1.06 \pm 0.03) \cdot 10^3$
0.24	$(1.122 \pm 0.013) \cdot 10^3$	0.87	$(6.293 \pm 0.092) \cdot 10^2$	0.48	$(8.72 \pm 0.19) \cdot 10^2$
0.26	$(8.247 \pm 0.100) \cdot 10^2$	0.88	$(5.217 \pm 0.084) \cdot 10^2$	0.52	$(7.11 \pm 0.16) \cdot 10^2$
0.28	$(6.093 \pm 0.074) \cdot 10^2$	0.89	$(4.296 \pm 0.066) \cdot 10^2$	0.56	$(5.68 \pm 0.14) \cdot 10^2$
0.30	$(4.501 \pm 0.180) \cdot 10^2$	0.90	$(3.391 \pm 0.052) \cdot 10^2$	0.60	$(4.46 \pm 0.21) \cdot 10^2$
0.32	$(3.026 \pm 0.057) \cdot 10^2$	0.91	$(2.815 \pm 0.061) \cdot 10^2$	0.64	$(3.52 \pm 0.11) \cdot 10^2$
0.34	$(2.229 \pm 0.050) \cdot 10^2$	0.92	$(2.075 \pm 0.057) \cdot 10^2$	0.68	$(2.74 \pm 0.09) \cdot 10^2$
0.36	$(1.549 \pm 0.046) \cdot 10^2$	0.93	$(1.626 \pm 0.032) \cdot 10^2$	0.72	$(2.08 \pm 0.08) \cdot 10^2$
0.38	$(1.095 \pm 0.028) \cdot 10^2$	0.94	$(1.221 \pm 0.026) \cdot 10^2$	0.76	$(1.54 \pm 0.06) \cdot 10^2$
0.40	$(7.100 \pm 0.210) \cdot 10^1$	0.95	$(8.154 \pm 0.260) \cdot 10^1$	0.80	$(1.03 \pm 0.04) \cdot 10^2$
0.42	$(4.437 \pm 0.180) \cdot 10^1$	0.96	$(5.193 \pm 0.190) \cdot 10^1$	0.84	$(6.66 \pm 0.31) \cdot 10^1$
0.44	$(2.684 \pm 0.190) \cdot 10^1$	0.97	$(3.165 \pm 0.130) \cdot 10^1$	0.88	$(3.89 \pm 0.20) \cdot 10^1$
0.46	$(1.439 \pm 0.150) \cdot 10^1$	0.98	$(1.312 \pm 0.094) \cdot 10^1$	0.92	$(1.71 \pm 0.19) \cdot 10^1$
0.48	$(6.447 \pm 0.560) \cdot 10^0$	0.99	$(2.769 \pm 0.260) \cdot 10^0$	0.96	$(2.60 \pm 1.30) \cdot 10^0$

factor of more than 2 with the inclusion of the radiative corrections. This feature is demonstrated in Fig. (5.9), where we show the scale dependence of the leading and NLO prediction for the average value of the thrust minor (above $T_{\min} = 0.02$). The leading and NLO curves run almost parallel down to $x_\mu \simeq 0.2$, only the latter is shifted to larger values. The large renormalization scale dependence indicates that the higher order corrections are important. One may conclude that, these distributions cannot be reliably calculated in fixed order perturbation theory and cannot be used for precision tests of QCD.

5.3 Four-Jet angular correlation

This type of the jet observables measures the correlation between the jets. Fist, we have to select the four jet events from final state and determine the the momenta

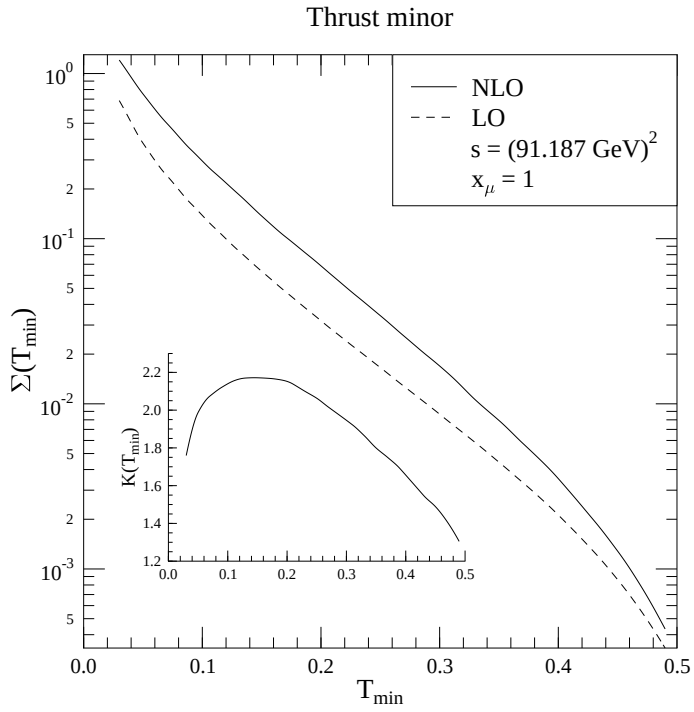

Figure 5.8: The leading-order (dashed) and the NLO (solid) QCD prediction for the $T_{\rm min}$ variable with renormalization scale $x_\mu = 1$. The inset shows the K factor of the distribution.

of the jets. For this selection we can use one of the jet clustering algorithms defined in Sec. (3.2). We will use the Durham and Cambridge jet clustering algorithms at a fixed jet resolution parameter $y_{cut} = 0.008$ which is the value used by the ALEPH Collaboration [66]. Using the Cambridge algorithm, the hadronization corrections are expected to be much smaller therefore, the perturbative prediction is more reliable.

In order to define the angular variables we denote the three-momenta of the four jets by $\vec{p}_i$, $(i = 1, 2, 3, 4)$ and label jets in order of descending jet energy, such that jet 1 has the highest energy and jet 4 has the smallest. The four variables are the Körner-Schierholz-Willrodt variable [20],
$\cos\phi_{\rm KSW}$ is the cosine of the average of two angles between planes spanned by the jets,

$$\phi_{\rm KSW} = \frac{1}{2}\left(\arccos\left(\frac{(\vec{p}_1\times\vec{p}_4)\cdot(\vec{p}_2\times\vec{p}_3)}{|\vec{p}_1\times\vec{p}_4||\vec{p}_2\times\vec{p}_3|}\right) + \arccos\left(\frac{(\vec{p}_1\times\vec{p}_3)\cdot(\vec{p}_2\times\vec{p}_4)}{|\vec{p}_1\times\vec{p}_3||\vec{p}_2\times\vec{p}_4|}\right)\right); \tag{5.20}$$

the modified Nachtmann-Reiter variable [21], $|\cos\theta^*_{\rm NR}|$ is the absolute value of the

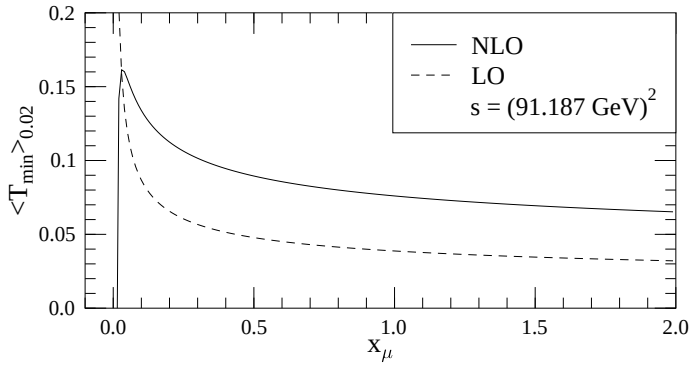

Figure 5.9: The renormalization scale dependence of the average values of thrust minor ($< T_{\rm min} >_{0.02}$) at leading and next-to-leading order.

cosine of the angle between the vectors $\vec{p}_1 - \vec{p}_2$ and $\vec{p}_3 - \vec{p}_4$,

$$\cos\theta^*_{\rm NR} = \frac{(\vec{p}_1 - \vec{p}_2)\cdot(\vec{p}_3 - \vec{p}_4)}{|\vec{p}_1 - \vec{p}_2||\vec{p}_3 - \vec{p}_4|}\,; \tag{5.21}$$

$\cos\alpha_{34}$ [24], the cosine of the angle between the two smallest energy jets,

$$\cos\alpha_{34} = \frac{\vec{p}_3\cdot\vec{p}_4}{|\vec{p}_3||\vec{p}_4|}\,; \tag{5.22}$$

the Bengtsson-Zerwas correlation [23], $|\cos\chi_{\rm BZ}|$ is the absolute value of the cosine of the angle between the plane spanned by jets 1 and 2 and that by jets 3 and 4,

$$\cos\chi_{\rm BZ} = \frac{(\vec{p}_1\times\vec{p}_2)\cdot(\vec{p}_3\times\vec{p}_4)}{|\vec{p}_1\times\vec{p}_2||\vec{p}_3\times\vec{p}_4|}\,; \tag{5.23}$$

The NLO differential cross sections of these variables are given in the following general form

$$\frac{1}{\sigma_0}\frac{d\sigma}{dz}(z) = \eta(\mu)^2 B(z) + \eta(\mu)^3\left[B(z)\frac{\beta_0}{C_F}\ln\frac{\mu^2}{s} + C(z)\right]\,, \tag{5.24}$$

where $\eta(\mu) = \alpha_s(\mu)/(2\pi)C_F$ is the coupling constant and $z = \cos\phi_{\rm KSW}$, $|\cos\theta^*_{\rm NR}|$, $\cos\alpha_{34}$, $|\cos\chi_{\rm BZ}|$. σ_0 denotes the Born cross section for the process $e^+e^- \to \bar{q}q$, s is the total c.m. energy squared, μ is the renormalization scale, while B_{O_4} and $C(z)$ are scale independent functions, $B(z)$ is the Born approximation and $C(z)$ is the radiative correction. We use the two-loop expression for the running coupling in Eq. (2.42) and set the number of light quark flavours to $n_f = 5$.

The Born approximation and the higher order correction are linear and quadratic forms of ratios of the color charges (see Appendix A and B)

$$B = B_0 + B_x\,x + B_y\,y\,, \tag{5.25}$$

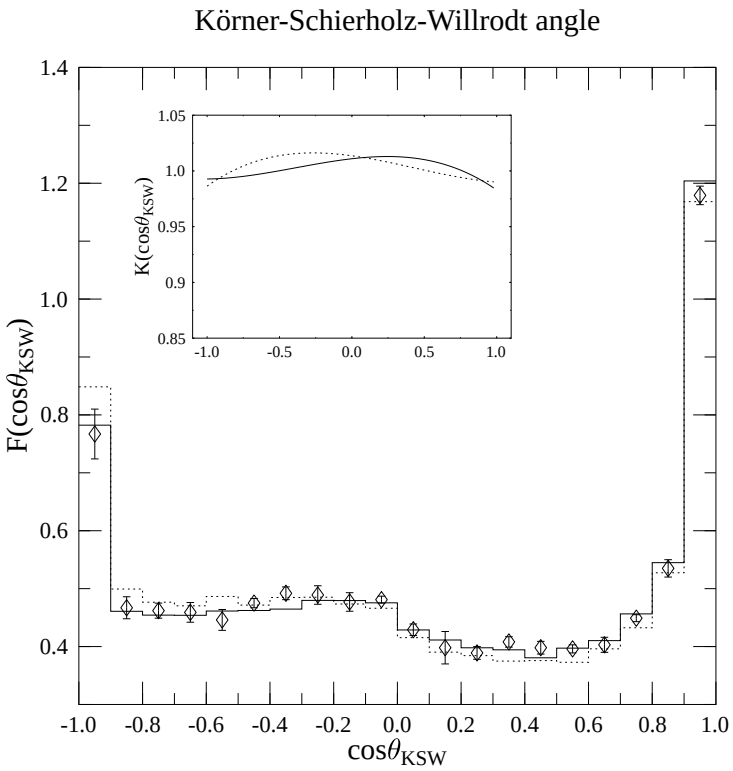

Figure 5.10: Comparison of the NLO QCD prediction for the $\cos\phi_{\rm KSW}$ distribution obtained using Durham (solid) and Cambridge (dotted) jet algorithm with ALEPH data (diamonds). In the window the K factor of the distribution with Durham (solid) and with the Cambridge (dotted) algorithm is shown.

and

$$C = C_0 + C_x\, x + C_y\, y + C_z\, z + C_{xx}\, x^2 + C_{xy}\, x\, y + C_{yy}\, y^2 \ , \qquad (5.26)$$

where the ratio z appears that is related to the square of a cubic Casimir

$$C_3 = \sum_{a,b,c=1}^{N_A} {\rm Tr}(t^a t^b t^c){\rm Tr}(t^c t^b t^a) \ , \qquad z = \frac{C_3}{N_c C_F^3} \ . \qquad (5.27)$$

The Born functions B_i are obtained by integrating the fully exclusive O(α_s^2) ERT matrix elements [48] and were used by the experimental collaborations [67, 24, 68, 69, 66]. At the end of this section in Tables (5.7–5.14) we tabulated the numerical value of the NLO kinematic functions C_i for these angular variables for the Durham and Cambridge clustering algorithms. We do not show the value of the C_z functions in Ref. [5] because they turn out to be negligible. The C values were obtained according

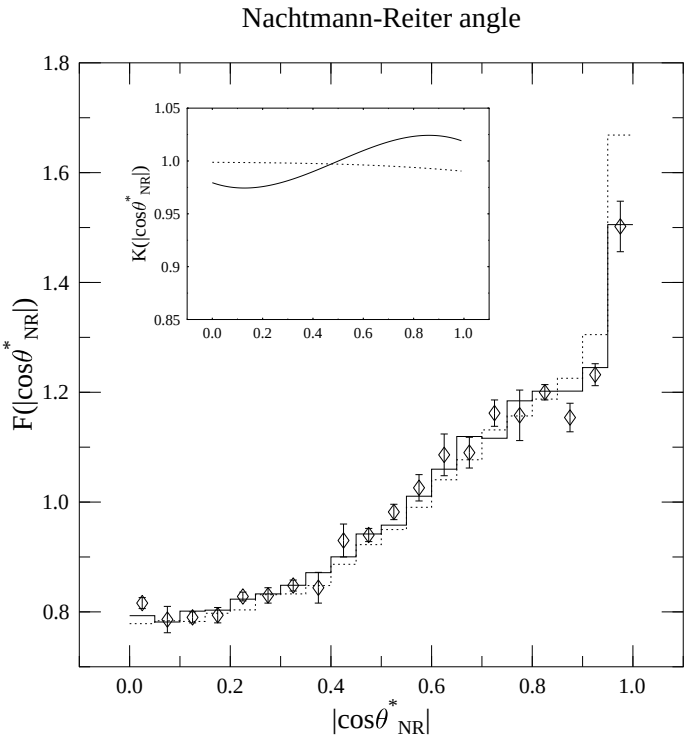

Figure 5.11: Comparison of the NLO QCD prediction for the $|\cos\theta^*_{\rm NR}|$ distribution obtained using Durham (solid) and Cambridge (dotted) jet algorithm with ALEPH data (diamonds). In the window the K factor of the distribution with Durham (solid) and with the Cambridge (dotted) algorithm is shown.

to Eq. (5.26). Comparing the size of the corrections for these two algorithms, we see that in general the C_i functions in the case of the Cambridge algorithm are 10–20 % smaller.

We use the numerical values for the kinematic functions to calculate the NLO QCD predictions for the SU(3) values $x = 9/4$, $y = 3/8$ according to Eq. (5.24) at $x_\mu = \mu/\sqrt{s} = 1$. We compare our predictions for the Durham algorithm (solid histograms) to ALEPH data (diamonds) in Figs. (5.10–5.13). In order to make this comparison we normalize the histograms to one, therefore

$$F(z) = \frac{1}{\sigma}\frac{d\sigma}{dz}(z) \ , \qquad \sigma = \int dz \ \frac{d\sigma}{dz}(z) \ . \tag{5.28}$$

The qualitative agreement between data and theory is very good. Also shown in these figures our results for the Cambridge algorithm (dotted histograms). The statistical error of the Monte Carlo integrals is below 1.5 % for the Durham algorithm

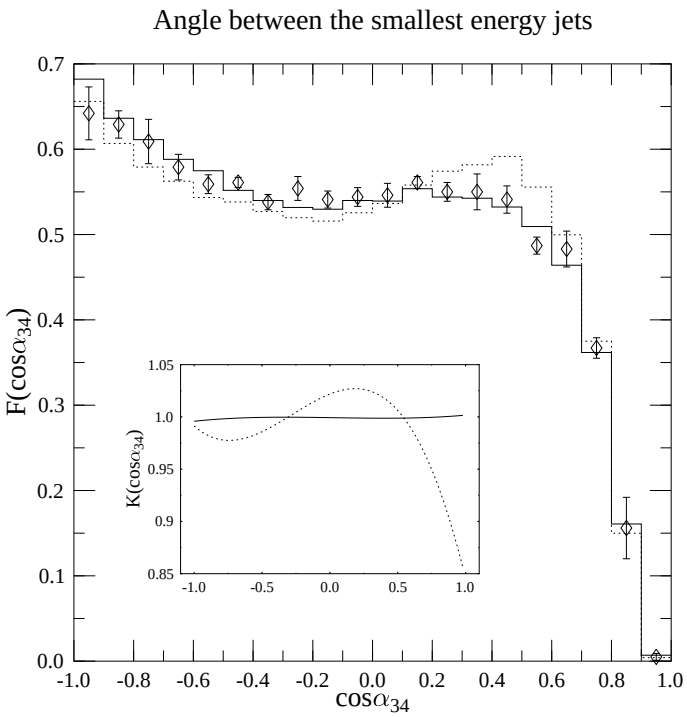

Figure 5.12: Comparison of the NLO QCD prediction for the $\cos\alpha_{34}$ distribution obtained using Durham (solid) and Cambridge (dotted) jet algorithm with ALEPH data (diamonds). In the window the K factor of the distribution with Durham (solid) and with the Cambridge (dotted) algorithm is shown.

and below 2 % in the case of the Cambridge algorithm in each of the bins. In the same figures, the windows show polynomial fits to the $K(z) = F_{NLO}(z)/F_{LO}(z)$ factors of the normalized distributions. The $\chi^2/N_{\rm dof}$ of these fits is between (1.5–7)/20. The K factors for the $|\cos\chi_{\rm BZ}|$ distributions, for the $\cos\alpha_{34}$ distribution with Durham algorithm and for the $|\cos\theta^*_{\rm NR}|$ distribution with the Cambridge algorithm are approximately constant 1 over the whole range, therefore the shape of the leading and NLO distributions are very similar in these cases.

Leading order versus next-to-leading order

A quantitative comparison of the data for the angular distributions to the NLO prediction decomposed in a quadratic form of the color factor ratios with group independent kinematical functions as coefficients makes possible a simultaneous fit of the strong coupling and the color charge ratios. That procedure would require a full experimental analysis which is not our goal. What we would like to do is to give a reliable estimate

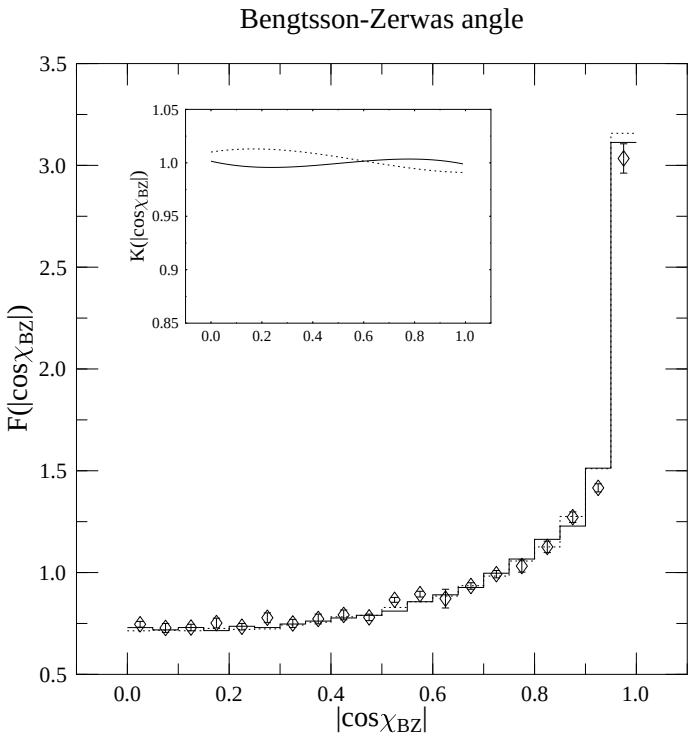

Figure 5.13: Comparison of the NLO QCD prediction for the $|\cos\chi_{\rm BZ}|$ distribution obtained using Durham (solid) and Cambridge (dotted) jet algorithm with ALEPH data (diamonds). In the window the K factor of the distribution with Durham (solid) and with the Cambridge (dotted) algorithm is shown.

of the systematic theoretical uncertainty coming from the use of the leading order perturbative prediction instead of the NLO one in a color charge measurement. We "produce" data using our NLO prediction with $SU(3)$ values $x = 9/4$ and $y = 3/8$ and perform a leading order fit of x and y using the B_0, B_x and B_y functions. We use χ^2 minimalization to obtain the best values with

$$\chi^2 = \sum_i \frac{1}{w_i^2}\left(\frac{B_0(z_i) + xB_x(z_i) + yB_y(z_i)}{\sigma_0 + x\sigma_x + y\sigma_y} - \frac{1}{\sigma_{\rm NLO}}\frac{d\sigma_{\rm NLO}}{dz}(z_i)\right)^2 \quad , \qquad (5.29)$$

where w_i denotes the statistical error of the normalized NLO distribution in the ith bin, the summation runs over the bins and σ_j ($j = 0$, x, y or NLO) defined as

$$\sigma_j = \int dz\, B_j(z)\,, \qquad \sigma_{\rm NLO} = \int dz\, \frac{d\sigma_{\rm NLO}}{dz}(z) \ . \qquad (5.30)$$

As a check of the fit we also performed a linear fit to the not normalized distributions in the form

$$\chi^2 = \sum_i \frac{1}{w_i^2} \left(\eta(B_0(z_i) + xB_x(z_i) + yB_y(z_i)) - \frac{d\sigma_{\rm NLO}}{dz}(z_i) \right)^2 , \qquad (5.31)$$

where w_i is the statistical error of the NLO distribution in the ith bin, and with η fitted as well. The two procedures give the same result for x and y to very good accuracy.

Table 5.5: Leading order fit of the color charge ratios to the next-to-leading order differential distributions of the angular correlations.

Observable	x	y
	Durham algorithm	
$\cos\phi_{\rm KSW}$	2.21 ± 0.05	0.58 ± 0.07
$\lvert\cos\theta^*_{\rm NR}\rvert$	1.41 ± 1.43	0.08 ± 0.11
$\cos\alpha_{34}$	2.08 ± 0.21	0.57 ± 0.23
$\lvert\cos\chi_{\rm BZ}\rvert$	1.15 ± 1.43	0.12 ± 0.31
all four	2.32 ± 0.03	0.29 ± 0.02
	Cambridge algorithm	
$\cos\phi_{\rm KSW}$	2.30 ± 0.08	0.52 ± 0.09
$\lvert\cos\theta^*_{\rm NR}\rvert$	0.99 ± 2.70	0.21 ± 0.31
$\cos\alpha_{34}$	0.34 ± 0.42	2.65 ± 0.48
$\lvert\cos\chi_{\rm BZ}\rvert$	3.53 ± 2.80	0.82 ± 0.68
all four	2.29 ± 0.05	0.45 ± 0.03

We performed the fit for each angular distribution separately, as well as for the four angular variables combined. Table (5.5) contains the results of these fits. We see that the shifts in the x–y values are quite large. Looking at the errors, one finds that the shift is significant only if the K factor of the corresponding distribution (see Figs. (5.10–5.13)) ííis not constant 1. For those cases when the shapes of the leading order and the NLO distributions are very similar, i.e. the $K \simeq 1$, then the fits give values compatible with the canonical QCD values. The origin of the large errors in some fits is the global correlation between the two parameters x and y in the fit. In these cases — $|\cos\theta^*_{\rm NR}|$, $\cos\alpha_{34}$ and $|\cos\chi_{\rm BZ}|$ distributions — one cannot fit both variables reliably. Instead, one can fit either the ratio of the two parameters, or fix one parameter to the SU(3) value and fix the other. For instance, fixing $x = 9/4$ one obtains the fitted values for y as given in Table (5.6). We observe from Figs. (5.10–5.13)) and Table (5.6) that in those cases, when $K \simeq 1$ the result of the fit is in agreement with SU(3) — Durham $\cos\alpha_{34}$, $|\cos\chi_{\rm BZ}|$ and Cambridge $|\cos\theta^*_{\rm NR}|$ distributions —, while for the rest of the distributions we obtain fit parameter different from the SU(3) value because the shapes of the leading and NLO distributions are

different. We show the result of the combined fit of all four variables in Fig. (5.14) in the form of 68.3 % and 95 % confidence level contours in the x–y plane with ellipses centered on the best x–y pair. There are five contours sitting on three different centers in each plot. The fits with both 1- and 2-σ contours were obtained using all four angular distributions with all bins included. The fit with only 1-σ contour shown corresponds to the "ALEPH choice": using all four variables with fit ranges $0.1 \leq |\cos\chi_{\rm BZ}|,\ |\cos\theta^*_{\rm NR}| \leq 0.9$ and $-0.8 \leq \cos\alpha_{34},\ \cos\phi_{\rm KSW} \leq 0.8$.

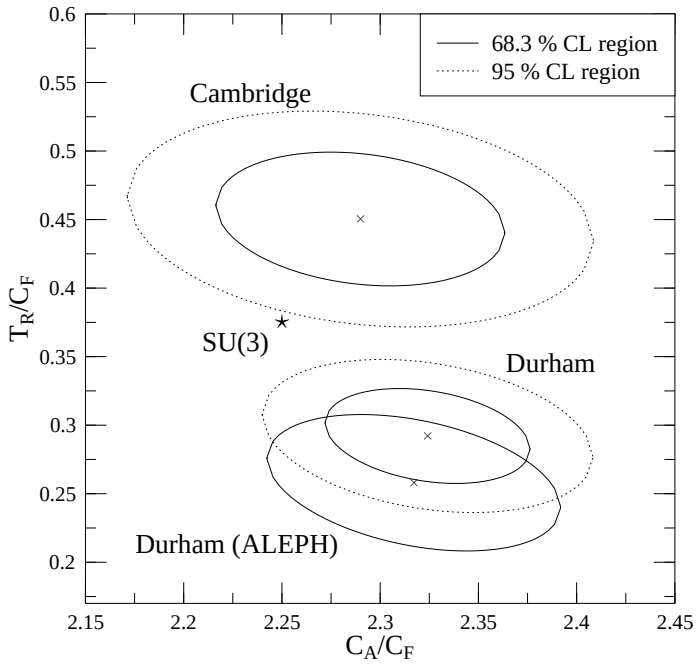

Figure 5.14: Confidence level contours of the leading order fits of the color charges x and y for the Durham and Cambridge clustering at $y_{cut} = 0.008$.

We observe from Fig. (5.14), that the leading order fit results in overestimating the C_A/C_F ratio by 2–3 % no matter which clustering algorithm is used. For the T_R/C_F ratio the leading order fit underestimates the result by 20–30 % of a NLO fit when the the Durham algorithm is used, while in the case of Cambridge clustering the leading order fit gives an overestimate of about 20 %. This systematic bias appears significant in both cases. Although the two parameters are slightly correlated when all four variables are used, the fit is reliable. The result of the fit depends on the jet algorithm because the different jet finders lead to different jet momenta from which our test variables are built. We also see that constraining the fit range as the ALEPH collaboration did does not alter our conclusions significantly. We would like to emphasize that the significant shift from the SU(3) values does not mean the

Table 5.6: Leading order fit the color charge ratio y to the next-to-leading order differential distributions of the angular correlations with $x = 9/4$ fixed.

Observable	Durham algorithm	Cambridge algorithm
$\cos\phi_{\rm KSW}$	0.57 ± 0.06	0.55 ± 0.08
$\lvert\cos\theta^{*}_{\rm NR}\rvert$	0.15 ± 0.03	0.36 ± 0.05
$\cos\alpha_{34}$	0.39 ± 0.05	0.56 ± 0.08
$\lvert\cos\chi_{\rm BZ}\rvert$	0.35 ± 0.05	0.51 ± 0.06
all four	0.31 ± 0.02	0.46 ± 0.03

exclusion of QCD, but simply gives an estimate of the systematic theoretical error in the color charge measurements when leading order fits are used.

One may ask how the light gluino exclusion significance changes in the recent analysis of Csikor and Fodor [15], which used the results of four-jet analyses, if one takes into account the systematic theoretical error discussed above. Assuming that the shifts of x and y are similar in the light gluino extension of QCD, our conclusion suggests that the radiative corrections induce a shift of order $2\alpha_s$ times the tree-level value for x and y. Lacking this piece of information Csikor and Fodor have increased the axes of the error ellipses by a factor of α_s times the theoretical x and y values. Implementing our results to a Csikor-Fodor type analysis for the four-jet events would decrease their confidence levels for the light gluino exclusion from 99.9 % (Csikor-Fodor value) to $\simeq$98 %, which is, however, still much higher than a 2-σ exclusion.

Table 5.7: Next-to-leading order kinematical functions to the $\cos\phi_{\rm KSW}$ angular distribution. The Durham jet algorithm is used.

$\cos\phi_{\rm KSW}$	C_4	C_0	C_x	C_y	C_{xx}	C_{xy}	C_{yy}
-0.950	1190.6 ± 25.0	-159.3	655.2	-1504.8	129.7	-235.6	-128.0
-0.850	686.5 ± 21.2	-86.7	381.8	-889.8	70.7	-109.6	-127.9
-0.750	696.9 ± 19.4	-67.5	353.1	-826.6	73.3	-82.4	-157.4
-0.650	707.5 ± 22.6	-73.8	352.2	-822.8	73.9	-61.5	-179.4
-0.550	722.0 ± 20.9	-73.7	366.5	-851.9	70.9	-48.2	-196.7
-0.450	716.2 ± 19.7	-77.9	373.9	-881.7	67.0	-32.6	-203.8
-0.350	708.5 ± 19.6	-87.8	390.4	-893.5	57.8	-10.3	-206.5
-0.250	763.1 ± 20.6	-78.2	418.1	-959.0	57.5	-2.0	-207.1
-0.150	752.5 ± 19.7	-77.7	435.4	-982.8	46.9	10.4	-197.2
-0.050	730.7 ± 18.8	-104.0	457.3	-1039.0	41.1	16.1	-191.6
0.050	665.5 ± 18.7	-90.7	420.7	-934.2	31.6	30.0	-176.1
0.150	652.9 ± 18.0	-84.7	431.0	-935.4	21.2	40.6	-157.4
0.250	631.6 ± 17.0	-86.2	424.2	-904.9	17.5	40.2	-147.9
0.350	633.7 ± 15.6	-83.3	433.1	-929.5	14.5	44.2	-137.6
0.450	576.9 ± 29.9	-105.1	404.6	-923.4	18.9	47.5	-127.2
0.550	628.8 ± 29.5	-100.3	484.4	-980.6	-4.0	52.6	-122.8
0.650	628.4 ± 16.2	-114.0	483.6	-1041.5	2.3	59.3	-119.7
0.750	711.1 ± 15.9	-132.8	578.1	-1197.2	-9.8	68.2	-118.2
0.850	836.8 ± 15.6	-169.5	675.8	-1444.1	-3.3	74.0	-130.3
0.950	1820.0 ± 22.9	-399.8	1547.2	-3258.7	-29.1	168.9	-252.6

Table 5.8: Next-to-leading order kinematical functions to the $|\cos\theta^*_{\rm NR}|$ angular distribution. The Durham jet algorithm is used.

$\lvert\cos\theta^*_{\rm NR}\rvert$	C_4	C_0	C_x	C_y	C_{xx}	C_{xy}	C_{yy}
0.025	1184.8 ± 26.6	-164.6	757.6	-1769.9	46.2	161.7	-459.4
0.075	1130.0 ± 35.3	-170.6	757.8	-1755.2	36.7	156.8	-450.0
0.125	1204.4 ± 37.0	-164.8	780.8	-1783.0	43.0	150.8	-451.7
0.175	1190.0 ± 39.9	-170.9	764.6	-1813.6	52.0	142.6	-451.4
0.225	1239.0 ± 37.9	-172.1	801.1	-1828.6	47.1	139.5	-432.3
0.275	1247.5 ± 32.2	-172.4	796.1	-1832.1	54.2	115.2	-423.6
0.325	1268.2 ± 33.5	-189.6	828.9	-1885.8	54.7	100.1	-408.9
0.375	1311.9 ± 40.1	-187.4	824.8	-1903.0	68.5	74.3	-386.8
0.425	1358.3 ± 41.6	-177.3	888.3	-1986.6	56.5	55.9	-374.3
0.475	1456.3 ± 38.0	-201.0	916.8	-2044.7	74.9	38.5	-356.7
0.525	1443.4 ± 41.3	-225.8	951.0	-2130.4	69.0	34.1	-342.0
0.575	1570.0 ± 60.5	-208.6	980.2	-2198.9	89.4	-11.4	-317.0
0.625	1662.7 ± 59.7	-249.2	1085.3	-2305.5	79.1	-30.2	-300.8
0.675	1806.9 ± 60.9	-233.2	1146.4	-2448.1	92.6	-61.2	-276.8
0.725	1689.3 ± 62.1	-279.2	1129.5	-2503.3	93.3	-83.3	-249.5
0.775	1913.3 ± 50.4	-263.6	1244.8	-2605.8	93.6	-105.4	-226.0
0.825	1931.5 ± 52.0	-290.4	1269.4	-2670.3	101.2	-139.6	-200.1
0.875	1907.6 ± 50.7	-284.7	1254.5	-2691.0	106.3	-160.8	-173.4
0.925	1979.0 ± 56.1	-302.0	1297.6	-2777.3	116.5	-196.4	-151.9
0.975	2426.4 ± 68.3	-399.1	1658.0	-3469.3	122.2	-241.3	-137.8

Table 5.9: Next-to-leading order kinematical functions to the $\cos\alpha_{34}$ angular distribution. The Durham jet algorithm is used.

$\cos\alpha_{34}$	C_4	C_0	C_x	C_y	C_{xx}	C_{xy}	C_{yy}
-0.950	1038.4 ± 17.9	-227.3	901.2	-1888.6	-20.6	77.1	-106.0
-0.850	988.9 ± 19.5	-187.7	830.9	-1717.5	-19.0	73.8	-109.0
-0.750	948.7 ± 19.4	-177.0	777.1	-1628.8	-10.4	67.2	-116.9
-0.650	911.1 ± 22.2	-162.4	716.5	-1500.5	-0.9	54.8	-123.8
-0.550	899.6 ± 26.1	-144.1	684.6	-1427.9	3.4	47.9	-132.5
-0.450	849.9 ± 22.1	-131.0	629.7	-1381.1	12.9	43.0	-141.0
-0.350	827.5 ± 21.1	-133.5	597.8	-1268.9	16.0	38.1	-148.8
-0.250	816.0 ± 19.0	-126.8	566.3	-1235.8	25.9	26.5	-158.2
-0.150	810.4 ± 19.8	-125.3	546.5	-1200.7	32.2	20.0	-171.5
-0.050	843.6 ± 21.4	-118.9	534.6	-1187.5	44.4	7.4	-187.6
0.050	829.9 ± 21.7	-126.0	510.9	-1152.5	53.0	-1.4	-203.9
0.150	879.4 ± 23.4	-105.2	484.1	-1100.1	69.4	-14.5	-219.1
0.250	834.2 ± 21.6	-104.4	450.9	-1055.2	74.0	-28.7	-233.1
0.350	837.2 ± 23.9	-93.4	426.1	-999.6	83.0	-43.0	-244.0
0.450	828.0 ± 24.0	-79.6	382.7	-915.3	93.2	-55.2	-249.9
0.550	793.7 ± 22.2	-72.9	343.9	-854.5	100.1	-70.2	-252.9
0.650	719.8 ± 21.9	-59.1	305.2	-763.9	94.0	-74.7	-238.4
0.750	546.0 ± 15.0	-52.5	238.4	-602.4	73.0	-66.1	-184.8
0.850	245.2 ± 9.3	-24.0	130.1	-302.8	24.8	-31.7	-62.8
0.950	12.5 ± 2.4	-1.9	9.2	-17.7	0.2	-0.4	-0.9

Table 5.10: Next-to-leading order kinematical functions to the $|\cos\chi_{\rm BZ}|$ angular distribution. The Durham jet algorithm is used.

$\lvert\cos\chi_{\rm BZ}\rvert$	C_4	C_0	C_x	C_y	C_{xx}	C_{xy}	C_{yy}
0.025	1133.9 ± 39.7	-171.8	748.6	-1623.5	29.2	161.8	-400.9
0.075	1087.1 ± 47.9	-170.2	724.3	-1689.3	34.9	164.9	-395.9
0.125	1147.7 ± 49.5	-163.0	771.0	-1640.7	23.1	153.2	-395.1
0.175	1075.4 ± 45.9	-160.2	719.1	-1665.6	33.6	159.0	-391.4
0.225	1144.5 ± 42.5	-177.8	752.8	-1659.9	36.9	135.4	-381.4
0.275	1110.3 ± 43.5	-172.6	741.9	-1634.2	33.4	121.7	-361.1
0.325	1152.2 ± 42.3	-142.2	744.5	-1651.3	39.0	110.2	-350.3
0.375	1181.2 ± 43.1	-175.4	794.6	-1741.2	35.9	106.1	-340.5
0.425	1210.8 ± 47.8	-155.7	798.5	-1693.3	37.9	72.5	-330.6
0.475	1213.1 ± 44.5	-185.8	762.7	-1749.9	66.2	56.7	-322.3
0.525	1236.6 ± 38.9	-195.1	819.6	-1801.7	53.0	44.5	-310.7
0.575	1337.2 ± 42.9	-182.4	847.8	-1855.7	65.6	19.1	-299.8
0.625	1383.5 ± 44.4	-201.5	891.7	-1983.3	72.4	-2.5	-292.6
0.675	1415.8 ± 44.2	-197.9	916.5	-2050.8	74.8	-22.5	-279.9
0.725	1551.9 ± 44.0	-283.2	1039.4	-2150.5	74.9	-45.4	-268.6
0.775	1659.4 ± 47.8	-152.9	1020.2	-2357.4	99.2	-75.9	-262.1
0.825	1828.2 ± 48.2	-251.4	1166.8	-2553.8	105.5	-102.4	-248.7
0.875	1791.5 ± 245.1	-316.9	1236.4	-2863.7	110.1	-146.7	-243.1
0.925	2455.5 ± 246.3	-318.9	1528.1	-3230.3	151.2	-217.0	-249.3
0.975	4804.5 ± 70.2	-731.4	3109.1	-6806.4	320.2	-552.9	-445.9

Table 5.11: Next-to-leading order kinematical functions to the $\cos\phi_{\rm KSW}$ angular distribution. The Cambridge jet algorithm is used.

$\cos\phi_{\rm KSW}$	C_4	C_0	C_x	C_y	C_{xx}	C_{xy}	C_{yy}
-0.950	1085.9 ± 44.0	-287.0	713.0	-1754.9	135.1	-280.6	-143.7
-0.850	658.4 ± 35.4	-164.3	404.4	-986.2	81.7	-134.9	-134.0
-0.750	617.4 ± 27.0	-139.8	366.6	-932.2	78.5	-108.1	-170.1
-0.650	620.0 ± 23.2	-124.2	355.9	-924.0	74.7	-71.1	-196.1
-0.550	662.8 ± 23.0	-130.5	377.7	-961.9	75.7	-59.5	-210.4
-0.450	605.2 ± 24.4	-145.8	380.8	-954.7	60.8	-30.6	-216.4
-0.350	658.4 ± 23.8	-143.1	405.4	-1004.1	60.9	-13.3	-224.1
-0.250	653.0 ± 25.4	-148.1	421.2	-1035.8	54.3	-4.2	-219.6
-0.150	610.7 ± 25.0	-173.7	431.9	-1044.3	44.3	13.4	-213.7
-0.050	603.3 ± 23.6	-176.6	449.2	-1078.7	36.9	16.1	-192.3
0.050	548.4 ± 21.4	-147.6	401.7	-970.0	30.8	28.0	-171.0
0.150	514.7 ± 19.3	-161.5	414.3	-952.0	18.2	37.2	-161.0
0.250	508.4 ± 17.1	-153.8	407.1	-942.3	17.3	38.5	-147.1
0.350	500.3 ± 17.0	-158.0	425.3	-974.9	9.9	42.6	-140.6
0.450	497.7 ± 18.5	-164.4	429.0	-996.6	10.0	44.7	-129.7
0.550	471.1 ± 16.9	-177.1	444.7	-1027.1	1.1	52.3	-124.8
0.650	510.0 ± 16.8	-195.1	489.6	-1085.2	-4.2	56.5	-120.9
0.750	560.0 ± 17.4	-207.1	545.7	-1217.8	-8.4	65.2	-118.7
0.850	681.4 ± 22.0	-264.5	687.5	-1514.9	-16.0	78.5	-129.7
0.950	1493.1 ± 25.4	-630.2	1574.3	-3435.0	-48.4	176.7	-252.8

Table 5.12: Next-to-leading order kinematical functions to the $|\cos\theta^*_{\rm NR}|$ angular distribution. The Cambridge jet algorithm is used.

$\lvert\cos\theta^*_{\rm NR}\rvert$	C_4	C_0	C_x	C_y	C_{xx}	C_{xy}	C_{yy}
0.025	1016.1 ± 30.2	-233.6	750.2	-1827.3	34.8	160.4	-449.3
0.075	1023.7 ± 38.2	-237.2	734.5	-1817.0	46.1	136.2	-450.5
0.125	1011.2 ± 44.1	-224.1	756.4	-1848.0	31.7	157.7	-441.6
0.175	1038.5 ± 44.3	-249.2	760.8	-1867.3	44.8	126.8	-450.3
0.225	1037.3 ± 42.3	-240.7	760.2	-1867.6	43.9	117.8	-430.8
0.275	1112.1 ± 42.0	-253.5	807.4	-1937.9	47.7	117.0	-426.1
0.325	1078.7 ± 37.7	-260.3	808.9	-1937.7	44.1	99.2	-416.5
0.375	1074.5 ± 37.2	-277.2	797.5	-1997.0	57.6	87.5	-403.2
0.425	1147.9 ± 39.6	-314.1	896.8	-2103.0	46.6	57.1	-385.7
0.475	1222.8 ± 43.0	-294.4	911.7	-2166.9	58.9	38.1	-370.6
0.525	1238.6 ± 46.5	-343.9	944.9	-2233.5	62.5	29.5	-352.4
0.575	1295.5 ± 45.3	-351.4	969.0	-2346.7	78.8	-4.6	-334.3
0.625	1371.8 ± 45.0	-393.9	1069.7	-2488.9	72.3	-39.0	-315.0
0.675	1403.5 ± 55.5	-452.3	1134.1	-2606.4	75.7	-73.7	-294.4
0.725	1504.7 ± 61.1	-455.9	1183.5	-2732.3	85.6	-86.4	-274.2
0.775	1479.6 ± 59.4	-539.4	1202.1	-2802.7	99.7	-126.3	-250.6
0.825	1527.5 ± 63.3	-566.6	1268.4	-2896.6	94.9	-142.1	-230.8
0.875	1585.8 ± 64.0	-629.1	1318.0	-2971.0	110.0	-196.0	-204.7
0.925	1706.3 ± 87.7	-625.3	1357.8	-3096.3	130.8	-234.3	-180.9
0.975	2243.9 ± 92.8	-842.0	1818.8	-4041.0	160.3	-329.7	-171.8

Table 5.13: Next-to-leading order kinematical functions to the $\cos\alpha_{34}$ angular distribution. The Cambridge jet algorithm is used.

$\cos\alpha_{34}$	C_4	C_0	C_x	C_y	C_{xx}	C_{xy}	C_{yy}
-0.950	827.2 ± 21.4	-373.0	904.6	-1956.5	-30.4	79.5	-105.8
-0.850	786.6 ± 41.6	-333.1	819.7	-1750.8	-22.2	70.2	-108.9
-0.750	731.5 ± 40.2	-310.3	760.7	-1686.0	-15.0	64.5	-118.2
-0.650	726.5 ± 21.4	-285.2	718.2	-1607.3	-6.1	56.4	-126.8
-0.550	691.0 ± 30.1	-257.9	666.9	-1473.9	-4.3	48.0	-133.0
-0.450	704.7 ± 32.9	-242.1	635.0	-1439.9	8.5	40.2	-143.0
-0.350	692.8 ± 23.8	-211.5	590.3	-1344.2	14.2	35.6	-149.0
-0.250	690.1 ± 21.9	-203.2	563.4	-1266.4	20.0	24.9	-158.9
-0.150	670.2 ± 22.9	-193.3	531.8	-1250.5	28.9	17.4	-174.4
-0.050	699.2 ± 23.9	-180.2	511.6	-1212.6	38.8	13.9	-185.9
0.050	720.4 ± 30.1	-176.5	499.8	-1163.4	48.0	-7.5	-202.7
0.150	769.0 ± 31.7	-158.3	487.1	-1185.0	62.2	-10.5	-223.5
0.250	791.6 ± 33.7	-163.2	477.7	-1163.8	74.3	-31.5	-239.8
0.350	790.2 ± 28.0	-159.0	451.3	-1119.0	86.1	-54.3	-260.3
0.450	816.2 ± 33.8	-143.8	426.7	-1095.9	100.2	-69.3	-273.9
0.550	733.4 ± 30.9	-148.9	370.3	-1033.3	110.4	-98.8	-277.3
0.650	634.0 ± 35.4	-143.2	333.7	-942.1	98.3	-97.3	-263.6
0.750	434.4 ± 22.9	-122.8	235.7	-732.8	80.7	-91.5	-201.8
0.850	150.1 ± 14.0	-79.6	135.6	-355.6	20.2	-41.5	-69.4
0.950	0.9 ± 1.7	-7.2	5.1	-13.8	0.5	-0.9	-0.7

Table 5.14: Next-to-leading order kinematical functions to the $|\cos\chi_{\rm BZ}|$ angular distribution. The Cambridge jet algorithm is used.

$\lvert\cos\chi_{\rm BZ}\rvert$	C_4	C_0	C_x	C_y	C_{xx}	C_{xy}	C_{yy}
0.025	950.6 ± 40.9	-233.8	718.7	-1751.2	28.4	156.9	-398.6
0.075	968.5 ± 53.7	-242.8	762.8	-1695.1	11.9	151.7	-395.7
0.125	949.3 ± 52.6	-245.5	718.9	-1784.5	31.7	168.0	-404.9
0.175	989.3 ± 45.2	-246.1	751.7	-1713.5	22.8	141.4	-390.4
0.225	959.7 ± 45.3	-260.6	722.5	-1707.9	34.8	138.6	-383.3
0.275	940.8 ± 45.5	-288.5	736.2	-1702.2	33.1	114.1	-373.5
0.325	989.1 ± 48.3	-224.8	710.5	-1744.9	45.0	108.5	-367.0
0.375	1011.7 ± 52.2	-257.5	781.7	-1804.6	30.5	96.4	-358.6
0.425	1055.0 ± 49.7	-262.7	767.8	-1870.0	55.2	75.1	-345.1
0.475	1015.4 ± 71.3	-378.7	862.4	-1902.1	31.6	63.9	-344.3
0.525	1110.7 ± 89.5	-194.5	764.8	-1943.5	63.6	46.9	-328.1
0.575	1136.4 ± 75.5	-297.7	834.4	-1991.1	67.3	8.2	-308.5
0.625	1156.8 ± 50.0	-313.0	893.3	-2106.2	58.5	-7.5	-311.5
0.675	1223.0 ± 60.9	-379.1	947.1	-2229.2	74.0	-31.0	-298.0
0.725	1257.6 ± 65.3	-391.6	1005.7	-2386.4	72.3	-51.3	-288.4
0.775	1355.8 ± 56.8	-435.0	1058.5	-2530.1	93.4	-92.2	-273.9
0.825	1386.3 ± 70.3	-527.7	1179.4	-2785.3	87.8	-119.5	-269.5
0.875	1636.2 ± 70.6	-568.2	1311.0	-2996.6	109.3	-165.5	-256.2
0.925	1994.9 ± 111.6	-674.3	1553.8	-3496.2	146.4	-261.0	-264.5
0.975	4032.8 ± 121.5	-1362.2	3169.4	-7444.4	329.2	-646.6	-473.7

Summary of the results

In this dissertation I analyze the four-jet production in electron-positron annihilation. In the fist part of this thesis I reviewed the basic element of the QCD and the properties of the hadronic events. I discussed those algorithms and shape variables which help us to characterize the structure of the hadronic events. I discussed a calculation method of NLO jet cross sections in detail. I applied this method for the process $e^+e^- \to 4$ jets and the most interesting results were discussed in Chapter 5. Finally, my results can be summarized in the following items

1. I calculated the five parton two lepton tree level matrix element in Weyl-spinor basis (see Appendix A).[6]

2. I gave the group independent color decomposition of the four parton two lepton one-loop matrix elements (see Appendix B). [2]

3. I developed a Monte Carlo event generator which can calculate 3- and 4-jet cross sections at next-to-leading order and 5-jet cross sections at leading order in e^+e^- annihilation. [9]

4. I showed that in the case of four-jet shape variables, the NLO corrections (with the exception of y_4 jet shape variable) are more than 100 %. The residual renormalization scale dependence is large indicating that even higher orders are important. One may conclude that these distributions cannot be reliable calculated in fix order perturbation theory and cannot be use for precision test of QCD. [1, 4, 6]

5. I showed that in the case of four-jet rates, the radiative corrections are about 100 % for JADE-type clustering algorithms [1], while for the Durham algorithm it is less than 60 % and even smaller for the Cambridge algorithm. The scale dependence for the latter algorithms is substantially reduced. The agreement between data and theory for the Durham clustering is very good and extends to small values of y_{cut} when one matches the fixed order prediction with improved resummed next-to-leading logarithmic approximation. [6]

6. I showed that in the case of normalized angular distributions the corrections are small as expected (the K factors are close to 1). The renormalization

scale dependence is small, which however, does not mean that the effect of the radiative corrections on the measurement of the QCD color charges is negligible. The measured value of the T_R/C_F ratio may differ up to 25 % when leading, or NLO QCD predictions are used in the color charge fits. [5]

7. I showed from the comparison of the Durham four-jet rate and the measured data that the existence of the light gluinos can be excluded at the 90 % confidence level. [3]

8. I showed that the NLO perturbative prediction, matched with the next-to-leading logarithmic approximation for predicting both 2-, 3- and 4-jet rates using the Durham jet-clustering algorithm, gives a very accurate description of the data obtained at the LEP. [7]

9. I performed the measurement of strong coupling constant using the 3- and 4-jet rates. The results is $\alpha_s(M_{Z^0}) = 0.1173 \pm 0.0018$, where the error doesn't contain the systematic error of the experiment.

Összefoglalás

(This is the hungarian review of the thesis.)

Általános hit, hogy az erős kölcsönhatást, mely a hadronok öszetevői között hat, a kvantum színdinamika (QCD) elmélete írja le. Két típusa van az összetevőknek, melyeket közösen partonoknak nevezünk, a kvarkok és a gluonok. Elméleti illetve kísérleti indukációk vannak arra nézve, hogy a partonok csak kötött állapotban létezhetnek a természetben, tehát a világ "színtelen". Elméletileg valamely erősen kölcsönható folyamatra a QCD jóslat megkapható, de a gyakorlatban ez kivitelezhetetlen. Azért a helyzet nem olyan rossz. Speciális feltételek mellett a számolások elvégezhetők a perturbatív módszer segítségével. Ezt a megközelítést a QCD aszimtotikus szabadsága teszi lehetővé. Használva a QCD tulajdonságait és a renormálási csoport technikát, lehet definiálni az $\alpha_s(Q)$ futó csatolási állandót, melynek értéke nullához tart a nagyenergiás tartományban ($Q \to 0$). Ez a viselkedés a nagyenergiás tartományban megengedi, hogy perturbatív sorfejtést alkalmazzunk az $\alpha_s(Q)$ változóban. A legalacsonyabb rendje ennek a sorfejtésnek a naív parton modell közelítésnek felel meg vagy más néven a vezetőrendű közelítésnek (LO). A LO eredmény csak egy durva közelítését tudja adni az éppen számolt mennyiségnek. A perturbatív sorfejtés pontossága a magasabb rendű járulékok nagysága által van kontrolálva. Számos QCD jóslat megköveteli legalább a vezető rendre következő járulékot (NLO) és az NLO definícióját a hozzá kapcsolódó mennyiségeknek (pl. $\alpha_s(Q)$).

Ilyen magasabb rendű számolások az elmúlt húsz év során el lettek végezve néha sokkal később, mint azt a kísérleti adatok megkövetelték volna. Ennek a késésnek az volt az oka, hogy nagyon nehéz egy általános és egyszerű számolási módszert kifejleszteni.

Az egyik nehézség, amivel szembe kell nézni az a mátrixelemek kezelése. A nemábeli vertexek komplexitása miatt a mátrix elemek kifejezései óriásivá válnak a külső lábak számának emelése által. Ez a probléma már vezető rendben is jelentkezik. Ezt szemléletesen alátamasztja a A és a B függelékekben megadott mátrix elemek is. Másrészt a hurok amplitudók hurok impulzus feletti integrálást tartalmaznak. Elméletileg és néhány fontos esetben [42] egy hurok szinten el tudjuk végezni őket, de már kéthurok rendben csak néheny speciális integrált tudunk kiszámolni. Jelenleg a magasabb hurok amplitudók számolása reménytelen.

A másik nehézség az ütközési folyamat rövid és hosszú hatótávolságú részeinek faktorizálása. A hosszú hatótávolságú részdivergenciák jelenlétét eredményezi a perturbatív számolás során. Az NLO vagy magasabb rendű számolások fő feladata a divergenciák kiejtése. Az irodalomban számos átalános módszert fejlesztettek ki [8, 50, 51, 52, 53] NLO hatáskeresztmetszetek számolására.

A disszertációmban elektron-pozitron megsemmisülésben való négy-jet keletkezés elméleti leírását tűztem ki célul.

Az elektron-pozitron megsemmisülés a legegyszerűbb és legtisztább folyamat a kvantum színdinamika (QCD) tesztelésére, mivel a kezdeti állapot egyszerű és jól ismert. A tisztán hadronikus események nagy száma lehetővé teszik az α_s erő csatolási állandó preciziós mérését.

A QCD elméletének másik "paramétere" a mérték szimmetriát meghatározó mérték csoport. Habár manapság senki sem kérdőjelezi meg azt, hogy a QCD SU(3)-as mértékelmélet ennek ellenére a QCD *teljes* mérése (az α_s erős csatolási állandó és a mértékcsoport C_A, C_F kvadratikus Casimirjeinek a szimultán mérése) nem pusztán elméleti feladat. Lehetséges létezése a könnyű gluinoknak, befolyásolja mind az α_s értékét mind pedig a színtöltések mért értékét (vagy rögzítve a mérték szimmetriát SU(3)-ra, akkor a fermionikus szabadságfokok számát befolyásolja). Így szimultán fit segítségével ellenőrízhetjük az extra fermionikus szabadságfokok létezését.

A harmadik terület, ahol a négy-jet események súlya meghatározó, az az, hogy a QCD esemenyek adják a legnagyobb háttért más nem QCD folyamatokhoz (pl. $e^+e^- \to W^+W^-$ folyamathoz). Ezek a csatornák fontosak a Higgs illetve más új részecskék keresése szempontjából.

Hadronikus állapotok szerkezete

A nagyenergiás elemirész folyamatokban a legmeghatározóbb az, amikor a végállapot tisztán hadronikus. A LEP1-en az ilyen események a teljes események 70%-át adják. Az ilyen folyamatokban nagy számmal vannak olyan események, melyekben jól elkülöníthető hadronnyalábok figyelhetők meg. Ezeket a hadronnyalábokat nevezzük hadronikus jeteknek. Tehát a hadronikus végállapotoknak szerkezete van, melyet az elméletnek le kell tudni írnia.

A nagyenergiás folyamatokban keletkező hadronikus eseményeket többféle módon jellemezhetjük. Vizsgálhatjuk az esemény geometriáját, azaz megnézhetjük, hogy egy esemény mennyire kollineáris, vagy éppen mennyire koplanáris. Másképpen fogalmazva feltehetjük a kérdést úgy is, hogy mekkora az olyan események súlya, melynek az $O_1, O_2, ...$ paraméterekkel jellemzett geometriai tulajdonsága $C_1, C_2, ...$, ahol $C_1, C_2, ...$ rögzített. Az $O_1, O_2, ...$ paramétereket alakváltozóknak (*event shapes*) nevezzük. Fontos, hogy a hadronikus eseményeket jellemző alakváltozók nem rendezik a hadronokat jetekbe, de kiemelhetik a jetszerű eseményeket. Természetesen definiálhatunk olyan algoritmust, amely a hadronokat jetekbe rendezi. Ekkor már beszélhetünk arról, hogy a végállapotban 2,3,4... jet van,illetve arról, hogy mekkora annak az n-jet események súlya. Az ilyen algoritmusokat nevezzük jetkereső algo-

ritmusoknak (*jet finding algorithm*). Nézzünk egy-egy példát a fent említett fizikai mennyiségekre.

Legyen m darab hadron a végállapotban, mely e^+e^- annihilációban keletkezett

$$e^+(p_+) + e^-(p_-) \longrightarrow h_1(p_1) + \cdots + h_m(p_m) \ , \qquad p_+ + p_- = Q \ , \tag{1}$$

ahol p_+, p_- a bejövő elektron-pozitron impulzusa, $p_1, ..., p_m$ a végállapoti hadronok impulzusai. Az impulzusok (p_+, p_-) tömegközépponti rendszerben vannak értve. A legismertebb alakváltozók egyike a **thrust** [16], mely az események kollinearitását méri és a következő kifejezéssel van definiálva

$$T(p_1, ..., p_m) = \max_{\vec{n}_T} \frac{\sum_{i=1}^{m} |\vec{p}_i \cdot \vec{n}_T|}{\sum_{i=1}^{m} |\vec{p}_i|} \ , \tag{2}$$

ahol az $\vec{n}_T$ vektort úgy definiáljuk, hogy T-t maximalizálja. Ha csak két hadron van a végállapotban, akkor $T = 1$. Általános esetben $0.5 \leq T \leq 1$. Azon események súlya, melyeknek a thrust-ja T és $T + \Delta T$ közé esik a következő

$$\Sigma(T) = \frac{1}{N} \sum_{\substack{i=1 \\ \text{események}}}^{N} \int_{T}^{T+\Delta T} dT \; T \; \delta \left(T - T(p_1, ..., p_{m_i}) \right) \ , \tag{3}$$

ahol $p_1, ..., p_{m_i}$ az i-edik esemény hadronjainak impulzusa. További két thrust-szerű mennyiség vezethető be, a **thrust major** T_{maj} és a **thrust minor** T_{min}. Ezeket szintén a (2) kifejezéssel definiáljuk azzal a különbséggel, hogy a thrust major $\vec{n}_{T_{\text{maj}}}$ tengelye merőleges az $\vec{n}_T$ thrust tengelyre, míg a thrust minor $\vec{n}_{T_{\text{min}}}$ tengelye merőleges mind a $\vec{n}_T$ mind a $\vec{n}_{T_{\text{maj}}}$ tengelyekre.

A jetkereső algoritmusokat átalában iterativ algoritmusok segítségével definiáljuk. Ilyen algoritmus a **Durham** algoritmus [25] is, mely a következő módon van definiálva:

1. Definiáljuk az y_{cut} feloldási változót.

2. Minden h_k, h_l párra számoljuk ki az y_{kl}-lel jelölt feloldási változót

$$y_{kl} = \frac{2 \min(E_k^2, E_l^2)}{Q^2} (1 - \cos\theta_{kl}) \ , \tag{4}$$

   ahol E_i az i-edik hadron energiáját és θ_{ij} az i-edik és a j-edik hadron impulzusai által bezárt szöget.

3. Jelölje y_{ij} a legkisebb értéket a 2. pontban számolt y_{kl}-eknek. Ha $y_{ij} < y_{cut}$, akkor kombinálja össze (p_i, p_j)-t egyetlen $p_{(ij)}$ pszeudorészecskévé a rekombinációs előírás szerint

$$p_{(ij)}^{\mu} = p_i^{\mu} + p_j^{\mu} \ . \tag{5}$$

4. Ismételje az eljárást a 2. ponttól egészen addig, míg az $y_{ij} > y_{cut}$ feltétel nem teljesül.

A maradék objektumok (pszeudorészecskék) definiálják a jeteket. Látható, hogy az y_{cut} függvényében a jetkereső algoritmus megmondja, hogy az adott esemény hány jetnek felel meg. Jelölje $r^{(n)}$ a következő függvény

$$r^{(n)}(p_1,...,p_m;y_{cut}) = \begin{cases} 1 & \text{ha az algoritmus talált } n \text{ jetet} \\ 0 & \text{ha nem talált } n \text{ jetet} \end{cases} \tag{6}$$

ahol $p_1,...,p_m$ a keletkezett m darab hadron négyes impulzusa, y_{cut} a feloldási változó.

Annak a súlya, hogy a végállapotban n-jetet találunk, a következő

$$R_n(y_{cut}) = \frac{1}{N} \sum_{\substack{i=1 \\ \text{események}}}^{N} r^{(n)}(p_1,...,p_{m_i};y_{cut}) \ . \tag{7}$$

A jet ráta fenti definiciójából következik, hogy

$$\sum_{n=2}^{\infty} R_n(y_{cut}) \ = \ 1 \ . \tag{8}$$

Látható, hogy mind az alakváltozók, mind a jet ráták esetén a keletkezési valószínűségeket a következő átalános alakban írhatjuk

$$P(O_1,O_2,...) = \frac{1}{N} \sum_{\substack{i=1 \\ \text{események}}}^{N} F_J^{(m_i)}(p_1,...,p_{m_i};O_1,O_2,...) \ . \tag{9}$$

Az $F_J^{(m_i)}$ függvényt jet mérőfüggvénynek nevezzük.

Jetkeletkezés elméleti leírása

Kísérleti tapasztalatok szerint a 2,3,4,.. jetkeletkezési valószínűségek a következő szabályszerűséget mutatták

$$2\text{jet} : 3\text{jet} : 4\text{jet} : ... = \mathcal{O}(\alpha_S^0) : \mathcal{O}(\alpha_S^1) : \mathcal{O}(\alpha_S^2) : ... \tag{10}$$

Ez azt indukálta, hogy a perturbatív QCD-ben szereplő partonok jó leírást adhatnak a hadronikus jetekre. Tehát megpróbálkozhatunk egy olyan leírásmóddal, hogy a hadronikus végállapotot partonikussal helyettesítjük. Ha szerencsenk van akkor ez jó közelítést adhat. A jet mérőfüggvény egy vágást jelent a hadronikus állapotok terébe. Azt viszont semmi sem garantálja, hogy ennek a vágásnak megtaláljuk az egzakt parton szintű megfelelőjét. A partonszint és a hadronszint között a különbség $\mathcal{O}(1/Q)$, ahol Q a releváns impulzusskála. Így a partonikus jet mérőfüggvényre a következő adódik

$$\bar{F}_J^{(n)}(p_1,...,p_n;O_1,O_2,...) = F_J^{(n)}(p_1,...,p_n;O_1,O_2,...) + \mathcal{O}\left(\frac{1}{Q}\right) \ , \tag{11}$$

ahol $\bar{F}_J^{(n)}$ a partonszintű, $F_J^{(n)}$ a hadronszintű jet mérőfüggvény, $p_1, ..., p_n$ parton-impulzusok. Ezek szerint a perturbációszámolás legalacsonyabb rendjében minden partonnak egy-egy jet felel meg. Ez a (3.21) szabálynak felel meg. Figyelembe kell venni a hadronizációs korrekciókat, amelyeket hadronizációs modellek segítségével számolunk. Ilyen modell a húrmodell [29] (string model), vagy a klaszter modell [30].

Így a jet hatáskeresztmetszetet a következő formulával számolhatjuk a regularizált elméletben, ahol a téridő dimenziója $d = 4 - 2\epsilon$

$$\sigma(O_1, O_2, ...) = \sum_{m=2}^{\infty} \int_m d\sigma_m(O_1, O_2, ...) \ , \tag{12}$$

ahol $d\sigma_m$ differenciális hatáskeresztmetszetek

$$\begin{aligned} d\sigma_m(O_1, O_2, ...) \quad = \quad & \sum_{\{m\}} d\Gamma^{(m)}(p_1, ..., p_m; Q) \, \frac{1}{S_{\{m\}}} \, |M_m(p_1, ..., p_m)|^2 \\ & \cdot \ F_J^{(m)}(p_1, ..., p_m, O_1, O_2, ...) \ , \end{aligned} \tag{13}$$

kifejezéssel vannak definiálva. $\sum_{\{m\}}$ jelöli az m-partonos konfigurációk feletti összegzést a $S_{\{m\}}$ Bose szimmetria factorral. M_m az m partonos renormált amplitudó és $d\Gamma^{(m)}$ az m partonos fázistér mérték.

Elvégezve a perturbatív sorfejtést α_s-ben egy NLO jet hatáskeresztmetszet σ általánosan a következő alakban írható fel

$$\sigma = \sigma^{LO} + \sigma^{NLO} \ . \tag{14}$$

Itt a vezetőrendű jet hatáskeresztmetszet σ^{LO}, melyet úgy kapunk, hogy a $d\sigma^B$ exkluzív hatáskeresztmetszetet integrálom a fázistér fölött azon a tartományon, amit a jet mérőfüggvény kijelöl. Ha m parton van a végállapotban

$$\sigma^{LO} = \int_m d\sigma^B \ , \tag{15}$$

ahol az összes mennyiség $d = 4 - 2\epsilon$ dimenzióban van értelmezve.

Nézzük most a korrekciót. A hatáskeresztmetszet két tagra bontható; egy $d\sigma^R$ tagra, mely $m+1$ partont tartalmaz a végállapotban és egy $d\sigma^V$ tagra, mely $m+1$ partont tartalmaz a végállapotban és egyben az 1-hurok korrekciókat adja

$$\sigma^{NLO} \equiv \int d\sigma^{NLO} = \int_{m+1} d\sigma^R + \int_m d\sigma^V \ . \tag{16}$$

A két integrál az (16) egyenlet jobb oldalán külön-külön divergens $d = 4$ dimenzióban, de az összegük véges. Ezek a szingularitások az infravörös divergenciák, melyek a kölcsönhatás hosszúhatótávolságú részét jellemzik. A dimenzionális regularizáció segítségével az egyes tagokban szeparálni tudom a szingularitásokat és el tudom végezni a kiejtést. A cél az, hogy a (16) egyenletet olyan alakban írjuk fel, mely nem tartalmaz szingularitásokat. Ezt a (16) egyenlet azonos átírásával érjük el

$$d\sigma^{NLO} = \left[d\sigma^R - d\sigma^A\right] + d\sigma^A + d\sigma^V \ , \tag{17}$$

ahol $d\sigma^A$ a $d\sigma^R$ közelítése ugyanolyan szingiuláris viselkedést mutat (d dimenzióban) mint $d\sigma^R$. Látszik, hogy $d\sigma^A$ lokális levonási tagként működik. Bevezetve a fázistér integrált a (17) a következő alakban írható fel

$$\sigma^{NLO} = \int_{m+1} \left[d\sigma^R - d\sigma^A \right] + \int_{m+1} d\sigma^A + \int_m d\sigma^V \ , \tag{18}$$

most már biztonságosan elvégezhető $\epsilon \to 0$ limesz az integrandusban. Az első tag már integrálható numerikusan (Monte Carlo program segítségével).

Az összes szingularitás az (4.9) egyenlet utolsó két tagjában van. Ha $d\sigma^A$ -t ki tudjuk integrálni egy egypartonos fázistér fölött (melyből a pólusok jönnek), akkor ϵ pólusokat összekombinálva $d\sigma^V$ ϵ pólusaival és elvégezve $\epsilon \to 0$ limeszt, egy m partonos integrálom marad, amely nem tartalmaz szingularitásokat és szintén jól kezelhető Monte Carlo programmal. Tehát a végső formulát a következő alakban írhatjuk

$$\sigma^{NLO} = \int_{m+1} \left[d\sigma^R_{\epsilon=0} - d\sigma^A_{\epsilon=0} \right] + \int_m \left[d\sigma^V + \int_1 d\sigma^A \right]_{\epsilon=0} \ . \tag{19}$$

A divergenciák kiejtését az $F_J^{(m)}$ jetfüggvény garantálja. Ez a függvény úgy van definiálva, hogy az értéke független a lágy és kollineáris hadronok (partonok) számától. Vagy másképp fogalmazva a függvény értéke ugyanaz egy adott m parton konfigurációra és egy vele kinematikusan degenerált $m+1$ partonos konfigurációra (ha egy parton lággyá vagy két parton kollineárisá válik)

$$F_J^{(m+1)} \longrightarrow F_J^{(m)} \ . \tag{20}$$

Az ilyen mennyiségeket nevezzük *infrared safe* fizikai mennyiségeknek. A korábban definiált fizikai mennyiségek eleget tesznek ennek a feltételnek.

A levonási procedurának a kulcsa a $d\sigma^A$. A következő tulajdonságokat kell kielégíteni $d\sigma^A$-nak

1. tetszőleges folyamatra meg lehessen konstruálni
2. ugyanolyan szinguláris viselkedést kell mutatnia d dimenzióban, mint $d\sigma^R$-nek
3. tudni kell implementálni Monte Carlo programba
4. integrálni kell tudni analitikusan egy egypartonos fázistér fölött

Ilyen levonási tag többféleképpen [8, 52, 53] definiálható. Ebben a dolgozatban a Catani-Seymour [53] által definiát levonási tagot használtam a négy-jet hatáskeresztmetszetek kiszámolására.

Négyjet keletkezés e^+e^- megsemmisülésben

Ebben az alfejezetben a korábban tárgyalt mószerekkel kapott négyjet hatáskeresztmetszeteket ismertetem a teljesség igénye nélkül. Helyszűke miatt, itt a magyar nyelvű áttekintőben csak a fenomenológiai szempontból legérdekesebb fizikai mennyiségekkel foglalkozunk.

A négyjet mennyiségek három csoportba rendezhetők: négyjet ráták, négyjet alakváltozók, négyjet szögkorrelációk. Mindhárom típusra részletes analízist végeztünk. A jet rátákat kiszámoltuk JADE-E0, Durham, Geneva és Cambridge algoritmusokra [1, 6]. Az alakváltozók közül kiszámoltuk a D-paraméter az akoplanaritás [1], a Π_1 és Π_4 Fox-Wolfram momentumokat [4], az y_4, a $T_{\min}$ és a C-paraméter ($C > 0.75$) [6] differenciális hatáskeresztmetszetét. A szögeloszlások közül meghatároztuk a Bengtsson-Zerwas (BZ), a Nachtman-Reiter (NR), a Körner-Schierholz-Wilrodt (KSW) és a legkisebb energiájú jetek szöge (α_{34}) eloszlásokat [5].

A fent említett mennyiségek közül néhányat, tölünk függetlenül másik három csoport is kiszámolta [70, 72, 73], így lehetőség nyílt a közvetlen összehasonlításra. Az

1. táblázat: Négyjet ráták külömböző y_{cut} értékeknél

Algoritmus	y_{cut}	MENLO PARC	DEBRECEN
Durham	0.005	$(1.04 \pm 0.02) \cdot 10^{-1}$	$(1.05 \pm 0.01) \cdot 10^{-1}$
	0.01	$(4.70 \pm 0.06) \cdot 10^{-2}$	$(4.66 \pm 0.02) \cdot 10^{-2}$
	0.03	$(6.82 \pm 0.08) \cdot 10^{-3}$	$(6.87 \pm 0.04) \cdot 10^{-3}$
	y_{cut}	EERAD2	MERCUTIO
	0.005	$(1.05 \pm 0.01) \cdot 10^{-1}$	$(1.06 \pm 0.01) \cdot 10^{-1}$
	0.01	$(4.65 \pm 0.02) \cdot 10^{-2}$	$(4.72 \pm 0.01) \cdot 10^{-2}$
	0.03	$(6.86 \pm 0.03) \cdot 10^{-3}$	$(6.96 \pm 0.03) \cdot 10^{-3}$

1. táblázatban összehasonlítjuk a négyjet rátákat különböző y_{cut} értékek mellett az általam írt DEBRECEN és az irodalomban fellelhető másik három programmal (MENLO PARC [70], EERAD2 [72], MERCUTIO [73]). Az 1. táblázatból jól látszik, hogy a négy program hibán belül ugyanazt az eredményt adja.

Négyjet ráták

A legfontosabb fizikai mennyiségek a jet ráták. Elektron-pozitron megsemmisülésben a legelterjedtebben használt jet-algoritmus a Durham-algoritmus. A négyjet rátát a négyjet hatáskeresztmetszet, és a totális hatáskeresztmetszet hányadosaként definiáljuk,

$$R_4 = \frac{\sigma_{4-\text{jet}}}{\sigma_{\text{tot}}}(y_{cut}) = \eta^2 B_4(y_{cut}) + \eta^3 \left(C_4(y_{cut}) - \frac{3}{2} B_4(y_{cut}) \right) \quad , \tag{21}$$

ahol $\sigma_{\rm tot} = \sigma_0(1 + 1.5\eta)$ és $\eta = \alpha_s C_F/(2\pi)$. A renormálási skálától való függést a következő helyettesítéssel kaphatjuk:

$$\eta \to \eta(\mu)\left(1 + \frac{\beta_0}{C_F}\,\eta(\mu)\,\ln x_\mu\right) \quad , \qquad x_\mu = \frac{\mu}{\sqrt{s}} \quad . \tag{22}$$

A skálafüggetlen $B_4(y_{cut})$ és $C_4(y_{cut})$ együtthatókat a DEBRECEN programmal számoltuk. Az 1. ábrán jól látható a LO és az NLO jóslatok sávok formájában.

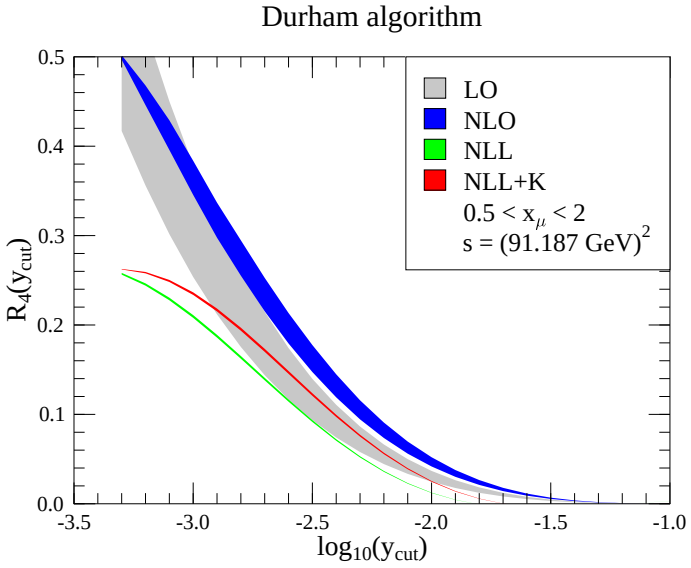

1. ábra: A Durham algoritmusra kapott négyjet ráták különböző elméleti jóslatai: LO (széles világosszürke sáv), NLO (széles sötétszürke sáv), NLLA ($K = 0$ alsó keskeny sáv), javított NLLA ($K \neq 0$ felső keskeny sáv).

A négyjet ráták gyorsan csökkennek a feloldási változó y_{cut} növekedésével, amiből az következik, hogy a jó statisztikájú adatok a kis y_{cut} tartományban érhető el. Másrészt tudjuk, hogy a perturbációszámítás nem megbízható ebben a tartományban, ugyanis a perturbációs kifejtési paraméter $\alpha_s/2\pi \ln^2 y_{cut}$ logaritmikusan felerősíti a magasabbrendű járulékokat. A problémát úgy oldjuk meg, hogy felösszegezzük a vezető-, illetve az arra következő logaritmusokat, amely az NLLA közelítést adja (next-to-leading log approximation). Durham algoritmus esetén ez megtehető [36]. Ez a közelítés csak a kis y_{cut} tartományokban működik jól. Másrészt tudjuk, hogy a nagy y_{cut} tartományokban a fix-order számolás jó közelítést ad, tehát a két eredményt egyeztetni kell. Mi az R-matching sémát használtuk, mely a következők szerint van definiálva

$$R_4^{\rm R-match} = R_4^{\rm NLL} + \eta^2\left(B_4 - B_4^{\rm NLL}\right) + \eta^3\left(C_4 - C_4^{\rm NLL} - \frac{3}{2}\left(B_4 - B_4^{\rm NLL}\right)\right), \tag{23}$$

ahol $R_4^{\rm NLL}$ az NLLA közelítés, $B_4^{\rm NLL}$ és $C_4^{\rm NLL}$ ennek az α_s szerinti sorfejtésének az együtthatói.

$$\begin{aligned} R_4^{\rm NLL} &= 2[\Delta_q(Q)]^2\Bigg[\left(\int_{Q_0}^{Q} dq\,\Gamma_q(Q,q)\,\Delta_g(q,Q_0)\right)^2 \\ &+ \int_{Q_0}^{Q} dq\,\Gamma_q(Q,q)\,\Delta_g(q,Q_0) \\ &\quad\cdot\int_{Q_0}^{q} dq'\left(\Gamma_g(q,q')\,\Delta_g(q',Q_0)+\Gamma_f(q')\Delta_f(q',Q_0)\right)\Bigg] \ . \end{aligned} \tag{24}$$

A (24) egyenletben $\Delta_a(Q,Q_0)$ a Sudakov alak faktorok, amely annak a valószínűségét fejezi ki, hogy valamely jetnek a $Q_0 = Q\sqrt{y_{cut}}$ skáláról a Q skálára való fejlődése közben ne legyen feloldodó elágazás. A Sudakov faktorokat a következő alakban írhatjuk

$$\Delta_q(Q,Q_0) = \exp\left(-\int_{Q_0}^{Q} dq\,\Gamma_q(Q,q)\right) \ , \tag{25}$$

$$\Delta_g(Q,Q_0) = \exp\left(-\int_{Q_0}^{Q} dq\,\left[\Gamma_g(Q,q)+\Gamma_f(q)\right]\right) \ , \tag{26}$$

$$\Delta_f(Q,Q_0) = \frac{\left[\Delta_q(Q,Q_0)\right]^2}{\Delta_g(Q,Q_0)} \ , \tag{27}$$

illetve az emissziós valószínűségek

$$\Gamma_q(Q,q) = \frac{2C_F}{\pi}\frac{\alpha_s(q)}{q}\left[\left(1+\frac{\alpha_s(q)}{2\pi}\,K\right)\ln\frac{Q}{q}-\frac{3}{4}\right] \ , \tag{28}$$

$$\Gamma_g(Q,q) = \frac{2C_A}{\pi}\frac{\alpha_s(q)}{q}\left[\left(1+\frac{\alpha_s(q)}{2\pi}\,K\right)\ln\frac{Q}{q}-\frac{11}{12}\right] \ , \tag{29}$$

$$\Gamma_f(Q,q) = \frac{n_f}{3\pi}\frac{\alpha_s(q)}{q} \ . \tag{30}$$

A K paraméter értéke függ a renormálási sémától, melynek értéke $\overline{\rm MS}$ séma esetén

$$K = C_A\left(\frac{67}{18}-\frac{\pi^2}{6}\right)-\frac{10}{9}T_R n_f \ , \qquad \beta_0 = \frac{11}{3}C_A-\frac{4}{3}T_R n_f \ , \tag{31}$$

ahol $C_A = 3$, $C_F = 4/3$, $T_R = 1/2$ $SU(3)$ mértékcsoport esetén. Az aktív kvark kvark flavour-ök száma n_f.

Használva a 23 illesztési egyenletet jó közelítést kaphatunk a kísérletileg mért adatokkal. A 2. ábráról leolvashatjuk, hogy javított felösszegzéssel ($K \neq 0$) kapott elméleti eredmény látványos egyezést mutat az ALEPH [58] detektorral mért kísérleti eredményekkel. Az is jól leolvasható, hogy az egyre pontosabb elméleti eredmények hogyan válnak "egyre jobbá". Ezek az eredmények azt sugalják, hogy a jet ráták jól használhatók a QCD pontos ellenőrzésére, pl. az erős csatolás mérésére.

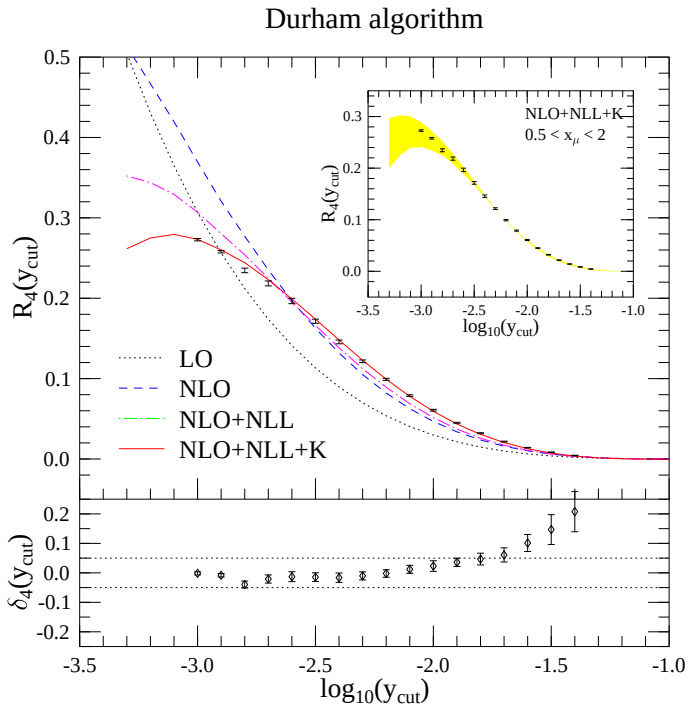

2. ábra: A QCD jóslat a négyjet rátára. A véges rendű (LO: pontozott vonal, NLO: szaggatott vonal), illetve az R-illesztett ($K = 0$: pontozott szaggatott vonal, $K \neq 0$: folytonos vonal) QCD jóslatok a Durham négyjet rátára $x_\mu = 1$ skálaválasztás mellett. A hibákkal feltüntetett pontok az ALEPH [58] kísérleti csoport eredményei.Az ábra alsó részén a kísérleti és az elméleti (R-illesztett $K \neq 0$ mellett) eredmények relatív eltérését mutatja ($\delta = 1 - \text{kísérlet/elmélet}$). A kis ábra az elméleti eredmény renormálási skálától való függését mutatja a $0.5 < x_\mu < 2$ tartományon.

Alakváltozók

Az alakváltozók közül itt csak a thrust minort vizsgáljuk. Tapasztalataink a többi alakváltozóra is érvényes. A thrust minor esetében az NLO korrekció 80%-120% között van, ami megkérdőjelezi a perturbációszámítás használhatóságát. A nagy korrekció azt eredményezi, hogy a renormálási skálától való függés nem csökken lényegesen, ami a 3. ábrán is jól látszik, ahol

$$\langle T_{\min} \rangle_{0.02} = \int_{0.02}^{0.5} dT_{\min} \Sigma(T_{\min}) \ , \tag{32}$$

ahol $\Sigma(T_{\min})$ a (3) egyenletben már definiáltunk. Látható, hogy a korrekció hatása inkább a normálás növelése és csak kevésbé a skálafüggés csökkentése. Ez a viselkedés jól látszik a 4. ábrán is.

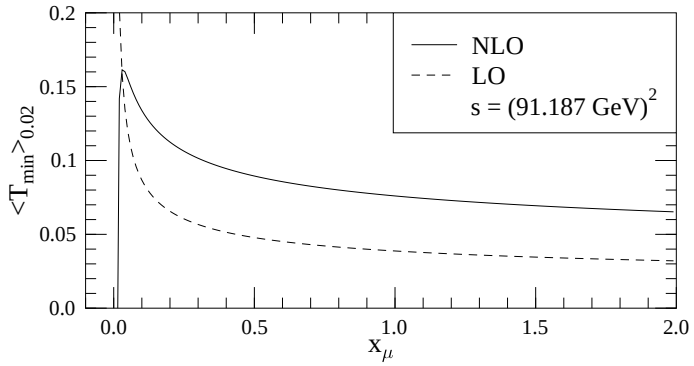

3. ábra: A $T_{\min}$ átlagának a renormálási skálától való függése

A fentiek alapján mondhatjuk azt, hogy a négyjet alakváltozók esetében szükségesek a magasabb rendű korrekciók ismerete is. Így az NLO eredmények nem alkalmasak pontos QCD tesztek elvégzésére.

Normált szögeloszlások

A normált szögeloszlások definiálásához először a négyjet eseményeket kell szelektálnunk. Ezt a Durham algoritmus segitségével végezték el az $y_{cut} = 0.08$ választással. A jetek impuzusát $\vec{p}_i$-vel $(i = 1, 2, 3, 4)$ jelöljük és a jeteket energiájuk szerint rendezzük úgy, hogy a legnagyobb energiája az első jetnek, a legkisebb a negyediknek van.

Itt most csak a legkisebb energiájú jetek szögeloszlását tárgyaljuk, melyet a következő módon definiálunk

$$\cos\alpha_{34} = \frac{\vec{p}_3 \cdot \vec{p}_4}{|\vec{p}_3||\vec{p}_4|} \quad . \tag{33}$$

A 5. ábrán láthatjuk a fenti mennyiségnek a

$$F(\cos\alpha_{34}) = \frac{1}{\sigma}\frac{d\sigma}{d\cos\alpha_{34}}(\cos\alpha_{34}) \quad , \qquad \sigma = \int_{-1}^{1} d\cos\alpha_{34}\,\frac{d\sigma}{d\cos\alpha_{34}}(\cos\alpha_{34}) \tag{34}$$

egyenlet szerint értelmezett normált szögeloszlását az ALEPH által mért adatokkal összehasonlítva. A belső ábrán az NLO korrekció nagyságát jellemző

$$K(\cos\alpha_{34}) = \frac{F_{NLO}(\cos\alpha_{34})}{F_{LO}(\cos\alpha_{34})} \tag{35}$$

faktor értéke található. Látható, hogy a K factor értéke közel egy, ami azt jelenti, hogy az NLO korrekció kicsi. Figyelemre méltó, hogy az NLO jóslat 5%-os pontossággal leírja a kísérleti adatokat, tehát a szögeloszlások is jól használhatók a QCD pontos ellenőrzésére, elsősorban az alapvető mértékcsoport mérésére.

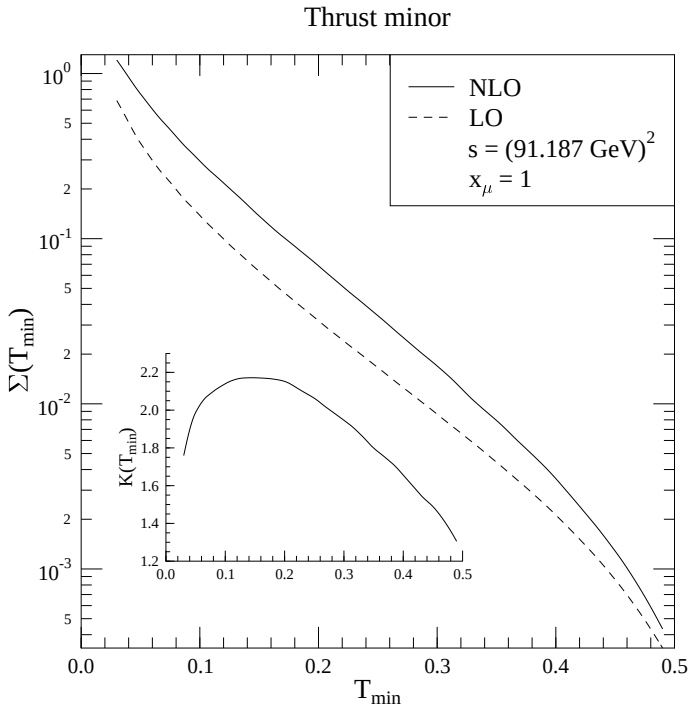

4. ábra: A LO (szaggatott) és az NLO (folytonos) QCD jóslatok a $T_{\rm min}$ disztribúcióra $x_\mu = 1$ skálaválasztás mellett.

Négyjet mennyiségek sugárzási korrekciói: összefoglalás

A négyjet mennyiségek esetén a vezető rendű jóslatok sokszor lényegesen kisebb ($x_\mu = 1$ skálaválasztás mellett), mint a kísérleti adatok, amiből az következik, hogy az elméletnek a valósággal való összehasonlításához szükséges az NLO korrekciók ismerete. Az eredmények azt mutatják, hogy a korrekciók nagyok és figyelembevételük lényegesen javitja a mért értékekkel való egyezést. Konkrétan a következőket állapíthatjuk meg:

i) A négyjet ráták esetén a sugárzási korrekciók nagyok, a JADE algoritmus esetén 100% körüli érték [1, 70], a Durham algoritmus esetén 60% körüli érték [6] és Cambridge algoritmus esetén még ennél is kisebb [6]. A renormálási skálától való függés a JADE algoritmustól eltekintve jelentősen csökken. A Durham algoritmus esetében figyelembe véve a logaritmus felösszegzésből jövő járulékokat, látványos egyezést kapunk a kísérleti adatokkal (3%-on belül).

ii) Az alakváltozók esetében a korrekciók általában 100%-nál is nagyobbak. A renormálási skálától való függés nem javul a korrekció figyelembevételével, csak az abszolút normálást emeli. A következtetésünk az, hogy az alakváltozók dif-

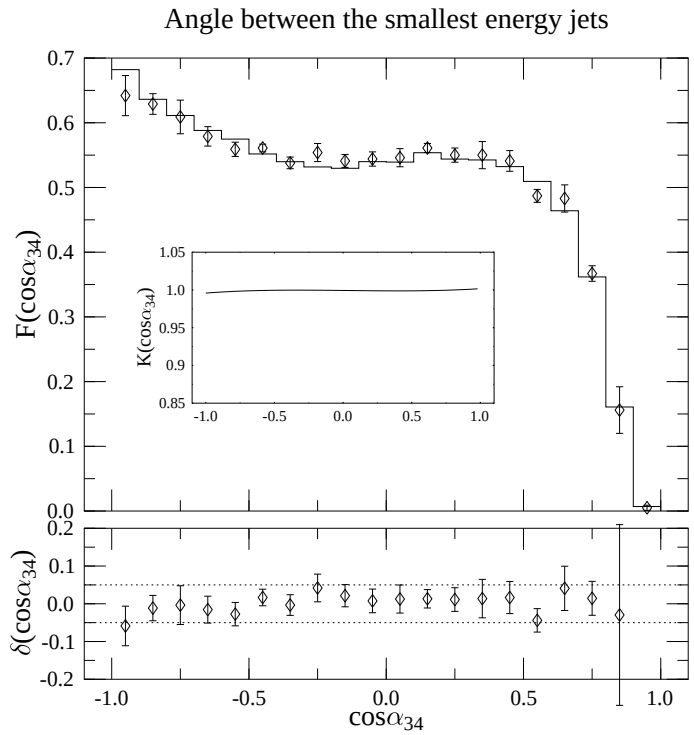

5. ábra: Az α_{34} szögeloszlás NLO elméleti jóslata összevetve az ALEPH által mért adatokkal. Az ábra alsó részén $\delta = \text{kísérlet/elmélet} - 1$, relatív eltérés látható. A könnyebb összehasonlítás végett az 5%-os sávot behúztuk.

ferenciális hatáskeresztmetszetei rögzített rendű NLO perturbációszámításban nem határozhatók meg megbizhatóan , ezért nem használhatók pontos QCD tesztekre. Itt fontos megjegyezni, hogy a logaritmus felösszegzés segíthet a helyzeten, de sajnos ezek a számolások még nem elérhető az irodalomban.

iii) A normál szögeloszlások eseteben az NLO korrekciók a várakozásnak megfelelően kicsik. A renormálási skálától való függése kicsi, azonban ez nem jelenti azt, hogy a hatásuk elhanyagolható lenne a QCD színtöltéseinek mérése során. Becslésünk szerint [5] a T_R/C_F hányados mért értéke akár 25%-ot is változhat, ha az NLO hatáskeresztmetszetet használjuk a színtöltés mérésekor a LO jóslat helyett.

Acknowledgments

My sincere thanks to *Dr. Zoltán Trócsányi*, for his skillful guidance as my supervisor for these years, to *Prof. Isván Lovas* and *Dr. Kornél Sailer* (the head of the Dept. of Theoretical Physics of University of Debrecen) for them constant support.

This work was sponsored in part by the EU Fourth Framework Programme "Training and Mobility of Researchers", Network "Quantum Chromodynamics and the Deep Structure of Elementary Particles", contract FMRX-CT98-0194 (DG 12 - MIHT), as well as by the Hungarian Scientific Research Fund grant OTKA T-025482, the Research Group in Physics of the Hungarian Academy of Sciences, Debrecen and the Universitas Foundation of the Hungarian Commercial Bank.

Appendix A

The tree level matrix elements

In this appendix we present analytic formulas for the four- and five-parton tree-level helicity amplitudes of the relevant subprocesses. These amplitudes were first calculated in Refs. [40]. The reason for presenting our results [6] here is twofold. On one hand we express the relevant color subamplitudes in terms of Weyl spinors $|k\pm\rangle$, which were also employed in the case of the one-loop four-parton amplitudes [47], while on the other we found that our expressions in the case of the four-quark processes are more compact and the corresponding computer code is faster than earlier ones. Another new feature of the amplitudes in this appendix is that we allow for the existence of light fermionic degrees of freedom in the adjoint representation of the gauge group (light gluinos). In calculating the amplitudes, we used quark and gluon currents [41, 39] and standard helicity techniques [41, 38].

A.1 Helicity amplitudes

We consider three subprocesses, each involving a vector boson $V(Q)$ carrying total four-momentum Q and n QCD partons ($n = 4$, or 5 here). The first subprocess is the production of a quark-antiquark pair and $n-2$ gluons. The second one is the production of two quark-antiquark pairs (of equal, or unequal flavor) and $n-4$ gluons. Finally, the third process is the production of a quark-antiquark pair, a light-gluino pair and $n-4$ gluons:

$$\begin{aligned}
\ell^+(-p_\ell) + \ell^-(-p_{\bar{\ell}}) &\rightarrow q(p_1) + g_1(p_2) + \cdots + g_{n-2}(p_{n-1}) + \bar{q}(p_n) \ , \quad \text{(A.1)} \\
\ell^+(-p_\ell) + \ell^-(-p_{\bar{\ell}}) &\rightarrow q(p_1) + \bar{q}(p_2) + Q(p_3) + \bar{Q}(p_4) \\
&+ \ g_1(p_5) + \cdots + g_{n-4}(p_n) \ , \quad \text{(A.2)} \\
\ell^+(-p_\ell) + \ell^-(-p_{\bar{\ell}}) &\rightarrow q(p_1) + \bar{q}(p_2) + \tilde{g}(p_3) + \tilde{g}(p_4) \\
&+ \ g_1(p_5) + \cdots + g_{n-4}(p_n) \ . \quad \text{(A.3)}
\end{aligned}$$

We have chosen the crossing invariant all particle outgoing kinematics with corresponding particle-antiparticle assignment, therefore, momentum conservation means

$$p_\ell + p_{\bar{\ell}} + p_1 + p_2 + p_3 + p_4 + p_5 + \ldots + p_n = 0 \ . \tag{A.4}$$

We shall express the amplitudes in terms of color subamplitudes. In the case of process (A.1), the color basis is chosen to be product of generators in the fundamental representation (in this appendix we use the normalization $T_R = 1$ in $\mathrm{Tr}(t^a t^b) = T_R\,\delta^{ab}$ for the generators of the symmetry group), therefore, the helicity amplitudes have the decomposition:

$$|1_f^{h_1}, 2_g^{h_2}, ..., n_{\bar{f}}^{h_n} >_n^{(0)} = \mathrm{g}_s^{(n-2)} \sum_{\{2,...,n-1\}} (t^{a_2} \cdots t^{a_{n-1}})_{i_1 \bar{i}_n}\ m(1_f^{h_1}, ..., n_{\bar{f}}^{h_n}) \ , \tag{A.5}$$

where $\{2, ..., n-1\}$ denotes all permutations of the labels $(2, ..., n-1)$ and $m(1, ..., n)$ are the color subamplitudes and g_s is the strong coupling constant. In Eq. (A.5) and in the following formulas the lepton labels are suppressed.

In the case of the four-fermion subprocesses (processes (A.2) and (A.3)) we decompose the helicity amplitudes as follows:

$$|1_{f_1}^{h_1}, 2_{f_2}^{h_2}, 3_{f_3}^{h_3}, 4_{f_4}^{h_4}, 5_g^{h_5}, ..., n_g^{h_n} >_n^{(0)} = \sum_{\{5,...,n\}} \sum_{\{1,3\}} (-1)^P \sum_{\{2,4\}} (-1)^P \mathcal{A}_n(1, 2, 3, 4, 5, ..., n) \ , \tag{A.6}$$

where $P = 0$ if the elements are in the canonical order ((1,3), or (2,4)) and $P = 1$ if the elements are permuted ((3,1), or (4,2)). The partial amplitudes $\mathcal{A}_n$ can be decomposed further in color space. In the case of four-quark production,

$$\mathcal{A}_4(1_q, 2_{\bar{q}}, 3_Q, 4_{\bar{Q}}) = \mathrm{g}_s^2 \sum_{b=1}^{N_A} t^b_{i_1 \bar{i}_2}\, t^b_{i_3 \bar{i}_4}\, M(1_{f_1}^{h_1}, 2_{f_2}^{h_2}, 3_{f_3}^{h_3}, 4_{f_4}^{h_4}) \ , \tag{A.7}$$

where $M(1_{f_1}^{h_1}, 2_{f_2}^{h_2}, 3_{f_3}^{h_3}, 4_{f_4}^{h_4})$ are the color subamplitudes.

In the case of four-quark plus one-gluon production, there are four independent basis vectors in color space:

$$\mathcal{A}_5(1_q, 2_{\bar{q}}, 3_Q, 4_{\bar{Q}}, 5_g) = \mathrm{g}_s^3 \sum_{i=1}^{4} T_i(1, 2, 3, 4, 5)\, M_i(1_{f_1}^{h_1}, 2_{f_2}^{h_2}, 3_{f_3}^{h_3}, 4_{f_4}^{h_4}, 5^{h_5}) \ , \tag{A.8}$$

where $T_i(1, 2, 3, 4, 5)$ are the color basis vectors:

$$T_1(1, ..., 5) = \sum_{b=1}^{N_A} (t^{a_5} t^b)_{i_1 \bar{i}_2}\, t^b_{i_3 \bar{i}_4} \ , \quad T_2(1, ..., 5) = \sum_{b=1}^{N_A} (t^b t^{a_5})_{i_1 \bar{i}_2}\, t^b_{i_3 \bar{i}_4} \ , \tag{A.9}$$

$$T_3(1, ..., 5) = \sum_{b=1}^{N_A} t^b_{i_1 \bar{i}_2}\, (t^{a_5} t^b)_{i_3 \bar{i}_4} \ , \quad T_4(1, ..., 5) = \sum_{b=1}^{N_A} t^b_{i_1 \bar{i}_2}\, (t^b t^{a_5})_{i_3 \bar{i}_4} \ . \tag{A.10}$$

The partial amplitudes for the process (A.3) can be written in terms of the color subamplitudes of the process (A.2), only the color basis differs. When $n = 4$,

$$\mathcal{A}_4(1_q, 2_{\bar{q}}, 3_{\tilde{g}}, 4_{\tilde{g}}) = \mathrm{g}_s^2 \sum_{b=1}^{N_A} t^b_{i_1\bar{i}_2}\, \widetilde{M}(1^{h_1}_{f_1}, 2^{h_2}_{f_2}, 3^{h_3}, 4^{h_4}) \ , \tag{A.11}$$

Finally, for $n = 5$ we have

$$\mathcal{A}_5(1_q, 2_{\bar{q}}, 3_{\tilde{g}}, 4_{\tilde{g}}, 5_g) = \mathrm{g}_s^3 \sum_{i=1}^{4} \widetilde{T}_i(1,2,3,4,5)\, \widetilde{M}_i(1^{h_1}_{f_1}, 2^{h_2}_{f_2}, 3^{h_3}, 4^{h_4}, 5^{h_5}) \ , \tag{A.12}$$

where

$$\widetilde{T}_1(1,...,5) = \sum_{b=1}^{N_A} (t^{a_5} t^b)_{i_1\bar{i}_2}\, F^b_{a_3 a_4} \,, \qquad \widetilde{T}_2(1,...,5) = \sum_{b=1}^{N_A} (t^b t^{a_5})_{i_1\bar{i}_2}\, F^b_{a_3 a_4} \,, \tag{A.13}$$

$$\widetilde{T}_3(1,...,5) = \sum_{b=1}^{N_A} t^b_{i_1\bar{i}_2}\, (F^{a_5} F^b)_{a_3 a_4} \,, \quad \widetilde{T}_4(1,...,5) = \sum_{b=1}^{N_A} t^b_{i_1\bar{i}_2}\, (F^b F^{a_5})_{a_3 a_4} \,. \tag{A.14}$$

In the following subsections we give explicit formulas for the color subamplitudes with a common coefficient factored out:

$$m(1^{h_1}_{f_1}, \ldots, n^{h_n}_{f_n}) = C^{h_\ell, h_1}_{f_1 f_n}\, A(1^{h_1}, \ldots, n^{h_n}) \ , \tag{A.15}$$

$$M(1^{h_1}_{f_1}, 2^{-h_1}_{f_2}, 3^{h_3}_{f_3}, 4^{-h_4}_{f_4}) = C^{h_\ell, h_1}_{f_1 f_2}\, \delta_{f_3 f_4}\, A(1^{h_1}, 2^{-h_1}, 3^{h_3}, 4^{-h_3}) \ , \tag{A.16}$$

$$M_i(1^{h_1}_{f_1}, 2^{-h_1}_{f_2}, 3^{h_3}_{f_3}, 4^{-h_3}_{f_4}, 5^{h_5}) = C^{h_\ell, h_1}_{f_1 f_2}\, \delta_{f_3 f_4}\, A_i(1^{h_1}, 2^{-h_1}, 3^{h_3}, 4^{-h_3}, 5^{h_5}) \ , \tag{A.17}$$

$$\widetilde{M}(1^{h_1}_{f_1}, 2^{-h_1}_{f_2}, 3^{h_3}, 4^{-h_4}) = C^{h_\ell, h_1}_{f_1 f_2}\, A(1^{h_1}, 2^{-h_1}, 3^{h_3}, 4^{-h_3}) \ , \tag{A.18}$$

$$\widetilde{M}_i(1^{h_1}_{f_1}, 2^{-h_1}_{f_2}, 3^{h_3}, 4^{-h_3}, 5^{h_5}) = C^{h_\ell, h_1}_{f_1 f_2}\, A_i(1^{h_1}, 2^{-h_1}, 3^{h_3}, 4^{-h_3}, 5^{h_5}) \ , \tag{A.19}$$

with $s = Q^2 = (p_\ell + p_{\bar{\ell}})^2$. The C coefficients contain the electroweak couplings. If the vector boson V is γ or Z^0 this coefficient is defined by

$$C^{h_\ell, h_{f_1}}_{f_1 f_2} = 2\, e^2 \left(-Q^{f_1}\, \mathcal{P}_\gamma(s) + v^{h_\ell}_\ell v^{h_{f_1}}_{f_1}\, \mathcal{P}_Z(s) \right) \delta_{f_1 f_2} \ , \tag{A.20}$$

where f_1, f_2 are the flavour indices of the quark antiquark pair that couples to the vector boson and

$$v^-_\ell = \frac{-1 + 2\sin^2\theta_W}{\sin 2\theta_W} \ , \qquad v^+_\ell = \frac{2\sin^2\theta_W}{\sin 2\theta_W} \ , \tag{A.21}$$

$$v^-_f = \frac{\pm 1 - 2Q_f \sin^2\theta_W}{\sin 2\theta_W} \ , \qquad v^+_f = -\frac{2Q_f \sin^2\theta_W}{\sin 2\theta_W} \ , \tag{A.22}$$

are the left- and right-handed couplings of leptons and quarks to neutral gauge bosons. In Eqs. (A.21,A.22) θ_W denotes the Weinberg angle, Q_f is the electric charge of the

quark of flavor f in units of e and the two signs in Eq. (A.22) correspond to up $(+)$ and down $(-)$ type quarks. The coupling C contains the propagators of Z^0 and photon,

$$\mathcal{P}_\gamma(s) = \frac{\mathrm{i}}{s + \mathrm{i}0}\,, \qquad \mathcal{P}_Z(s) = \frac{\mathrm{i}}{s - M_Z^2 + \mathrm{i}\Gamma_Z\, M_Z}\,, \tag{A.23}$$

where M_Z and Γ_Z are the mass and width of the Z^0.

If the vector boson V is a W^+ or a W^-, then the couplings take the form

$$C_{f_1 f_2}^{h_\ell, h_{f_1}} = 2\, e^2\, v_\ell^{h_\ell} v_{f_1}^{h_{f_1}}\, \mathcal{P}_W(s)\, \delta_{\tilde{f}_1 f_2}\,, \tag{A.24}$$

where $\tilde{f}_1$ denotes the partner of quark f_1 in the SU(2)$_L$ doublet and, for the sake of simplicity, we set the Kobayashi-Maskawa mixing matrix to unity. In Eq. (A.24) the left- and right-handed couplings differ from the corresponding expressions in Eqs. (A.21,A.22):

$$v_\ell^- = v_f^- = \frac{1}{2\sqrt{2}\sin\theta_W}\,, \qquad v_\ell^+ = v_f^+ = 0\,. \tag{A.25}$$

In this case $\mathcal{P}_W(s)$ denotes $W^\pm$ propagator,

$$\mathcal{P}_W(s) = \frac{\mathrm{i}}{s - M_W^2 + \mathrm{i}\Gamma_W\, M_W}\,, \tag{A.26}$$

where M_W and Γ_W are the mass and width of the $W^\pm$.

Four-parton color subamplitudes

In this subsection, we present all four-parton color subamplitudes for the helicity configuration $h_q = +$ and $h_\ell = +$. The amplitudes for the reversed helicity configurations can be obtained from these amplitudes by applying parity operation P, which amounts to making the substitutions $\langle ij\rangle \equiv \langle k_i^-|k_j^+\rangle \leftrightarrow [ji] \equiv \langle k_j^+|k_i^-\rangle$. The amplitudes when only the lepton helicities are reversed can be obtained simply by exchanging the lepton labels and flipping the lepton helicity in the coupling factors $C_{f_1 f_2}^{h_\ell, h_{f_1}}$ We use the notation

$$\begin{aligned}
\langle i|lm\ldots|j\rangle &\equiv k_l^\mu k_m^\nu \langle k_i^-|\gamma_\mu\gamma_\nu\ldots|k_j^\pm\rangle\,, &\text{(A.27)}\\
[i|lm\ldots|j] &\equiv k_l^\mu k_m^\nu \langle k_i^+|\gamma_\mu\gamma_\nu\ldots|k_j^\pm\rangle\,, &\text{(A.28)}\\
\langle i|(l+m)\ldots|j\rangle &\equiv (k_l^\mu + k_m^\mu)\ldots\langle k_i^-|\gamma_\mu\ldots|k_j^\pm\rangle\,, &\text{(A.29)}\\
[i|(l+m)\ldots|j] &\equiv (k_l^\mu + k_m^\mu)\ldots\langle k_i^+|\gamma_\mu\ldots|k_j^\pm\rangle\,, &\text{(A.30)}
\end{aligned}$$

and the two- and three-particle invariants $s_{ij} \equiv (k_i + k_j)^2$ and $t_{ijl} \equiv (k_i + k_j + k_l)^2$. Labels 5 and 6 refer to the positron and electron respectively. The two-quark two-

gluon color subamplitudes are as follows:

$$A(1_q^+,2_g^+,3_g^+,4_{\bar{q}}^-) = -\frac{\langle 45\rangle^2[56]}{\langle 12\rangle\langle 23\rangle\langle 34\rangle} \ , \tag{A.31}$$

$$A(1_q^+,2_g^-,3_g^-,4_{\bar{q}}^-) = -\frac{[16]^2\langle 56\rangle}{[12][23][34]} \ , \tag{A.32}$$

$$\begin{aligned} A(1_q^+,2_g^+,3_g^-,4_{\bar{q}}^-) &= -\frac{\langle 31\rangle[12]\langle 45\rangle\langle 3|(1+2)|6\rangle}{\langle 12\rangle s_{23}t_{123}} \\ &+ \frac{\langle 34\rangle[42][16]\langle 5|(3+4)|2\rangle}{[34]s_{23}t_{234}} + \frac{\langle 5|(3+4)|2\rangle\langle 3|(1+2)|6\rangle}{\langle 12\rangle[34]s_{23}} \ , \end{aligned} \tag{A.33}$$

$$\begin{aligned} A(1_q^+,2_g^-,3_g^+,4_{\bar{q}}^-) &= \frac{[13]^2\langle 45\rangle\langle 2|(1+3)|6\rangle}{[12]s_{23}t_{123}} - \frac{[13]\langle 24\rangle[16]\langle 45\rangle}{[12]\langle 34\rangle s_{23}} \\ &- \frac{\langle 24\rangle^2[16]\langle 5|(2+4)|3\rangle}{\langle 34\rangle s_{23}t_{234}} \ . \end{aligned} \tag{A.34}$$

In the four-quark case, we have only one independent helicity amplidute. The nonzero helicity configurations are as follows

$$A(1_q^+,2_{\bar{q}}^-,3_Q^+,4_{\bar{Q}}^-) = \frac{[13]\langle 25\rangle\langle 4|(1+3)|6\rangle}{t_{134}s_{34}} + \frac{\langle 42\rangle[16]\langle 5|(2+4)|3\rangle}{t_{234}s_{34}} \ , \tag{A.35}$$

$$A(1_q^+,2_{\bar{q}}^-,3_Q^-,4_{\bar{Q}}^+) = A(1_q^+,2_{\bar{q}}^-,4_Q^+,3_{\bar{Q}}^-) \ . \tag{A.36}$$

Five-parton color subamplitudes

In this subsection, we present all five-parton color subamplitudes for the helicity configuration $h_q = +$ and $h_\ell = +$. The amplitudes for the remaining helicity configurations can be obtained from these amplitudes as in the $n = 4$ case. Labels 6 and 7 refer to the positron and electron respectively. First we list the two-quark three-gluon amplitudes. In this case the *maximally helicity violating* (MHV) amplitudes (which are not independent) can be writen in the followings simple form

$$A(1_q^+,2_g^+,3_g^+,4_g^+,5_{\bar{q}}^-) = -\frac{\langle 65\rangle^2[67]}{\langle 12\rangle\langle 23\rangle\langle 34\rangle\langle 45\rangle} \ , \tag{A.37}$$

$$A(1_q^+,2_g^-,3_g^-,4_g^-,5_{\bar{q}}^-) = P\,A(5_q^+,4_g^+,3_g^+,2_g^+,1_{\bar{q}}^-)\Big|_{6\leftrightarrow 7} \ . \tag{A.38}$$

These amplitudes have very simple structure. The other helicity configurations is given by

$$
\begin{aligned}
A(1_q^+,2_g^+,3_g^+,4_g^-,5_{\bar{q}}^-) \;=\; & -\frac{[17]\langle 6|(1+7)|2\rangle\langle 45\rangle^2[53]^2}{[45]\langle 42\rangle s_{34}t_{345}t_{167}} \\
& + \frac{\langle 4|(5+6)|7\rangle\langle 6|(5+4)|3\rangle}{\langle 12\rangle\langle 23\rangle\langle 34\rangle[34][45]} - \frac{\langle 4|(1+2)|7\rangle\langle 6|(5+4)|3\rangle\langle 45\rangle[53]}{\langle 12\rangle\langle 24\rangle[45]s_{34}t_{345}} \\
& + \frac{\langle 65\rangle\langle 4|(5+6)|7\rangle}{\langle 23\rangle\langle 34\rangle[34]t_{567}}\left(\frac{[23]\langle 4|(2+3)|1\rangle}{t_{234}} + \frac{\langle 4|(1+2)|3\rangle}{\langle 12\rangle}\right) \\
& + \frac{[17]\langle 45\rangle[53]}{\langle 23\rangle[34][45]t_{167}}\left(\frac{\langle 6|(1+7)|2\rangle}{\langle 34\rangle} + \frac{\langle 6|(1+7)|3\rangle}{\langle 24\rangle}\right) \\
& - \frac{[17]\langle 45\rangle[23]}{\langle 23\rangle[34]t_{234}t_{167}}\left(\frac{\langle 6|(1+7)|2\rangle\langle 24\rangle}{\langle 34\rangle} + \langle 6|(1+7)|3\rangle\right) \quad , \qquad \text{(A.39)}
\end{aligned}
$$

$$
\begin{aligned}
A(1_q^+,2_g^+,3_g^-,4_g^+,5_{\bar{q}}^-) = & \frac{\langle 31\rangle[12]\langle 3|(1+2)|4\rangle\langle 3|(5+6)|7\rangle\langle 65\rangle}{\langle 12\rangle\langle 34\rangle s_{23}t_{123}t_{567}} \\
& + \frac{\langle 31\rangle[12]\langle 3|(1+2)|7\rangle\langle 65\rangle\langle 35\rangle}{\langle 12\rangle\langle 34\rangle\langle 45\rangle s_{23}t_{123}} - \frac{\langle 3|(1+2)|7\rangle\langle 6|(1+7)|2\rangle\langle 35\rangle^2}{\langle 12\rangle\langle 23\rangle\langle 34\rangle\langle 45\rangle[23]t_{345}} \\
& + \frac{\langle 3|(1+2)|7\rangle\langle 6|(5+3)|4\rangle\langle 35\rangle[42]}{[23]\langle 12\rangle\langle 23\rangle s_{34}t_{345}} - \frac{[42]^2[17]\langle 6|(1+7)(2+4)|3\rangle\langle 35\rangle}{s_{23}s_{34}t_{234}t_{167}} \\
& + \frac{[42]\langle 3|(5+6)|7\rangle\langle 65\rangle}{s_{23}s_{34}t_{567}}\left(\frac{[42]\langle 3|(2+4)|1\rangle}{t_{234}} - \frac{\langle 3|(1+2)|4\rangle}{\langle 12\rangle}\right) \\
& + \frac{[17]\langle 6|(1+7)|2\rangle\langle 35\rangle^2}{s_{23}t_{345}t_{167}}\left(\frac{\langle 3|(5+4)|2\rangle}{\langle 34\rangle\langle 45\rangle} + \frac{[42][54]}{s_{34}}\right) \quad , \qquad \text{(A.40)}
\end{aligned}
$$

$$
\begin{aligned}
A(1_q^+,2_g^-,3_g^+,4_g^+,5_{\bar{q}}^-) = & \frac{[43]^2\langle 2|(3+4)|1\rangle\langle 2|(5+6)|7\rangle\langle 65\rangle}{s_{23}s_{34}t_{234}t_{567}} \\
& + \frac{[13]\langle 2|(3+4)|1\rangle\langle 2|(5+6)|7\rangle\langle 65\rangle}{[12]\langle 34\rangle\langle 42\rangle s_{23}t_{567}} - \frac{[13]^2\langle 2|(1+3)|4\rangle\langle 2|(5+6)|7\rangle\langle 65\rangle}{[12]\langle 24\rangle s_{23}t_{123}t_{567}} \\
& + \frac{[17]\langle 6|(1+7)|3\rangle\langle 25\rangle}{\langle 24\rangle s_{23}t_{345}t_{167}}\left(\langle 2|(5+4)|3\rangle\left(\frac{\langle 25\rangle}{\langle 45\rangle} - \frac{\langle 32\rangle}{\langle 34\rangle}\right) - \langle 2|(5+3)|4\rangle\frac{\langle 42\rangle}{\langle 34\rangle}\right) \\
& + \frac{[13][17]\langle 25\rangle}{[12]s_{23}\langle 24\rangle t_{345}}\left(\langle 6|(5+4)|3\rangle\left(\frac{\langle 25\rangle}{\langle 45\rangle} - \frac{\langle 32\rangle}{\langle 34\rangle}\right) - \langle 6|(5+3)|4\rangle\frac{\langle 42\rangle}{\langle 34\rangle}\right) \\
& - \frac{[13]^2\langle 2|(1+3)|7\rangle\langle 65\rangle\langle 25\rangle}{[12]\langle 24\rangle\langle 45\rangle s_{23}t_{123}} - \frac{[17]\langle 25\rangle[43]^2\langle 6|(1+7)(3+4)|2\rangle}{s_{23}s_{34}t_{234}t_{167}} \quad , \qquad \text{(A.41)}
\end{aligned}
$$

$$
\begin{aligned}
A(1_q^+,2_g^+,3_g^-,4_g^-,5_{\bar{q}}^-) &= \frac{[12][2|(3+4)(5+6)|7]\langle 65\rangle}{s_{23}t_{567}}\left(\frac{\langle 43\rangle^2}{s_{34}t_{234}}-\frac{\langle 31\rangle}{[34][42]\langle 12\rangle}\right)\\
&-\frac{\langle 31\rangle^2[12]^2\langle 4|(5+6)|7\rangle\langle 65\rangle}{\langle 12\rangle[24]s_{23}t_{123}t_{567}}+\frac{\langle 31\rangle[12]\langle 3|(1+2)|7\rangle\langle 6|(5+4)|2\rangle}{\langle 12\rangle[24][45]s_{23}t_{123}}\\
&+\frac{\langle 3|(1+2)|7\rangle\langle 6|(1+7)|2\rangle}{\langle 12\rangle[34][45]s_{23}}+\frac{[17]\langle 6|(1+7)|2\rangle\langle 3|(5+4)|2\rangle}{[34][45]s_{23}t_{167}}\\
&-\frac{[17]\langle 6|(1+7)|2\rangle\langle 5|(3+4)|2\rangle\langle 43\rangle^2}{s_{23}s_{34}t_{234}t_{167}}\ , \qquad \text{(A.42)}
\end{aligned}
$$

$$
\begin{aligned}
A(1_q^+,2_g^-,3_g^-,4_g^+,5_{\bar{q}}^-) &= \frac{\langle 23\rangle^2[14][4|(2+3)(5+6)|7]\langle 65\rangle}{s_{23}s_{34}t_{234}t_{567}}\\
&-\frac{[14]\langle 3|(5+6)|7\rangle\langle 65\rangle}{[42]s_{34}t_{123}t_{567}}\left(\frac{[4|(2+3)(1+2+3)|4]}{[23]}-\frac{[14]\langle 3|(1+2)|4\rangle}{[12]}\right)\\
&-\frac{[14]\langle 65\rangle\langle 35\rangle}{[42]\langle 45\rangle s_{34}t_{123}}\left(\frac{[4|(2+3)(1+2+3)|7]}{[23]}-\frac{[14]\langle 3|(1+2)|7\rangle}{[12]}\right)\\
&+\frac{[14][17]\langle 6|(5+3)|4\rangle\langle 35\rangle^2}{[12][24]\langle 45\rangle s_{34}t_{345}}-\frac{[17]\langle 6|(1+7)|4\rangle\langle 2|(5+3)|4\rangle\langle 35\rangle^2}{[42]\langle 45\rangle s_{34}t_{345}t_{167}}\\
&-\frac{[17]\langle 6|(1+7)|4\rangle\langle 5|(2+3)|4\rangle}{s_{34}t_{167}}\left(\frac{\langle 35\rangle}{\langle 45\rangle[42][23]}+\frac{\langle 23\rangle^2}{s_{23}t_{234}}\right)\ . \qquad \text{(A.43)}
\end{aligned}
$$

The $(+,-,+,-,-)$ helicity configuration can be obtained using the charge conjugation

$$
A(1_q^+,2_g^-,3_g^+,4_g^-,5_{\bar{q}}^-) = P\,A(5_q^+,4_g^+,3_g^-,2_g^+,1_{\bar{q}}^-)_{|_{6\leftrightarrow 7}}\ . \qquad \text{(A.44)}
$$

The four-quark one-gluon amplitudes have are also listed. The first is

$$
\begin{aligned}
A_1(1_q^+,2_{\bar{q}}^-,3_Q^+,4_{\bar{Q}}^-,5_g^+) &= -\frac{[15]\langle 4|(1+5)|3\rangle\langle 4|(2+6)|7\rangle\langle 62\rangle}{\langle 45\rangle s_{15}s_{34}t_{267}}\\
&-\frac{[17]\langle 6|(1+7)|5\rangle\langle 42\rangle^2[23]}{\langle 45\rangle s_{34}t_{234}t_{167}}-\frac{\langle 4|(1+5)|7\rangle\langle 6|(2+4)|3\rangle\langle 42\rangle}{\langle 15\rangle\langle 54\rangle s_{34}t_{234}}\\
&+\frac{[53]\langle 4|(3+5)|1\rangle\langle 4|(2+6)|7\rangle\langle 62\rangle}{\langle 45\rangle s_{34}t_{345}t_{267}}\\
&+\frac{[17]\langle 6|(1+7)(3+5)|4\rangle[35]\langle 42\rangle}{\langle 45\rangle s_{34}t_{345}t_{167}}\ , \qquad \text{(A.45)}
\end{aligned}
$$

and for the other helicity configuration, the non zero color subamplitudes are given by the followings

$$A_1(1_q^+,2_{\bar{q}}^-,3_Q^+,4_{\bar{Q}}^-,5_g^-) = \frac{[13]^2\langle 51\rangle\langle 4|(2+6)|7\rangle\langle 62\rangle}{[35]s_{15}s_{34}t_{267}} + \frac{[17]\langle 6|(1+7)|3\rangle\langle 5|(2+4)|3\rangle\langle 42\rangle}{[35]s_{34}t_{234}t_{167}} - \frac{[13][17]\langle 6|(2+4)|3\rangle\langle 42\rangle}{[15][53]s_{34}t_{234}} + \frac{[13]\langle 54\rangle[3|(4+5)(2+6)|7]\langle 62\rangle}{[35]s_{34}t_{345}t_{267}} - \frac{[17]\langle 6|(1+7)|3\rangle\langle 54\rangle\langle 2|(4+5)|3\rangle}{[35]s_{34}t_{345}t_{167}} \quad , \tag{A.46}$$

$$A_2(1_q^+,2_{\bar{q}}^-,3_Q^+,4_{\bar{Q}}^-,5_g^+) = -\frac{[53]\langle 4|(3+5)|1\rangle\langle 4|(2+6)|7\rangle\langle 62\rangle}{\langle 45\rangle s_{34}t_{345}t_{267}} - \frac{[17]\langle 6|(1+7)|3\rangle[25]\langle 42\rangle^2}{\langle 45\rangle s_{25}s_{34}t_{167}} - \frac{[13]\langle 4|(1+3)|5\rangle\langle 4|(2+6)|7\rangle\langle 62\rangle}{\langle 45\rangle s_{34}t_{134}t_{267}} - \frac{[13]\langle 4|(1+3)|7\rangle\langle 42\rangle\langle 62\rangle}{\langle 45\rangle\langle 52\rangle s_{34}t_{134}} - \frac{[17]\langle 6|(1+7)(3+5)|4\rangle[35]\langle 42\rangle}{\langle 45\rangle s_{34}t_{345}t_{167}} \quad , \tag{A.47}$$

$$A_2(1_q^+,2_{\bar{q}}^-,3_Q^+,4_{\bar{Q}}^-,5_g^-) = -\frac{[13]\langle 54\rangle[3|(4+5)(2+6)|7]\langle 62\rangle}{[35]s_{34}t_{345}t_{267}} + \frac{[13]^2\langle 41\rangle\langle 5|(2+6)|7\rangle\langle 62\rangle}{[35]s_{34}t_{134}t_{267}} + \frac{[17]\langle 6|(1+7)|3\rangle\langle 54\rangle\langle 2|(4+5)|3\rangle}{[35]s_{34}t_{345}t_{167}} - \frac{[13]\langle 4|(1+3)|7\rangle\langle 6|(2+5)|3\rangle}{[35][52]s_{34}t_{134}} + \frac{[17]\langle 6|(1+7)|3\rangle\langle 52\rangle\langle 4|(2+5)|3\rangle}{[35]s_{25}s_{34}t_{167}} \quad , \tag{A.48}$$

$$A_3(1_q^+,2_{\bar{q}}^-,3_Q^+,4_{\bar{Q}}^-,5_g^+) = -\frac{[53]\langle 4|(3+5)|1\rangle\langle 4|(2+6)|7\rangle\langle 62\rangle}{\langle 45\rangle s_{35}t_{345}t_{267}} - \frac{[17]\langle 6|(1+7)(3+5)|4\rangle[35]\langle 42\rangle}{\langle 45\rangle s_{35}t_{345}t_{167}} \quad , \tag{A.49}$$

$$A_4(1_q^+,2_{\bar{q}}^-,3_Q^-,4_{\bar{Q}}^+,5_g^+) = \frac{[54]\langle 3|(4+5)|1\rangle\langle 3|(2+6)|7\rangle\langle 62\rangle}{\langle 35\rangle s_{45}t_{345}t_{267}} + \frac{[17]\langle 6|(1+7)(4+5)|3\rangle[45]\langle 32\rangle}{\langle 35\rangle s_{45}t_{345}t_{167}} \quad , \tag{A.50}$$

$$A_3(1_q^+,2_{\bar{q}}^-,3_Q^-,4_{\bar{Q}}^+,5_g^-) = -\frac{[14]\langle 53\rangle[4|(3+5)(2+6)|7]\langle 62\rangle}{[45]s_{35}t_{435}t_{267}} + \frac{[17]\langle 6|(1+7)|4\rangle\langle 53\rangle\langle 2|(3+5)|4\rangle}{[45]s_{35}t_{435}t_{167}} \ , \tag{A.51}$$

$$A_4(1_q^+,2_{\bar{q}}^-,3_Q^+,4_{\bar{Q}}^-,5_g^-) = \frac{[13]\langle 54\rangle[3|(4+5)(2+6)|7]\langle 62\rangle}{[35]s_{45}t_{345}t_{267}} - \frac{[17]\langle 6|(1+7)|3\rangle\langle 54\rangle\langle 2|(4+5)|3\rangle}{[35]s_{45}t_{345}t_{167}} \ . \tag{A.52}$$

The non independent color amplitudes are as follows

$$A_1(1_q^+,2_{\bar{q}}^-,3_Q^-,4_{\bar{Q}}^+,5_g^+) = A_1(1_q^+,2_{\bar{q}}^-,4_Q^+,3_{\bar{Q}}^-,5_g^+) \ , \tag{A.53}$$

$$A_1(1_q^+,2_{\bar{q}}^-,3_Q^-,4_{\bar{Q}}^+,5_g^-) = A_1(1_q^+,2_{\bar{q}}^-,4_Q^+,3_{\bar{Q}}^-,5_g^-) \ , \tag{A.54}$$

$$A_2(1_q^+,2_{\bar{q}}^-,3_Q^-,4_{\bar{Q}}^+,5_g^+) = A_2(1_q^+,2_{\bar{q}}^-,4_Q^+,3_{\bar{Q}}^-,5_g^+) \ , \tag{A.55}$$

$$A_2(1_q^+,2_{\bar{q}}^-,3_Q^-,4_{\bar{Q}}^+,5_g^-) = A_2(1_q^+,2_{\bar{q}}^-,4_Q^+,3_{\bar{Q}}^-,5_g^-) \ . \tag{A.56}$$

A.2 Matrix elements

In this appendix we present analytic formulas for the color-correlated four-parton Born-level matrix elements and for the four-, five-parton Born-level matrix elements. The calculation of the color-correlated four-parton amplitudes is a straightforward application of color algebra and the four-parton helicity amplitudes. However, to our knowledge these results were not published previously. The uncorrelated color sum was first calculated in Ref. [40]. We present our results in terms of the color subamplitudes of Appendix A.1. It is a new feature of the matrix elements in this appendix that they are given in terms of group independent functions and eigenvalues of the quadratic Casimir operators of the underlying gauge group.

Having the helicity amplitudes at our disposal, we calculate the squared matrix elements summed over final state colors without and with color-correlation:

$$|M_n^{(0)}(1,...,n)|^2 = {}_n^{(0)}\!<1,...,n|1,...,n>_n^{(0)} \ , \qquad n=4,5 \ , \tag{A.57}$$

$$|M_4^{(0)\,i,j}(1,...,4)|^2 = {}_n^{(0)}\!<1^{h_1},...,4^{h_4}|\,\boldsymbol{T}_i\cdot\boldsymbol{T}_j\,|1^{h_1'},...,4^{h_4'}>_n^{(0)} \ , \tag{A.58}$$

where in the latter case we leave the helicity indices explicit so that both correlated and uncorrelated helicity summation is possible. (Although we did not show the

flavor indices, the flavor summation is also left out, as will become clear later.) In the correlated case we have to insert the helicity matrix (see Eq. (4.21))

$$\boldsymbol{H}_{i,j}^{hh'} = \delta_{h_1 h'_1} ... \langle h_i | \, \boldsymbol{V}_{i,j} \, | h'_i \rangle ... \delta_{h_n h'_n} \quad , \tag{A.59}$$

and in the uncorrelated case

$$\boldsymbol{H}_{i,j}^{hh'} = \delta_{h_1 h'_1} \dots \delta_{h_i h'_i} \dots \delta_{h_n h'_n} \quad . \tag{A.60}$$

We evaluate the color sum in such a way that the matrix elements are given as polynomial expressions of the Casimir invariants of the gauge group with group independent kinematical coefficients. In addition to the usual quadratic Casimirs C_F and C_A, we shall also use a cubic Casimir C_3 that is defined as

$$C_3 = \sum_{a,b,c=1}^{N_A} \mathrm{Tr}(t^a t^b t^c) \mathrm{Tr}(t^c t^b t^a) \quad . \tag{A.61}$$

In the following subsections we list the explicit formulas for $|M_4^{(0)}|^2$, $|M_4^{(0)\,ij}|^2$ and $|M_5^{(0)}|^2$.

Four-parton color-summed matrix elements

In this subsection, we give explicit formulas for the color-summed Born matrix elements for four final state partons. There are four different cases: the two-quark two-gluon process and three four-fermion processes (two unequal flavor quark pairs, two equal flavor quark pairs and the two-quark two-gluino production). The color summation is straightforward in each cases, we simply list the results:

$$\begin{aligned}
|M_4^{(0)}(1_q, 2_g, 3_g, 4_{\bar{q}})|^2 &= N_c C_F^2 \Big\{ |m(1_{f_1}, 2, 3, 4_{f_4}) + m(1_{f_1}, 3, 2, 4_{f_4})|^2 \\
&- x \, \mathrm{Re}\big(m(1_{f_1}, 2, 3, 4_{f_4}) m(1_{f_1}, 3, 2, 4_{f_4})^* \big) \Big\} \quad , \qquad \text{(A.62)} \\
|M_4^{(0)}(1_q, 2_{\bar{q}}, 3_Q, 4_{\bar{Q}})|^2 &= N_c C_F^2 \Big\{ \\
&- 2 \, \mathrm{Re}\big(H(1_{f_1}, 2_{f_2}, 3_{f_3}, 4_{f_4}) H(1_{f_1}, 4_{f_4}, 3_{f_3}, 2_{f_2})^* \big) \\
&+ x \, \mathrm{Re}\big(H(1_{f_1}, 2_{f_2}, 3_{f_3}, 4_{f_4}) H(1_{f_1}, 4_{f_4}, 3_{f_3}, 2_{f_2})^* \big) \\
&+ y \, |H(1_{f_1}, 2_{f_2}, 3_{f_3}, 4_{f_4})|^2 \\
&+ y \, |H(1_{f_1}, 4_{f_4}, 3_{f_3}, 2_{f_2})|^2 \Big\} \quad , \qquad \text{(A.63)} \\
|M_4^{(0)}(1_q, 2_{\tilde{q}}, 3_{\tilde{g}}, 4_{\tilde{g}})|^2 &= N_c C_F^2 \, x \, |\widetilde{M}(1_{f_1}, 2_{f_2}, 3, 4)|^2 \quad , \qquad \text{(A.64)}
\end{aligned}$$

where x and y are ratios of the quadratic Casimirs ($x = C_A/C_F$, $y = T_R/C_F$ and $z = C_3/(N_c C_F^3)$) and $H(1_{f_1}, 2_{f_2}, 3_{f_3}, 4_{f_4})$ is defined by

$$H(1_{f_1}, 2_{f_2}, 3_{f_3}, 4_{f_4}) = M(1_{f_1}, 2_{f_2}, 3_{f_3}, 4_{f_4}) + M(3_{f_3}, 4_{f_4}, 1_{f_1}, 2_{f_2}) \quad . \tag{A.65}$$

Four-parton color-correlated matrix elements

In this subsection, we give explicit formulas for the color-correlated, color-summed Born matrix elements for four final state partons. We consider those four cases as in the previous subsection. The color summation is again fairly straightforward, therefore, we only record the results.

For the $V \to q\bar{q}gg$ subprocess

$$|M_4^{(0)\,ik}(1_q, 2_g, 3_g, 4_{\bar{q}})|^2 = -\frac{N_c C_F^3}{2}\left\{M_0^{ik} + xM_x^{ik} + x^2 M_{xx}^{ik}\right\} , \tag{A.66}$$

where the non-vanishing elements of the matrix $M_0^{(0)\,ik}$ are given by

$$M_0^{12} = 2(S_1 + S_2 + S_3) \ , \tag{A.67}$$

of matrix $M_x^{(0)\,ik}$ are given by

$$\begin{aligned} M_x^{12} &= -2S_1 - 2S_2 - 3S_3 \ , \\ M_x^{13} &= M_x^{14} = M_x^{23} = M_x^{24} = S_1 + S_2 + S_3 \ , \end{aligned} \tag{A.68}$$

and of matrix $M_x^{(0)\,ik}$ are given by

$$\begin{aligned} M_{xx}^{12} &= \frac{1}{2}(S_1 + S_2 + 2S_3) \ , & M_{xx}^{13} &= M_{xx}^{24} = -\frac{1}{2}(S_2 + S_3) \ , \\ M_{xx}^{14} &= M_{xx}^{23} = -\frac{1}{2}(S_1 + S_3) \ , & M_{xx}^{34} &= \frac{1}{2}(S_1 + S_2) \ , \end{aligned} \tag{A.69}$$

and the S_i functions are defined by

$$S_1 = m(1_{f_1}^{h_1}, 2^{h_2}, 3^{h_3}, 4_{f_4}^{h_4})^* m(1_{f_1}^{h'_1}, 2^{h'_2}, 3^{h'_3}, 4_{f_4}^{h'_4}) \ , \tag{A.70}$$

$$S_2 = m(1_{f_1}^{h_1}, 3^{h_3}, 2^{h_2}, 4_{f_4}^{h_4})^* m(1_{f_1}^{h'_1}, 3^{h'_3}, 2^{h'_2}, 4_{f_4}^{h'_4}) \ , \tag{A.71}$$

$$\begin{aligned} S_3 &= m(1_{f_1}^{h_1}, 2^{h_2}, 3^{h_3}, 4_{f_4}^{h_4})^* m(1_{f_1}^{h'_1}, 3^{h'_3}, 2^{h'_2}, 4_{f_4}^{h'_4}) \\ &+ m(1_{f_1}^{h_1}, 3^{h_3}, 2^{h_2}, 4_{f_4}^{h_4})^* m(1_{f_1}^{h'_1}, 2^{h'_2}, 3^{h'_3}, 4_{f_4}^{h'_4}) \ . \end{aligned} \tag{A.72}$$

In the case of four-quark production

$$\begin{aligned} |M_4^{(0)\,ik}(1_q, 2_{\bar{q}}, 3_Q, 4_{\bar{Q}})|^2 &= -\frac{N_c C_F^3}{2}\Big\{M_0^{ik} + xM_x^{ik} + yM_y^{ik} + zM_z^{ik} \\ &\quad + x^2 M_{xx}^{ik} + xyM_{xy}^{ik}\Big\}, \end{aligned} \tag{A.73}$$

where the non-zero element of the matrices M_0^{ik}, M_x^{ik}, M_y^{ik}, M_z^{ik}, M_{xx}^{ik}, M_{xy}^{ik} are also listed. The matrix M_0^{ik} is given by

$$M_0^{12} = M_0^{14} = M_0^{23} = M_0^{34} = -2S_3 \ , \qquad M_0^{13} = M_0^{24} = 2S_3 \ . \tag{A.74}$$

The matrix M_x^{ik} is given by

$$M_x^{12} = M_x^{14} = M_x^{23} = M_x^{34} = 2S_3 \ , \qquad M_x^{13} = M_x^{24} = -3S_3 \ . \tag{A.75}$$

The matrix M_y^{ik} is given by

$$M_y^{12} = M_y^{34} = 2S_1 \ , \qquad M_y^{14} = M_y^{23} = 2S_2 \ . \tag{A.76}$$

The matrix M_y^{ik} is given by

$$M_z^{12} = M_z^{34} = 2S_2 \ , \quad M_z^{14} = M_z^{23} = 2S_1 \ , \quad M_z^{13} = M_z^{24} = -2(S_1 + S_2) \tag{A.77}$$

The matrix M_y^{ik} is given by

$$M_{xx}^{12} = M_{xx}^{14} = M_{xx}^{23} = M_{xx}^{34} = -\frac{1}{2}S_3 \ , \qquad M_{xx}^{13} = M_{xx}^{24} = S_3 \ . \tag{A.78}$$

The matrix M_y^{ik} is given by

$$M_{xy}^{12} = M_{xy}^{34} = -S_1 \ , \quad M_{xy}^{14} = M_{xy}^{23} = -S_2 \ , \quad M_{xy}^{13} = M_{xy}^{24} = S_1 + S_2 \ . \tag{A.79}$$

For this case the S_i functions are defined as follows:

$$\begin{aligned}
S_1 &= H(1_{f_1}^{h_1}, 2_{f_2}^{h_2}, 3_{f_3}^{h_3}, 4_{f_4}^{h_4})^* H(1_{f_1}^{h'_1}, 2_{f_2}^{h'_2}, 3_{f_3}^{h'_3}, 4_{f_4}^{h'_4}) \ , && \text{(A.80)} \\
S_2 &= H(1_{f_1}^{h_1}, 4_{f_4}^{h_4}, 3_{f_3}^{h_3}, 2_{f_2}^{h_2})^* H(1_{f_1}^{h'_1}, 4_{f_4}^{h'_4}, 3_{f_3}^{h'_3}, 2_{f_2}^{h'_2}) \ , && \text{(A.81)} \\
S_3 &= H(1_{f_1}^{h_1}, 2_{f_2}^{h_2}, 3_{f_3}^{h_3}, 4_{f_4}^{h_4})^* H(1_{f_1}^{h'_1}, 4_{f_4}^{h'_4}, 3_{f_3}^{h'_3}, 2_{f_2}^{h'_2}) \\
&+ H(1_{f_1}^{h_1}, 4_{f_4}^{h_4}, 3_{f_3}^{h_3}, 2_{f_2}^{h_2})^* H(1_{f_1}^{h'_1}, 2_{f_2}^{h'_2}, 3_{f_3}^{h'_3}, 4_{f_4}^{h'_4}) \ , && \text{(A.82)}
\end{aligned}$$

where $H(1_{f_1}, 2_{f_2}, 3_{f_3}, 4_{f_4})$ is defined in Eq. (A.65).

Finally, for the $V \to q\bar{q}\tilde{g}\tilde{g}$ subprocess

$$|M_4^{(0)\,ik}(1_q, 2_{\bar{q}}, 3_{\tilde{g}}, 4_{\tilde{g}})|^2 = -\frac{N_c C_F^3}{2} \left\{ x\widetilde{M}_x^{ik} + x^2 \widetilde{M}_{xx}^{ik} \right\} , \tag{A.83}$$

where the non-vanishing elements of the matrices $\widetilde{M}_x^{ik}$ and $\widetilde{M}_{xx}^{ik}$ are given by

$$\widetilde{M}_x^{12} = 2|\widetilde{M}(1_{f_1}, 2_{f_2}, 3_{f_3}, 4_{f_4})|^2 \ ,$$

$$\begin{aligned}
&\widetilde{M}_{xx}^{12} = -\widetilde{M}_{xx}^{34} = -|\widetilde{M}(1_{f_1}, 2_{f_2}, 3_{f_3}, 4_{f_4})|^2 \ , \\
&\widetilde{M}_{xx}^{13} = \widetilde{M}_{xx}^{14} = \widetilde{M}_{xx}^{23} = \widetilde{M}_{xx}^{24} = \frac{1}{2}|\widetilde{M}(1_{f_1}, 2_{f_2}, 3_{f_3}, 4_{f_4})|^2 \ . && \text{(A.84)}
\end{aligned}$$

Five-parton color-summed matrix elements

In this subsection, we give explicit formulas for the color-summed Born matrix elements for five final state partons. There are again four different cases: the two-quark three-gluon process, the production of two equal, or unequal flavor quark pairs plus a gluon and the two-quark two-gluino one-gluon production.

In the case of the two-quark three-gluon process the color summation is straightforward and leads to the following expression:

$$M_5^{(0)}(1_q,2_g,3_g,4_g,5_{\bar{q}})|^2 = N_c C_F^3 \Big\{ M_0 - \frac{x}{2}(M_1+2M_0) \tag{A.85}$$

$$+ \frac{x^2}{4}(M_0+M_1+M_2) \Big\} \ , \tag{A.86}$$

where

$$M_0 = \Big| \sum_{\{2,3,4\}} m(1_{f_1},2,3,4,5_{f_5}) \Big|^2 \ , \tag{A.87}$$

$$M_2 = \sum_{\{2,3,4\}} |m(1_{f_1},2,3,4,5_{f_5})|^2 \ , \tag{A.88}$$

and

$$M_1 + 2\,M_2 = -2\,\mathrm{Re} \sum_{\{2,3,4\}'} \big\{ m(1_{f_1},2,3,4,5_{f_5})^* \cdot \big(m(1_{f_1},2,4,3,5_{f_5}) + m(1_{f_1},3,2,4,5_{f_5}) - m(1_{f_1},4,3,2,5_{f_5}) \big) \big\} \ , \tag{A.89}$$

where $\{2,3,4\}$ denotes the all permutation of the labels 2,3,4 and $\{2,3,4\}'$ denotes the cyclic permutations of these labels.

In the case of the four-quark one-gluon subprocesses the color decomposition of the matrix element squared for any flavor configuration can be written in the following form

$$|M_5^{(0)}(1_q,2_{\bar{q}},3_Q,4_{\bar{Q}},5_g)|^2 = N_c C_F^3 \big\{ M_0 + x M_x + y M_y + z M_z + x^2 M_{xx} + xy M_{xy} \big\} \ , \tag{A.90}$$

and the following abbreviations:

$$M_0 = B + C + E \ , \tag{A.91}$$

$$M_x = -\frac{1}{2}(3C+2E+B) \ , \quad M_y = A + D \ , \quad M_z = F + G \ , \tag{A.92}$$

$$M_{xx} = \frac{1}{4}(2C+E) \ , \qquad M_{xy} = -\frac{1}{2}(F+D) \ , \tag{A.93}$$

with the functions A, B, C, D, E, F defined as

$$A = \sum_{\{1,3\}}\sum_{\{2,4\}}\sum_{i=1}^{2}|H_i|^2 \ , \tag{A.94}$$

$$B = -2\mathrm{Re}\big(H_1H_1(2\leftrightarrow 4)^* + H_2H_2(1\leftrightarrow 3)^* + (1\leftrightarrow 3, 2\leftrightarrow 4)\big) \ , \tag{A.95}$$

$$C = -2\mathrm{Re}\big(H_1H_1(1\leftrightarrow 3)^* + H_2H_2(2\leftrightarrow 4)^* + (1\leftrightarrow 3, 2\leftrightarrow 4)\big) \ , \tag{A.96}$$

$$D = 2\mathrm{Re}\Big(\sum_{\{1,3\}}\sum_{\{2,4\}} H_1H_2^*\Big) \ , \tag{A.97}$$

$$\begin{aligned} E = & -2\mathrm{Re}\big((H_1 + H_1(1\leftrightarrow 3, 2\leftrightarrow 4))(H_2(1\leftrightarrow 3) + H_2(2\leftrightarrow 4))^* \\ & +(H_1\leftrightarrow H_2)\big) \ , \end{aligned} \tag{A.98}$$

$$\begin{aligned} F = & \ 2\mathrm{Re}\big(H_1H_1(1\leftrightarrow 3, 2\leftrightarrow 4)^* + H_1(1\leftrightarrow 3)H_1(2\leftrightarrow 4)^* \\ & + (H_1\leftrightarrow H_2)\big) \ , \end{aligned} \tag{A.99}$$

$$\begin{aligned} G = & \ 2\mathrm{Re}\big(H_1H_2(1\leftrightarrow 3, 2\leftrightarrow 4)^* + H_1(1\leftrightarrow 3)H_2(2\leftrightarrow 4)^* \\ & + (H_1\leftrightarrow H_2)\big) \ , \end{aligned} \tag{A.100}$$

where

$$\begin{aligned} H_1(1_{f_1}, 2_{f_2}, 3_{f_3}, 4_{f_4}, 5_g) &= M_1(1_{f_1}, 2_{f_2}, 3_{f_3}, 4_{f_4}, 5_g) \\ &+ M_3(3_{f_3}, 4_{f_4}, 1_{f_1}, 2_{f_2}, 5_g) \ , \end{aligned} \tag{A.101}$$

$$\begin{aligned} H_2(1_{f_1}, 2_{f_2}, 3_{f_3}, 4_{f_4}, 5_g) &= M_2(1_{f_1}, 2_{f_2}, 3_{f_3}, 4_{f_4}, 5_g) \\ &+ M_4(3_{f_3}, 4_{f_4}, 1_{f_1}, 2_{f_2}, 5_g) \ . \end{aligned} \tag{A.102}$$

For the $V \to q\bar{q}\tilde{g}\tilde{g}g$ process the square of the matrix element can be written in the form:

$$|M_5^{(0)}(1_q, 2_{\bar{q}}, 3_{\tilde{g}}, 4_{\tilde{g}}, 5_g)|^2 = N_c C_F^3 \left\{x\widetilde{M}_x + x^2\widetilde{M}_{xx}\right\} \ , \tag{A.103}$$

where

$$\widetilde{M}_x = |\widetilde{M}_1 + \widetilde{M}_2|^2 \tag{A.104}$$

$$\begin{aligned} \widetilde{M}_{xx} &= |\widetilde{M}_3 + \widetilde{M}_4|^2 \\ &+ \frac{1}{2}\mathrm{Re}\big((\widetilde{M}_1 + \widetilde{M}_2)(\widetilde{M}_3 + \widetilde{M}_4)^*\big) \\ &- \mathrm{Re}\big((\widetilde{M}_1 + \widetilde{M}_4)(\widetilde{M}_2 + \widetilde{M}_3)^*\big) \ . \end{aligned} \tag{A.105}$$

Appendix B

The one-loop level matrix elements

In this appendix we present the group independent color decomposition of four parton one-loop matrix elements in electron-positron annihilation (this results are published in [2]). In Refs. [45, 46] Campbell, Glover and Miller make FORTRAN programs for the NLO squared matrix elements of the $e^+e^- \to \gamma^* \to \bar{q}q\bar{Q}Q$ and $\bar{q}qgg$ processes publicly available. In Refs. [44, 47] Bern, Dixon, Kosower and Wienzierl give analytic formulæ for the helicity amplitudes of the same processes with the $e^+e^- \to Z^0 \to$ four partons channel included as well. In this presenting, we rely on the work of Bern, Dixon, Kosower and Wienzierl and we use the same notation as articles [44, 47] and introduce new ones but to the extent that is necessary.

Our aim is to give the NLO squared matrix elements for the $e^+e^- \to \bar{q}q\bar{p}p$ processes ($p = Q$, g, or $\tilde{g}$) in terms of color factors multiplied by group independent kinematic functions. In order to find a group independent decomposition of the squared matrix element, we have to give different color decompositions of the one-loop helicity amplitudes for the various processes than those presented in Refs. [44, 47], where the color charge information has been lost by the use of the SU(N_c) Fierz identity and SU(N_c) relations $C_F = (N_c^2 - 1)/N_c$, $C_A = 2N_c$ (for $T_R = 1$). In the new color decomposition we can only use the defining relation of the Lie algebra in Eq. (2.7) and definition of the quadratic Casimir invariants C_F, C_A in Eq. (2.8). Careful analysis of the color structure of the individual Feynman diagrams contributing to a given process shows that the color charge information can completely be recovered from the primitive amplitudes of Refs. [44, 47] for the QCD subprocesses, while in the case of two-quark two-gluino production minor modification of the partial amplitudes is necessary. In order we can use those primitive amplitudes we use $T_R = 1$ normalization.

In the next we give the color decomposition of the amplitudes of all relevant process.

Four quarks process

Let us first consider the $e^+e^- \to \bar{q}q\bar{Q}Q$ process. We are interested in the color decomposition of the amplitude $|1^{h_1}_{f_1}, 2^{h_2}_{f_2}, 3^{h_3}_{f_3}, 4^{h_4}_{f_4}; 5^{h_{\bar{\ell}}}_{\bar{\ell}}, 6^{h_\ell}_{\ell} >^{(0)}_4$ up to one-loop level. The 5,6 legs are the lepton pair, 1,3 legs are the outgoing quarks and 2,4 legs are the outgoing anti-quarks. The label f_1, f_2, f_3, f_4 denote the flavour of the legs 1,2,3,4 respectively. The color decomposition of the tree level helicity amplitude is given by

$$\begin{aligned} |1^{h_1}_{f_1}, 2^{h_2}_{f_2}, 3^{h_3}_{f_3}, 4^{h_4}_{f_4} >^{(0)}_4 \quad &= \quad \mathrm{g}_s^2 \sum_{\{1,3\}} \sum_{\{2,4\}} (-1)^{P(1,3)+P(2,4)} \sum_{c=1}^{N_A} t^c_{i_1\bar{i}_4} t^c_{i_3\bar{i}_2} \\ &\cdot \quad \widetilde{C}^{h_1 h_\ell}_{f_1 f_4} \tilde{A}_{6;0}(1^{h_1}_q, 2^{h_2}_{\bar{Q}}, 3^{h_3}_Q, 4^{h_4}_{\bar{q}}) \ , \end{aligned} \tag{B.1}$$

where $P(a,b) = 0$ if the element are in canonical order (a,b) and $P(b,a) = 1$ if the elements are permuted. The QCD coupling is denoted by g_s, h_x is the helicity of particle x and the coupling factors $\widetilde{C}^{h_q h_e}_{f_q f_{\bar{q}}} = s_{56}\, C^{h_q h_e}_{f_q f_{\bar{q}}}$ is defined in Eq. (A.20, A.24).

At one loop level the group independent color decomposition of the helicity amplitudes is given by

$$\begin{aligned} |1^{h_1}_{f_1}, 2^{h_2}_{f_2}, 3^{h_3}_{f_3}, 4^{h_4}_{f_4} >^{(1)}_4 = (4\pi \mathrm{g}_s)^2 \sum_{\{1,3\}} \sum_{\{2,4\}} (-1)^{P(1,3)+P(2,4)} \\ \cdot \left\{ \widetilde{C}^{h_1 h_\ell}_{f_1 f_4} \left[\tilde{A}_{6;1}(1^{h_1}_q, 2^{h_2}_{\bar{Q}}, 3^{h_3}_Q, 4^{h_4}_{\bar{q}}) \sum_{c=1}^{N_A} t^c_{i_1\bar{i}_4} t^c_{i_3\bar{i}_2} \right.\right. \\ \left.\left. + \ \tilde{A}_{6;2}(1^{h_1}_q, 2^{h_2}_{\bar{Q}}, 3^{h_3}_Q, 4^{h_4}_{\bar{q}}) \sum_{c,d=1}^{N_A} (t^c t^d)_{i_1\bar{i}_4} (t^d t^c)_{i_3\bar{i}_2} \right] \right. \\ \left. + \ \widetilde{C}^{h_e}_{\mathrm{ax}} \tilde{A}_{6;3}(1^{h_1}_q, 2^{h_2}_{\bar{Q}}, 3^{h_3}_Q, 4^{h_4}_{\bar{q}}) \sum_{c=1}^{N_A} t^c_{i_1\bar{i}_4} t^c_{i_3\bar{i}_2} \right\}, \end{aligned} \tag{B.2}$$

where $\widetilde{C}^{h_\ell}_{\mathrm{ax}}$ vanishes for the photon and $W^\pm$ boson, while for the $e^+e^- \to Z^0 \to \bar{q}q\bar{Q}Q$ process it is

$$\widetilde{C}^{+}_{\mathrm{ax}} = \frac{v^+_e}{\sin 2\theta_W}\, s_{56}\, \mathcal{P}_Z(s_{56}) \ , \qquad \widetilde{C}^{-}_{\mathrm{ax}} = \frac{v^-_e}{\sin 2\theta_W}\, s_{56}\, \mathcal{P}_Z(s_{56}) \ , \tag{B.3}$$

with θ_W being the Weinberg angle. In Eq. (B.2) we used the notation $\tilde{A}_{6;i}$ for the partial amplitudes in order to distinguish them from the $A_{6;i}$ functions introduced in Ref. [44], where the basic gauge invariant classes of colorless amplitudes, the 'primitive amplitudes' are also given explicitly. Our new partial amplitudes can be expressed in terms of the same primitive amplitudes multiplied by color factors. The expressions depend on the helicities of the partons. There are only two independent helicity configurations, which can be taken to be $(1^+_q, 2^\pm_{\bar{Q}}, 3^\mp_Q, 4^-_{\bar{q}}; 5^-_{\bar{\ell}}, 6^+_\ell)$, and from which the amplitudes of the other helicity configurations can be obtained [44].

Formulas (B.1) and (B.2) apply to the case of unequal quark flavors, $q \neq Q$. The equal flavor amplitude may be obtained from the unequal-flavor formula by subtracting the same formula with q and Q exchanged and then setting $Q = q$ in all the coupling constant prefactors [44].

The explicit expressions for the $\tilde{A}_{6;i}$ partial amplitudes in terms of primitive amplitudes are (we suppress the 5, 6 labels of the lepton pair)

$$\begin{aligned}
\tilde{A}_{6;0}(1_q^+, 2_{\bar{Q}}^+, 3_Q^-, 4_{\bar{q}}^-) &= A_6^{tree;++}(1,2,3,4) \ , \\
\tilde{A}_{6;1}(1_q^+, 2_{\bar{Q}}^+, 3_Q^-, 4_{\bar{q}}^-) &= -C_F A_6^{\rm sl}(2,3,1,4) + A_6^{t,++}(1,2,3,4) \qquad \text{(B.4)} \\
&+ \frac{C_A}{2}\left(A_6^{\rm sl}(2,3,1,4) - A_6^{+-}(1,3,2,4)\right) \\
&- n_f\left(A_6^{f,++}(1,2,3,4) + A_6^{s,++}(1,2,3,4)\right) \ , \qquad \text{(B.5)} \\
\tilde{A}_{6;2}(1_q^+, 2_{\bar{Q}}^+, 3_Q^-, 4_{\bar{q}}^-) &= A_6^{++}(1,2,3,4) + A_6^{+-}(1,3,2,4) \ , \qquad \text{(B.6)} \\
\tilde{A}_{6;3}(1_q^+, 2_{\bar{Q}}^+, 3_Q^-, 4_{\bar{q}}^-) &= \tilde{A}_6^{\rm ax}(1,4,2,3) \ , \qquad \text{(B.7)}
\end{aligned}$$

while for the other helicity configuration

$$\begin{aligned}
\tilde{A}_{6;0}(1_q^+, 2_{\bar{Q}}^-, 3_Q^+, 4_{\bar{q}}^-) &= A_6^{tree;+-}(1,2,3,4) \ , \\
\tilde{A}_{6;1}(1_q^+, 2_{\bar{Q}}^-, 3_Q^+, 4_{\bar{q}}^-) &= C_F A_6^{\rm sl}(3,2,1,4) + A_6^{t,+-}(1,2,3,4) \\
&- \frac{C_A}{2}\left(A_6^{\rm sl}(3,2,1,4) + A_6^{++}(1,3,2,4)\right) \\
&- n_f\left(A_6^{f,+-}(1,2,3,4) + A_6^{s,+-}(1,2,3,4)\right) \ , \qquad \text{(B.8)} \\
\tilde{A}_{6;2}(1_q^+, 2_{\bar{Q}}^-, 3_Q^+, 4_{\bar{q}}^-) &= A_6^{++}(1,3,2,4) + A_6^{+-}(1,2,3,4) \ , \qquad \text{(B.9)} \\
\tilde{A}_{6;3}(1_q^+, 2_{\bar{Q}}^-, 3_Q^+, 4_{\bar{q}}^-) &= -\tilde{A}_6^{\rm ax}(1,4,3,2) \ , \qquad \text{(B.10)}
\end{aligned}$$

where we redefined the amplitude $A_6^{\rm ax}(1,4,3,2)$. Thus we have

$$\begin{aligned}
\tilde{A}_6^{\rm ax}(1,2,3,4) &= -\frac{2{\rm i}}{(4\pi)^2}\frac{f(m_t; s_{12}, s_{34}, s_{56}) - f(m_b; s_{12}, s_{34}, s_{56})}{s_{56}} \\
&\cdot \left(\frac{[63]\langle 42\rangle\langle 25\rangle}{\langle 12\rangle} - \frac{[61][13]\langle 45\rangle}{[12]}\right) \qquad \text{(B.11)}
\end{aligned}$$

where $f(...)$ function is defined in Ref. [44] and m_t and m_b denote the mass of quark *botton* and *top* respectively.

Two quarks two gluinos process

The gluino is a majorana fermion in the adjoint representation of the gauge group and does not couple to the vector bosons directly. Therefore, the $e^+e^- \to \bar{q}q\tilde{g}\tilde{g}$ subprocesses has similar color decomposition to that of the $e^+e^- \to \bar{q}q\bar{Q}Q$ subprocess.

At tree level this decomposition reads

$$|1_{f_1}^{h_1},2_{\tilde{g}}^{h_2},3_{\tilde{g}}^{h_3},4_{f_4}^{h_4}>_4^{(0)}=\mathrm{g}_s^2\widetilde{C}_{f_1f_4}^{h_1h_\ell}\tilde{A}_{6;0}(1_q^{h_1},2_{\tilde{g}}^{h_2},3_{\tilde{g}}^{h_3},4_{\bar{q}}^{h_4})\sum_{c=1}^{N_A}t^c_{i_1\bar{i}_4}F^c_{\tilde{g}_2\tilde{g}_3}\ \ ,\quad(B.12)$$

while at one-loop it is

$$\begin{aligned}|1_{f_1}^{h_1},2_{\tilde{g}}^{h_2},3_{\tilde{g}}^{h_3},4_{f_4}^{h_4}>_4^{(1)}=(4\pi\mathrm{g}_s)^2\Bigg\{&\widetilde{C}_{f_1f_4}^{h_1h_\ell}\Bigg[\tilde{A}_{6;1}(1_q^{h_1},2_{\tilde{g}}^{h_2},3_{\tilde{g}}^{h_3},4_{\bar{q}}^{h_4})\sum_{c=1}^{N_A}t^c_{i_1\bar{i}_4}F^c_{\tilde{g}_3\tilde{g}_2}\\&+\tilde{A}_{6;2}(1_q^{h_1},2_{\bar{q}}^{h_2},3_{\bar{q}}^{h_3},4_{\bar{q}}^{h_4})\sum_{c,d=1}^{N_A}(t^ct^d)_{i_1\bar{i}_4}(F^dF^c)_{\tilde{g}_3\tilde{g}_2}\Bigg]\\&+\ \widetilde{C}_{\mathrm{ax}}^{h_\ell}\ \tilde{A}_{6;3}(1_q^{h_1},2_{\bar{q}}^{h_2},3_{\bar{q}}^{h_3},4_{\bar{q}}^{h_4})\sum_{c=1}^{N_A}t^c_{i_1\bar{i}_4}F^c_{\tilde{g}_3\tilde{g}_2}\Bigg\}.\end{aligned}\quad(B.13)$$

The $\tilde{A}_{6;i}$ partial amplitudes for the $e^+e^-\to\bar{q}q\tilde{g}\tilde{g}$ process are closely related to those of the $e^+e^-\to\bar{q}q\bar{Q}Q$ process. In fact, the $\tilde{A}_{6;2}$ and $\tilde{A}_{6;3}$ amplitudes are exactly the same,

$$\tilde{A}_{6;0}(1_q^+,2_{\tilde{g}}^\pm,3_{\tilde{g}}^\mp,4_{\bar{q}}^-)=\tilde{A}_{6;0}(1_q^+,2_{\bar{Q}}^\pm,3_Q^\mp,4_{\bar{q}}^-)\ \ ,\quad(B.14)$$

$$\tilde{A}_{6;2}(1_q^+,2_{\tilde{g}}^\pm,3_{\tilde{g}}^\mp,4_{\bar{q}}^-)=\tilde{A}_{6;2}(1_q^+,2_{\bar{Q}}^\pm,3_Q^\mp,4_{\bar{q}}^-)\ \ ,\quad(B.15)$$

$$\tilde{A}_{6;3}(1_q^+,2_{\tilde{g}}^\pm,3_{\tilde{g}}^\mp,4_{\bar{q}}^-)=\tilde{A}_{6;3}(1_q^+,2_{\bar{Q}}^\pm,3_Q^\mp,4_{\bar{q}}^-)\ \ ,\quad(B.16)$$

while the $\tilde{A}_{6;1}$ amplitudes differ in terms arising from fermion bubble and parent triangle diagrams [44],

$$\begin{aligned}\tilde{A}_{6;1}(1_q^+,2_{\tilde{g}}^\pm,3_{\tilde{g}}^\mp,4_{\bar{q}}^-)&=\tilde{A}_{6;1}(1_q^+,2_{\bar{Q}}^\pm,3_Q^\mp,4_{\bar{q}}^-)-(C_F-C_A)A_6^{\Delta,+\pm}(1,2,3,4)\\&-\ n_{\tilde{g}}\frac{C_A}{2}\left(A_6^{f,+\pm}(1,2,3,4)+A_6^{s,+\pm}(1,2,3,4)\right),\end{aligned}\quad(B.17)$$

where $n_{\tilde{g}}$ is the number of light gluino flavors and

$$\begin{aligned}&A_6^{\Delta,+\pm}(1,2,3,4)=\\&\quad c_\Gamma A_6^{\mathrm{tree},+\pm}(1,2,3,4)\left[-\frac{1}{\epsilon^2}\left(\frac{\mu^2}{-s_{23}}\right)^\epsilon-\frac{3}{2\epsilon}\left(\frac{\mu^2}{-s_{23}}\right)^\epsilon-\frac{7}{2}\right],\end{aligned}\quad(B.18)$$

with c_Γ and $A_6^{\mathrm{tree},++}$ given in Ref. [44]. We remark here that gluinos are Majorana fermions therefore, the cross section requires an identical-particle factor of $\frac{1}{2}$ in the phase-space measure.

Two quarks two gluons process

Finally, the new color decomposition of the helicity amplitudes for the $e^+e^- \to \bar{q}qgg$ process at tree level is given by

$$|1_{f_1}^{h_1}, 2_g^{h_2}, 3_g^{h_3}, 4_{f_4}^{h_4}>_4^{(0)} = \mathrm{g}_s^2 \widetilde{C}_{f_1 f_4}^{h_1 h_\ell} \Big[\tilde{A}_{6;0}(1_q^{h_q}, 2_g^{h_2}, 3_g^{h_3}, 4_{\bar{q}}^{h_4})(t^{g_2} t^{g_3})_{i_1 \bar{i}_4} + \tilde{A}_{6;0}(1_{\bar{q}}^{h_1}, 3_g^{h_3}, 2_g^{h_2}, 4_{\bar{q}}^{h_4})(t^{g_3} t^{g_2})_{i_1 \bar{i}_4} \Big], \quad \text{(B.19)}$$

and at one-loop it is

$$\begin{aligned}
|1_{f_1}^{h_1}, 2_g^{h_2}, 3_g^{h_3}, 4_{f_4}^{h_4}>_4^{(1)} = (4\pi \mathrm{g}_s)^2 \Bigg\{ & \\
& \widetilde{C}_{f_1 f_4}^{h_1 h_\ell} \Big[\tilde{A}_{6;1}(1_q^{h_1}, 2_g^{h_2}, 3_g^{h_3}, 4_{\bar{q}}^{h_4})(t^{g_2} t^{g_3})_{i_1 \bar{i}_4} \\
& \qquad + \tilde{A}_{6;2}(1_q^{h_1}, 2_g^{h_2}, 3_g^{h_3}, 4_{\bar{q}}^{h_4})(t^{g_3} t^{g_2})_{i_1 \bar{i}_4} \\
& \qquad + \tilde{A}_{6;3}(1_q^{h_1}, 2_g^{h_2}, 3_g^{h_3}, 4_{\bar{q}}^{h_4}) \sum_{c,d=1}^{N_A} (t^c t^d)_{i_1 \bar{i}_4} (F^d F^c)_{g_3 g_2} \Big] \\
& + \sum_{f=1}^{n_f} \frac{1}{2} \left(\widetilde{C}_{ff}^{+h_\ell} + \widetilde{C}_{ff}^{-h_\ell} \right) \tilde{A}_{6;4}(1_q^{h_1}, 2_g^{h_2}, 3_g^{h_3}, 4_{\bar{q}}^{h_4}) \\
& \qquad \cdot \sum_{c=1}^{N_A} \left[\mathrm{Tr}(t^{g_2} t^{g_3} t^c) t^c_{i_1 \bar{i}_4} + \mathrm{Tr}(t^{g_3} t^{g_2} t^c) t^c_{i_1 \bar{i}_4} \right] \\
& + \widetilde{C}_{\mathrm{ax}}^{h_\ell} \Big[\tilde{A}^A_{6;5}(1_q^{h_1}, 2_g^{h_2}, 3_g^{h_3}, 4_{\bar{q}}^{h_4})(t^{g_2} t^{g_3})_{i_1 \bar{i}_4} \\
& \qquad + \tilde{A}^B_{6;5}(1_q^{h_1}, 2_g^{h_2}, 3_g^{h_3}, 4_{\bar{q}}^{h_4})(t^{g_3} t^{g_2})_{i_1 \bar{i}_4} \\
& \qquad + \tilde{A}^C_{6;5}(1_q^{h_q}, 2_g^{h_2}, 3_g^{h_3}, 4_{\bar{q}}^{h_{\bar{q}}}) \\
& \qquad \cdot \sum_{c=1}^{N_A} \left[\mathrm{Tr}(t^{g_2} t^{g_3} t^c) t^c_{i_1 \bar{i}_4} + \mathrm{Tr}(t^{g_3} t^{g_2} t^c) t^c_{i_1 \bar{i}_4} \right] \Big] \Bigg\} \ . \qquad \text{(B.20)}
\end{aligned}$$

The partial amplitudes $\tilde{A}_{6;i}$ can easily be constructed from the primitive amplitudes of Ref. [47]:

$$\begin{aligned}
\tilde{A}_{6;0}(1_q^+, 2_g^{h_2}, 3_g^{h_3}, 4_{\bar{q}}^-) &= A_6^{tree}(1_q^+, 2_g^{h_2}, 3_g^{h_3}, 4_{\bar{q}}^-) \ , & \text{(B.21)} \\
\tilde{A}_{6;3}(1_q^+, 2_g^{h_2}, 3_g^{h_3}, 4_{\bar{q}}^-) &= A_{6;3}(1_q^+, 4_{\bar{q}}^-; 2_g^{h_2}, 3_g^{h_3}) \ , & \text{(B.22)} \\
\tilde{A}_{6;4}(1_q^+, 2_g^{h_2}, 3_g^{h_3}, 4_{\bar{q}}^-) &= A^{\mathrm{v}}_{6;4}(1_q^+, 4_{\bar{q}}^-; 2_g^{h_2}, 3_g^{h_3}) \ , & \text{(B.23)}
\end{aligned}$$

and the more complicate amplitudes are given by

$$\begin{aligned}\tilde{A}_{6;1}(1_q^+,2_g^{h_2},3_g^{h_3},4_{\bar{q}}^-) &= C_F A_6(1_q,4_{\bar{q}};3,2)+A_6^{t,++}(1_q,2,3,4_{\bar{q}})\\ &+\frac{C_A}{2}\left[A_6(1_q,2,3,4_{\bar{q}})-A_6(1_q,4_{\bar{q}};3,2)-A_{6;3}(1_q,4_{\bar{q}};3,2)\right]\\ &-n_f\left(A_6^{f,++}(1_q,2,3,4_{\bar{q}})+A_6^{s,++}(1_q,2,3,4_{\bar{q}})\right)\quad, \qquad \text{(B.24)}\\ \tilde{A}_{6;2}(1_q^+,2_g^{h_2},3_g^{h_3},4_{\bar{q}}^-) &= C_F A_6(1_q,4_{\bar{q}};2,3)+A_6^{t,++}(1_q,3,2,4_{\bar{q}})\\ &+\frac{C_A}{2}\left[A_6(1_q,3,2,4_{\bar{q}})-A_6(1_q,4_{\bar{q}};2,3)\right]\\ &-n_f\left(A_6^{f,++}(1_q,3,2,4_{\bar{q}})+A_6^{s,++}(1_q,3,2,4_{\bar{q}})\right)\quad, \qquad \text{(B.25)}\end{aligned}$$

and the axial amplitudes are

$$\begin{aligned}\tilde{A}^A_{6;5}(1_q^+,2_g^{h_2},3_g^{h_3},4_{\bar{q}}^-) &= \frac{1}{2}\left[A^{\rm ax}_{6;4}(1_q^+,4_{\bar{q}}^-;2_g^{h_2},3_g^{h_3})-A^{\rm ax}_{6;4}(1_q^+,4_{\bar{q}}^-;3_g^{h_3},2_g^{h_2})\right.\\ &\left.+A^{\rm ax}_{6;5}(1_q^+,4_{\bar{q}}^-;2_g^{h_2},3_g^{h_3})\right]\quad, \qquad \text{(B.26)}\\ \tilde{A}^B_{6;5}(1_q^+,2_g^{h_2},3_g^{h_3},4_{\bar{q}}^-) &= \frac{1}{2}\left[A^{\rm ax}_{6;4}(1_q^+,4_{\bar{q}}^-;3_g^{h_3},2_g^{h_2})-A^{\rm ax}_{6;4}(1_q^+,4_{\bar{q}}^-;2_g^{h_2},3_g^{h_3})\right.\\ &\left.+A^{\rm ax}_{6;5}(1_q^+,4_{\bar{q}}^-;2_g^{h_2},3_g^{h_3})\right]\quad, \qquad \text{(B.27)}\\ \tilde{A}^C_{6;5}(1_q^+,2_g^{h_2},3_g^{h_3},4_{\bar{q}}^-) &= \frac{1}{2}\left[A^{\rm ax}_{6;4}(1_q^+,4_{\bar{q}}^-;2_g^{h_2},3_g^{h_3})+A^{\rm ax}_{6;4}(1_q^+,4_{\bar{q}}^-;3_g^{h_3},2_g^{h_2})\right.\\ &\left.-A^{\rm ax}_{6;5}(1_q^+,4_{\bar{q}}^-;2_g^{h_2},3_g^{h_3})\right]\quad. \qquad \text{(B.28)}\end{aligned}$$

Before closing the discussion of the helicity amplitudes, we should remark that in order to take into account the effect of light gluinos in a NLO calculation fully, one has to make the change

$$n_f \to n_f + \frac{C_A}{2} n_{\tilde{g}} \qquad \text{(B.29)}$$

in Eqs. (B.4), (B.8) and (B.24), (B.25), where in SU(N_c) theory $C_A = 2N_c$ for $T_R = 1$.

As a next step we use Eqs. (B.1), (B.2), (B.12), (B.13), and (B.19), (B.20) to give a gauge independent decomposition of the NLO squared matrix elements. The general expression for these matrix elements is

$$d\sigma_4^{\rm NLO,\,virtual} \propto 2 \sum_{\rm helicities}\sum_{\rm colors} {\rm Re}\left[{}^{(0)}_{4}\!<1,...,m|1,...,m>^{(1),\,fin}_{4}\right]\quad, \qquad \text{(B.30)}$$

where color sum is evaluated in such a way that the group independent information is maintained. For this purpose, we use the commutation relation (2.7) together with the definition of the quadratic Casimirs, Eq. (2.8) to derive the necessary Lie-algebra relations.

The resulting differential cross sections can be written as a quadratic form:

$$\frac{1}{\sigma_0} d\sigma_4^{\mathrm{NLO,\,virtual}}(\vec{p}) = \left(\frac{\alpha_s C_F}{2\pi}\right)^3 [C_0(\vec{p}) + C_x(\vec{p})\, x + C_y(\vec{p})\, y + C_z(\vec{p})\, z + C_{xx}(\vec{p})\, x^2 + C_{xy}(\vec{p})\, x\, y + C_{yy}(\vec{p})\, y^2] \quad . \tag{B.31}$$

In this equation σ_0 denotes the Born cross section for the process $e^+e^- \to \bar{q}q$, $\vec{p}$ is the collection of the final state momenta, and x, y and z are ratios of eigenvalues of the Casimir operators defined as

$$x = \frac{C_A}{C_F} \ , \qquad y = \frac{T_R}{C_F} = \frac{N_c}{N_A} \ , \qquad z = \frac{C_3}{N_c C_F^2} \ . \tag{B.32}$$

These ratios are the sole quantities together with the overall normalization that carry group information. The coefficients $C_i(\vec{p})$ are the group independent kinematical functions that depend on the subprocess. Their explicit expressions are quite complicated, but can be obtained straightforwardly using the formulas of this appendix.

Bibliography

[1] Z. Nagy, Z. Trócsányi, Next-to-Leading Order Calculation of Four-Jet Shape Variables, Phys. Rev. Lett. **79**, 3604 (1997)

[2] Z. Nagy, Z. Trócsányi, Group independent color decomposition of next-to-leading order matrix elements for $e^+e^- \to$ four partons, Phys. Lett. **B414**, 187 (1997)

[3] Z. Nagy, Z. Trócsányi, Excluding light gluinos using four-jet LEP events: a next-to-leading order result, hep-ph/9708343

[4] Z. Nagy, Z. Trócsányi, Four-jet production in e^+e^- annihilation at next-to-leading order, Nucl. Phys. (Proc. Suppl.) **B64**, 63 (1998)

[5] Z. Nagy, Z. Trócsányi, Four-Jet angular distributions and color charge measurements: Leading order versus next-to-leading order, Phys. Rev. **D57**, 5793 (1998)

[6] Z. Nagy, Z. Trócsányi, Next-to-leading order calculation of four-Jet observables in electron-positron annihilation, Phys. Rev. **D59**, 014020 (1998)

[7] Z. Nagy, Z. Trócsányi, Multijet rates in e^+e^- annihilation: perturbative theory versus LEP data, Nucl. Phys. (Proc. Suppl.) **B74**, 44 (1999)

[8] Z. Nagy, Z. Trócsányi, Calculation of QCD jet cross sections at next-to-leading order, Nucl. Phys. **B486**, 189 (1997)

[9] `http://dtp.atomki.hu/~nagyz/NLO`

[10] C.N.Yang, R.L. Mills Phys. Rev. **96**, 191 (1954)

[11] T. Kinoshita, J. Math. Phys. **3** 650. (1962) ; T.D. Lee, M. Nauenberg, Phys. Rev. **B133**, 1549 (1964)

[12] M. Gell-Mann, Acta Phys. Aus., Suppl. **IX**, 733 (1972); H. Fritzsch and M. Gell-Mann, XVIth International Conference on High Energy Physics, Vol. II p.135 (1972); H. Fritzsch, M. Gell-Mann and H. Leutwyler, Phys. Lett. **47B**, 365 (1973); T. Muta, Foundation of Quantum Chromodynamics, World Scientific, (1987).

[13] G. Altarelli, G. Parisi, Nucl. Phys. **126**, 298 (1977)

[14] S.G. Gorishny, A.L. Kataev, S.A. Larin, Phys. Lett. **B259**, 144 (1991); L.R. Surguladze, M.A. Samuel, Phys. Rev. Lett. **66**, 560 (1991); K.G. Chetyrkin, Phys. Lett. **B391**, 402 (1997);

[15] F. Csikor and Z. Fodor, Phys. Rev. Lett. **78**, 4335 (1997); F. Csikor and Z. Fodor, preprint hep-ph/9712269

[16] E. Fahri, Phys. Rev. Lett. **39**, 1587 (1977)

[17] G. Parisi, Phys. Lett. **B74**, 65 (1978); J.F. Donoghue, F.E. Low, S.Y. Pi, Phys. Rev. **D20**, 2759 (1979)

[18] A. De Rújula *et al.*, Nucl. Phys. **B138**, 387 (1978)

[19] G.C. Fox and S. Wolfram, Phys. Lett. **B82**, 134 (1979)

[20] J.G. Körner, G. Schierholz, J. Willrodt, Nucl. Phys. **B185**, 365 (1981)

[21] O. Nachtman, A. Reiter, Zeit. Phys. C **16**, 45 (1982)

[22] JADE Collaboration, W. Bartel et al., Zeit. Phys. C **33**, 23 (1986); S. Bethke et al., Phys. Lett. **B213**, 235 (1988)

[23] M. Bengtsson, P.M. Zerwas, Phys. Lett. **B208**, 306 (1988)

[24] P. Abreu et al, DELPHI Collaboration, Phys. Lett. **255**, 466 (1991)

[25] S. Catani, Yu.L. Dokshitzer, M. Olsson, G. Turnock, B.R. Webber, Phys. Lett. **B269**, 432 (1991)

[26] S. Bethke, Z. Kunszt, D.E. Soper, W.J. Stirling, Nucl. Phys. **B370**, 310 (1992)

[27] Yu.L. Dokshitzer, G.D. Leder, S. Moretti, B.R, Webber, J. of High Energy Phys. **8**, 1 (1997)

[28] S. Bentvelsen and I. Meyer, hep-ph/9803322 .

[29] X. Artu, G. Mennessier, Nucl. Phys. **B70**, 93 (1974); M.G. Bowler, Zeit. Phys. C **11**, 169 (1981;)B. Anderson, G. Gustafson, B. Söderberg, Zeit. Phys. C **20**, 317 (1983); Nucl. Phys. **B264**, 29 (1986)

[30] D. Amati, G. Veneziano, Phys. Lett. **B83**, 87 (1979); A. Bassetto, M. Ciafaloni, G. Marchesini, Phys. Lett. **83**, 207 (1979); G. Marchesini, L. Trentadue, G. Veneziano, Nucl. Phys. **B181**, 335 (1980)

[31] G. Marchesini and B.R. Webber, Nucl. Phys. **B310**, 461 (1988); G. Marchesini, B.R. Webber, G. Abbiendi, I.G. Knowles, M.H. Seymour and L. Stanco, Comp. Phys. Comm. **67**, 465 (1992).

[32] T. Sjöstrand, Comp. Phys. Comm. **82**, 74 (1994).

[33] J. Kodaira and L. Trentadue, Phys. Lett. **B112**, 66 (1982); C.T.H. Davies, W.J. Stirling and B.R. Webber, Nucl. Phys. **B256**, 413 (1985); S. Catani, E. d'Emilio and L. Trentadue, Phys. Lett. **B211**, 335 (1988).

[34] S. Catani, G. Marchesini and B.R. Webber, Nucl. Phys. **B349**, 635 (1991).

[35] S. Catani, in QCD at 200 TeV, Proc. 17th INFN Eloisatron Project Workshop, ed.: L. Cifarelli and Yu.L. Dokshitzer, Plenum Press, New York (1992).

[36] S. Catani, Yu.L. Dokshitzer, M. Olsson, G. Turnock and B.R. Webber, Phys. Lett. B **269**, 432 (1991).

[37] G. Dissertori and M. Schmelling, Phys. Lett. B **361**, 167 (1995).

[38] P. de Causmaecker, R. Gastmans, W. Troost and T.T. Wu, Phys. Lett. **105B**, 215 (1981); R. Kleiss, Nucl. Phys. **B241**, 61 (1984); F.A. Berends, P.H. Daverveldt and R. Kleiss, *ibid* **253**, 441 (1985); J.F. Gunion and Z. Kunszt, Phys. Lett. **161B**, 333 (1985); Z. Xu, D.H. Zhang and L. Chang, Nucl. Phys. **B291**, 392 (1987).

[39] F.A. Berends and W.T. Giele, Nucl. Phys. **B306**, 759 (1988).

[40] K. Hagiwara and D. Zeppenfeld, Nucl. Phys. **B313**, 560 (1989); F.A. Berends, W.T. Giele and H. Kuijf, *ibid* **B321**, 39 (1989); N.K. Falk, D. Graudenz and G. Kramer, *ibid* **B328**, 317 (1989).

[41] M.L. Mangano, S.J. Parke, Phys. Rep. **200**, 301 (1991)

[42] Z. Bern, L. Dixon, D.A. Kosower, Phys. Lett. **B348**, 503 (1993), Nucl. Phys. **B412**, 616 (1994)

[43] Z. Kunszt, A. Signer, Z. Trócsányi Nucl. Phys. **B420**, 550 (1994); Nucl. Phys. **B411**, 397 (1994)

[44] Z. Bern, L. Dixon, D. A. Kosower and S. Wienzierl, Nucl. Phys. **B489**, 3 (1997);

[45] E.W.N. Glover and D.J. Miller, Phys. Lett. **B396**, 257 (1997).

[46] J.M. Campbell, E.W.N. Glover and D.J. Miller, preprint hep-ph/9706297.

[47] Z. Bern, L. Dixon and D. A. Kosower, Nucl. Phys. **B513**, 3 (1998).

[48] R.K. Ellis, D.A. Ross, A.E. Terrano, Nucl. Phys. **B178**, 421 (1981)

[49] Z. Kunszt, P. Nason, G. Marchesini and B.R. Webber, in 'Z Physics at LEP1', CERN 89-08, vol. 1, p. 373.

[50] W.T. Giele, E.W.N. Glover, Phys. Rev. **D46**, 1980 (1992)

[51] W.T. Giele, E.W.N. Glover, D.A. Kosower, Nucl. Phys. **B403**, 633 (1993)

[52] S.Frixione, Z. Kunszt, A. Signer, Nucl. Phys. **B467**, 399 (1996)

[53] S. Catani, M.H. Seymour, Phys. Lett. **B387**, 287 (1996); Nucl. Phys. **B485**, 291 (1997)

[54] S.D. Ellis, R. Kleiss, W.J. Stirling, Comp. Phys. Comm. **40**, 359 (1986)

[55] R. Pittau, Comp. Phys. Comm. **83**, 141 (1994)

[56] VENUS collaboration, K. Abe *et al.*, Phys. Lett. B **240**, 232 (1990); AMY collaboration, K.B. Lee *et al.*, *ibid* **313**, 469 (1993); TOPAZ collaboration, Y. Ohnishi *et al.*, *ibid* **313**, 475 (1993);

[57] Mark II collaboration, S. Komamiya *et al.*, Phys. Rev. Lett. **64**, 987 (1990); SLD collaboration, K. Abe *et al.*, Phys. Rev. D **51**, 962 (1995).

[58] ALEPH collaboration, D. Decamp *et al.*, Phys. Lett. B **257**, 479 (1991); *ibid* **284**, 163 (1992).

[59] DELPHI collaboration, P. Abreu *et al.*, Zeit. Phys. C **54**, 55 (1992); *ibid* **59**, 21 (1993).

[60] OPAL collaboration, P.D. Acton *et al.*, Zeit. Phys. C **55**, 1 (1992); *ibid* **59**, 93 (191); R. Akers *et al.*, *ibid* **68**, 519 (1995).

[61] L3 collaboration, O. Adriani *et al.*, Phys. Lett. B **284**, 471 (1992); Phys. Rep. **236**, 1 (1993).

[62] G.R. Farrar, Phys. Lett. B **265**, 395 (1991); Phys. Rev. D **51**, 3904 (1995;)J. Ellis, D. Nanopoulos and D. Ross, Phys. Lett. B **305**, 375 (1993); R. Muñoz-Tapia and W.J. Stirling, Phys. Rev. D **49**, 3763 (1994). F.E. Close, G.R. Farrar and Z.P. Li, *ibid* **55**, 5749 (1997); D.J. Chung, G.R. Farrar and E.W. Kolb, astro-ph/9707036;

[63] L3 Collaboration, B. Adeva *et al.*, Phys. Lett. B **248**, 227 (1990); DELPHI Collaboration, P. Abreu *et al.*, *ibid* **255**, 466 (1991); DELPHI Collaboration, P. Abreu *et al.*, Zeit. Phys. C **59**, 357 (1993); OPAL Collaboration, R. Akers *et al.*, *ibid* **65**, 367 (1995); ALEPH Collaboration, D. Decamp *et al.*, Phys. Lett. B **284**, 151 (1992); ALEPH Collaboration, R. Barate *et al.*, Zeit. Phys. C **76**, 1 (1997).

[64] ALEPH collaboration, R. Barate *et al.*, Phys. Rep. **294**, 1 (1998).

[65] OPAL Collaboration, M.Z. Akrawy *et al.*, Zeit. Phys. C **47**, 505 (1990); G. Alexander *et al.*, *ibid* **72**, 191 (1996); L3 Collaboration, B. Adeva *et al.*, *ibid* **55**, 39 (1992); DELPHI Collaboration, P. Abreu *et al.*, *ibid* **73**, 11 (1996).

[66] D. Decamp et al, ALEPH Collaboration, Phys. Lett. **B284**, 151 (1992); R. Barate et al, ALEPH Collaboration, Zeit. Phys. C **76**, 1 (1997)

[67] B. Adeva et al, L3 Collaboration, Phys. Lett. **B248**, 227 (1990)

[68] P. Abreu et al, DELPHI Collaboration, Zeit. Phys. C **59**, 357 (1993)

[69] R. Akers et al, OPAL Collaboration, Zeit. Phys. C **65**, 367 (1995)

[70] L. Dixon, A. Signer, Phys. Rev. Lett. **78**, 811 (1997); Phys. Rev. **D65**, 4031 (1997)

[71] L. Dixon and A. Signer, private communication.

[72] J.M. Campbell, M.A. Cullen, E.W.N. Glover, Eur.Phys.J. **C9**, 245 (1999)

[73] S. Weinzierl, D. A. Kosower, Phys. Rev. **D60**, 054028 (1999)